Desorption of Per-and Polyfluoroalkyl Substances from Powdered and Colloidal Activated Carbon

by

Andrew Michael Uramowski

A thesis

presented to the University of Waterloo

in fulfillment of the

thesis requirement for the degree of

Master of Applied Science

in

Civil Engineering (Water)

Waterloo, Ontario, Canada, 2024

© Andrew Michael Uramowski 2024

Author’s Declaration

I hereby declare that I am the sole author of this thesis. This is a true copy of the thesis, including any required final revisions, as accepted by my examiners.

I understand that my thesis may be made electronically available to the public.

Abstract

Per- and polyfluoroalkyl substances (PFAS) are a group of synthetic chemicals with unique heat-resistant properties, leading to their usage in aqueous film-forming foams (AFFF) for fighting fuel-based fires at airports and military bases. The application of AFFF at these facilities has led to the contamination of groundwater with PFAS, which can threaten the safety of nearby drinking water, agricultural, and industrial supply wells, as well as downgradient surface water bodies. Drinking water supplies contaminated with PFAS can result in human exposure, which has been linked to developmental, immunological, endocrine, and cardiovascular disorders, and cancer. Since PFAS are resistant to biodegradation and traditional destruction technologies, current remediation efforts are focused on immobilizing PFAS using adsorptive processes that sequester PFAS from the aqueous phase, concentrating them on an adsorbent media. The injection of activated carbon (AC) particulate amendments into the subsurface has been suggested as a promising technique for the in situ immobilization of plumes of PFAS and to protect downgradient receptors. To predict the long-term performance of these AC barriers, a thorough understanding of adsorption and desorption processes is required.

The objective of this research was to investigate the desorption behaviour of three PFAS (perfluorooctane sulfonic acid (PFOS), perfluorooctanoic acid (PFOA), and perfluorobutane sulfonic acid (PFBS)) from a powdered AC (PAC) and a colloidal AC (CAC). The research focused specifically on assessing whether desorption of PFOS, PFOA, and PFBS on these two AC materials was hysteretic. PFAS adsorption and desorption kinetic experiments using PAC or CAC were completed to determine the contact time required to reach near-equilibrium conditions. Adsorption experiments with PAC utilized the bottle-point method, and desorption experiments used a sequential desorption methodology where the aqueous phase of desorption reactors was replaced with an adsorbate-free solution. Adsorption of PFAS by CAC was also investigated using the bottle-point method; however, desorption experiments were conducted using two different methods: (1) a sub-sampling methodology where aliquots of slurry from a well-mixed adsorption isotherm bottle were diluted to initiate desorption, and

(2) a whole-bottle dilution method where the entire contents of adsorption reactors were diluted to larger volumes to initiate desorption.

The results indicated that for experiments utilizing PAC, adsorption and desorption equilibrium was established for all compounds within 72 h. Desorption of PFOS, PFOA and PFBS from PAC did not demonstrate hysteresis since all desorption data were contained within the 95% adsorption prediction band. For experiments using CAC, adsorption equilibrium was established by 120 h for all compounds, while desorption equilibrium was established by 120 h for PFOS, and 72 h for PFOA and PFBS. Desorption data using the sub-sampling method for PFOS, PFOA or PFBS and CAC were below and outside of the 95% adsorption prediction band. It was concluded that unrepresentative sub-sampling of CAC slurry occurred in the desorption step using this method. When the whole-bottle dilution method was adopted for PFOS, desorption data were within the 95% adsorption prediction band, indicating no evidence of hysteresis under the experimental conditions used. Since mass removal at each desorption step was extremely small compared to the sorbed fraction, desorption data did not reach aqueous equilibrium concentrations near the method detection limit.

The absence of hysteretic behaviour in this research demonstrates that sorption processes are reversible over the concentration ranges explored. This reversibility implies that PFAS sorbed within AC barriers can be released when the groundwater concentration is decreased, either due to temporal heterogeneity in concentration profiles, or the depletion of the source zone.

Acknowledgements

I want to preface this thesis by acknowledging those who have made my time as a master's student an incredible experience. Without encouragement provided by many who have crossed my path during this process, the research would not have made it to where it is today.

First, I would like to acknowledge my supervisors, Dr. Anh Pham and Dr. Neil Thomson, for an environment where curiosity is welcomed and encouraged. I valued our brainstorming sessions greatly. When the path forward wasn't clear, your continued vote of confidence was crucial to my perseverance during method development. And in the last stages of my degree, your detailed feedback has made me a better writer.

To the "Phamily" group, which is forever growing, I valued each discussion (work-related or personal) at our weekly Grad House coffee breaks. To those who I was fortunate enough to work with in DWE-2461 over the years, I thank you for making each day new and exciting; although, if I were to do it all over again, I would probably not put my laptop on top of the drawer labeled "strong magnet"… To Lara, our co-op student during the Winter 2023 term, thank you for all your hard work. I hope this experience fostered a curiosity within you for graduate studies. To Seyfollah, the core of the research group, thank you for all the guidance throughout this process. Your skillset and intuition in a research setting was invaluable to my success.

While this research was lab-based, my desire to gain field experience was made possible by opportunities within the extended research group. Through several trips to CFB Borden and one trip to NAS Jacksonville, I made some fond memories I won't soon forget. To Adam and Bill, thank you for having me along for part of the journey.

To Bekah, my rock throughout this process, your unconditional love has been crucial to staying motivated everyday. Thank you for supporting me through this academic journey; I couldn't have done it without you.

And last but not least, thank you to my parents and my brother for a life of learning through experiences, to gain an appreciation of the world we live in. You taught me to question

everything and be inquisitive in day-to-day life, which I'm proud to say has become key to my interest in environmental engineering and research. Your endless support has allowed me to reach outside my comfort zone in many aspects of life and continue to grow as an individual, and for that, I am forever grateful.

Dedication

This thesis is dedicated to my brother Jared, who I look up to in every endeavor. You have, and always will be my role model.

Table of Contents

Author's Declaration ii

Abstract iii

Acknowledgements v

Dedication vii

List of Figures x

List of Tables xiv

List of Abbreviations xv

Chapter 1 Introduction 1

1.1 Background 1

1.2 Research Scope 4

1.3 Thesis Overview 5

Chapter 2 Literature Review 6

2.1 Per- and polyfluoroalkyl Substances 6

2.2 PFAS Treatment Technologies 8

2.2.1 Degradation Technologies 8

2.2.2 Separation Technologies 10

2.3 Activated Carbon 12

2.3.1 Mechanisms of Adsorption to Activated Carbon 13

2.3.2 Adsorption Isotherm 14

2.4 Desorption and Hysteresis 17

2.5 Adsorption and Desorption of PFAS on Aquifer Materials 22

2.6 Adsorption and Desorption of PFAS on Engineered Adsorbents 23

Chapter 3 Materials and Methods 26

3.1 Materials 27

3.1.1 Adsorbents 27
3.1.2 Chemicals 27
3.2 Methods 28
3.2.1 Carbon Processing 28
3.2.2 Adsorption and Desorption Isotherm Experiments with PAC 30
3.2.3 Adsorption and Desorption Kinetic Experiments with PAC 32
3.2.4 Adsorption and Desorption Isotherm Experiments with CAC 33
3.2.5 Adsorption and Desorption Kinetic Experiments with CAC 36
3.2.6 Sample Preparation and Analysis 36
3.2.7 Data Analysis 37
Chapter 4 Results and Discussion 39
4.1 Powdered Activated Carbon Experiments 39
4.1.1 Adsorption and Desorption Kinetics 39
4.1.2 Adsorption and Desorption Isotherms 42
4.2 Colloidal Activated Carbon Experiments 48
4.2.1 Adsorption and Desorption Kinetics 48
4.2.2 Adsorption and Desorption Experiments 51
4.3 Discussion of Desorption Results Reported in the Literature 57
Chapter 5 Conclusions, Insights and Recommendations 59
5.1 Conclusions 59
5.2 Limitations and Recommendations 61
References 63
Appendix A Equipment Details 75
Appendix B Additional Figures 78

List of Figures

Figure 1.1: Schematic of PFAS immobilization using injectable AC at an AFFF-impacted site. 3

Figure 2.1: Chemical structures of PFOA, PFOS and 6:2 FTS 6

Figure 2.2: Schematic of activated carbon pore structure demonstrating the accumulation of PFAS ● on the surface of the carbon, and the adsorption of PFAS ● within the pore structure 13

Figure 2.3: Examples of adsorption ─○─, reversible sorption ─Δ─, and irreversible sorption ─▲─ in sequential desorption experimental data 19

Figure 2.4: Visual demonstration of hysteretic desorption data generated using the single-step desorption approach 21

Figure 2.5: Visual demonstration of irreversible desorption data generated using the batch serial dilution approach. D1 to D5 represent the desorption step number, where D5 intersects the y-axis (C_e = 0) at C_s > 0, indicating irreversible sorption 21

Figure 3.1: Comparison between (a) as-received WPC PAC and (b) retained WPC PAC. Image taken at 40x objective, 1.3 numerical aperture. Circular ordnances within the image are air bubbles trapped under the microscope cover slides..... 29

Figure 3.2: Schematic of the experimental approach used to investigate the desorption of PFBS, PFOA, and PFOS from PAC. After the adsorption bottle reached equilibrium (a-b), 10% of the aqueous phase (including all PAC) was transferred to a larger HDPE bottle (c). Multiple desorption steps (d-f) were then repeated where 90% of the supernatant was replaced with buffer solution, shaken for 7 days, then the aqueous concentration was determined..... 31

Figure 3.3: Schematic of the experimental approach used to study the desorption of PFOS, PFOA, and PFBS from CAC. After the top adsorption isotherm bottles reached equilibrium (ads bottle), aqueous phase concentrations were measured. Well-mixed aliquots (1, 2, 5, 10, 25 mL) were subsampled from these adsorption bottles and were then diluted to total volumes of 125 mL (bottles 1-5), shaken for 168 h, then the aqueous concentration was determined..... 34

Figure 3.4: Schematic of revised CAC desorption (whole bottle dilution) methodology. After the 50-mL adsorption bottles that replicate the top adsorption isotherm point reached equilibrium, entire bottle contents were poured into larger HDPE bottles (1-4), and filled to total volumes of 125, 250, 500, 1000 mL. 35

Figure 4.1: The concentration-time profiles for adsorption of PFOS, PFOA, and PFBS in 50-mL reaction solutions containing retained WPC PAC. Reaction solutions contained 0.1 g/L (PFOS), 0.16 g/L (PFOA) or 0.2 g/L (PFBS) of PAC, and either $[PFOS]_0$ = 4500 µg/L , $[PFOA]_0$ = 2500 µg/L, or $[PFBS]_0$ = 600 µg/L. Solid phase concentrations (C_s) were fit to the pseudo first-order kinetic function (the solid lines in the right panel). The model parameters were then used to generate predicted aqueous phase concentrations (solid lines in the left panel). Error bars represent one standard deviation..... 39

Figure 4.2: The concentration-time profiles for desorption of PFOS, PFOA, and PFBS in 50-mL reaction solutions containing retained WPC PAC. Reaction solutions contained 0.1 g/L (PFOS), 0.16 g/L (PFOA) or 0.2 g/L (PFBS) of PAC, and either $[PFOS]_0$ = 4500 µg/L , $[PFOA]_0$ = 2500 µg/L, or $[PFBS]_0$ = 600 µg/L, and were allowed 168 h to equilibrate. At a time of 0 h, 90% of the PAC-free solution was replaced with adsorbate-free buffer to initiate desorption. Solid phase concentrations (C_s) were fit to the first-order kinetic function (the solid lines in the right panel). The model parameters were then used to generate predicted aqueous phase concentrations (solid lines in the left panel). Error bars represent one standard deviation..... 41

Figure 4.3: Adsorption isotherms for PFOS, PFOA, and PFBS on retained WPC PAC. The experimental data (circles) are fit to the Freundlich Isotherm model (solid lines). Error bars on each point represent one standard deviation from the mean of three replicates. 43

Figure 4.4: Adsorption and desorption of PFOS on retained WPC PAC. The experimental data (circles) are fit to the Freundlich Isotherm model (solid line), with the 95% prediction band of adsorption overlayed (dotted lines). Adsorption reaction solutions contained a range of 0.08–1 g/L of retained WPC PAC, and $[PFOS]_0$ = 4500 µg/L. Following adsorption, 90% of the PAC-free supernatant from D0 was removed, and the remaining solution was diluted with adsorbate-free buffer to 1000 mL. Desorption points D1 through D5 (triangles) represent the sequential desorption steps completed. Error bars on each point represent one standard deviation from the mean of three replicates. 45

Figure 4.5: Adsorption and desorption of PFOA on retained WPC PAC. The experimental data (circles) are fit to the Freundlich Isotherm model (solid line), with the 95% prediction band of adsorption overlayed (dotted lines). Adsorption reaction solutions contained a range of 0.12–0.6 g/L of retained WPC PAC, and $[PFOA]_0$ = 2500 µg/L. Following adsorption, 90% of the PAC-free supernatant from D0 was removed, and the remaining solution was diluted with adsorbate-free buffer to 1000 mL. Desorption points D1 through D9 (triangles) represent the sequential desorption steps completed. Error bars on each point represent one standard deviation from the mean of three replicates. 46

Figure 4.6: Adsorption and desorption of PFBS on retained WPC PAC. The experimental data (circles) are fit to the Freundlich Isotherm model (solid line), with the 95% prediction band of adsorption overlayed (dotted lines). Adsorption reaction solutions contained a range of 0.12–1.2 g/L of retained WPC PAC, and $[PFBS]_0$ = 600 µg/L. Following adsorption, 90% of the PAC-free supernatant from D0 was removed, and the remaining solution was diluted

with adsorbate-free buffer to 500 mL. Desorption points D1 through D4 (triangles) represent the sequential desorption steps completed. Error bars on each point represent one standard deviation from the mean of three replicates. 47

Figure 4.7: The concentration-time profiles for adsorption of PFOS, PFOA, and PFBS in 125-mL reaction solutions containing polymer-free CAC. Reaction solutions contained 0.0712 g/L (PFOS) or 0.133 g/L (PFOA and PFBS) of CAC, and either $[PFOS]_0$ = 4500 µg/L, $[PFOA]_0$ = 2500 µg/L, or $[PFBS]_0$ = 500 µg/L. Solid phase concentrations (C_s) were fit to the pseudo first-order kinetic function (the solid lines in the right panel). The model parameters were then used to generate predicted aqueous phase concentrations (solid lines in the left panel). Error bars represent one standard deviation. 48

Figure 4.8: The concentration-time profiles for desorption of PFOS, PFOA, and PFBS in 125-mL reaction solutions containing polymer-free CAC. Original reaction solutions contained 0.0539 g/L (PFOS), or 0.0887 g/L (PFOA and PFBS) of CAC, and either $[PFOS]_0$ = 4500 µg/L , $[PFOA]_0$ = 2500 µg/L, or $[PFBS]_0$ = 500 µg/L, and were allowed 168 h to equilibrate. At a time of 0 h, 2 mL aliquots of well-mixed solution were diluted to 125 mL with adsorbate-free buffer to initiate desorption. Solid phase concentrations (C_s) were fit to the first-order kinetic function (the solid lines in the right panel). The model parameters were then used to generate predicted aqueous phase concentrations (solid lines in the left panel). Error bars represent one standard deviation..... 50

Figure 4.9: Adsorption isotherms for PFOS, PFOA, and PFBS on polymer-free CAC. The experimental data (circles) are fit to the Freundlich Isotherm model (solid lines). Error bars on each point represent one standard deviation from the mean of three replicates. 52

Figure 4.10: Adsorption and desorption of PFOS on polymer-free CAC. The adsorption data (circles) are fit to the Freundlich Isotherm model (solid line), with the 95% prediction band of adsorption overlayed (dotted lines). Adsorption reaction solutions contained a range of 0.054–0.36 g/L of polymer-free CAC, and $[PFOS]_0$ = 4500 µg/L. Following adsorption, varying sub-samples (1, 2, 5, 10, 25 mL) of D0 were diluted with adsorbate-free buffer to 125 mL to initiate desorption, creating desorption points D1 through D5 (triangles). Error bars on each point represent one standard deviation from the mean of three replicates. 53

Figure 4.11: Adsorption and desorption of PFOA on polymer-free CAC. The adsorption data (circles) are fit to the Freundlich Isotherm model (solid line), with the 95% prediction band of adsorption overlayed (dotted lines). Adsorption reaction solutions contained a range of 0.089–0.36 g/L of polymer-free CAC, and $[PFOA]_0$ = 2500 µg/L. Following adsorption, varying sub-samples (1, 2, 5, 10, 25 mL) of D0 were diluted with adsorbate-free buffer to 125 mL to initiate desorption, creating desorption points D1 through D5 (triangles). Error bars on each point represent one standard deviation from the mean of three replicates. 54

Figure 4.12: Adsorption and desorption of PFBS on polymer-free CAC. The adsorption data (circles) are fit to the Freundlich Isotherm model (solid line), with the 95% prediction band of adsorption overlayed (dotted lines). Adsorption reaction solutions contained a range of

0.089–0.89 g/L of polymer-free CAC, and $[PFBS]_0$ = 500 µg/L. Following adsorption, varying sub-samples (1, 2, 5, 10, 25 mL) of D0 were diluted with adsorbate-free buffer to 125 mL to initiate desorption, creating desorption points D1 through D5 (triangles). Error bars on each point represent one standard deviation from the mean of three replicates. 55

Figure 4.13: Adsorption and desorption of PFOS on polymer-free CAC. The adsorption data (circles) are fit to the Freundlich Isotherm model (solid line), with the 95% prediction band of adsorption overlayed (dotted lines). Adsorption reaction solutions contained a range of 0.067–0.44 g/L of polymer-free CAC, and $[PFOS]_0$ = 4500 µg/L. Following adsorption, whole bottles (50 mL) replicating D0 were diluted with adsorbate-free buffer to 125, 250, 500 and 1000 mL to initiate desorption, and represent desorption points D1 to D4 (triangles), respectively. Error bars on each point represent one standard deviation from the mean of three replicates. 56

Figure B.1: Comparisons of the adsorption data for PFOS, PFOA or PFBS on polymer-free CAC with contact times of 168 h (black circles) and 672 h (coloured circles). After the data was fit to the Freundlich isotherm model (not shown), the 95% confidence band of adsorption was overlayed (dashed lines). Error bars on each point represent one standard deviation from the mean of three replicates. Overlap of the 95% confidence bands indicates that the isotherms are not statistically different, at the 95% level of confidence..... 79

Figure B.2: Comparison of PAC (solid lines) to CAC (dashed lines) for the adsorption of PFOS —, PFOA —, PFBS —. 80

List of Tables

Table 2.1: Summary of Reported Freundlich Adsorption Parameters for PFOS, PFOA and PFBS on Carbon-Based Adsorbents 16

Table 4.1: Summary of PFAS Adsorption Kinetic Parameters for Retained WPC PAC 40

Table 4.2: Summary of PFAS Desorption Kinetic Parameters for Retained WPC PAC 42

Table 4.3: Summary of Freundlich Adsorption Parameters for Retained WPC PAC 44

Table 4.4: Summary of PFAS Adsorption Kinetic Parameters for Polymer-free CAC 49

Table 4.5: Summary of PFAS Desorption Kinetic Parameters for polymer-free CAC 51

Table 4.6: Summary of Freundlich Adsorption Parameters for Polymer-Free CAC 52

Table A.1: LC-MS/MS Setup 76

List of Abbreviations

AC	Activated Carbon
AFFF	Aqueous film-forming foams
AOPs	Advanced oxidation processes
BP	Bottle-point
CAC	Colloidal activated carbon
EO	Electrochemical oxidation
FFTA	Firefighting training area
GAC	Granular activated carbon
HALT	Hydrothermal alkaline treatment
HDPE	High-density polyethylene
IX	Ion Exchange
LC-MS/MS	Liquid chromatography-tandem mass spectrometry
MCLs	Maximum contaminant levels
MDL	Method detection limit
NF	Nanofiltration
PAC	Powdered activated carbon
PFAAs	Perfluoroalkyl acids
PFAS	Per-and polyfluoroalkyl substances
PFBA	Perfluorobutanoic acid
PFBS	Perfluorobutane sulfonic acid
PFCAs	Perfluoroalkyl carboxylates
PFSAs	Perfluoroalkyl sulfonates
PFDA	Perfluorodecanoic acid
PFHpA	Perfluoroheptanoic acid
PFHPS	Perfluoroheptane sulfonic acid
PFHxA	Perfluorohexanoic acid
PFHxS	Perfluorohexane sulfonic acid
PFNA	Perfluorononanoic acid
PFOA	Perfluorooctanoic acid
PFOAB	Perfluorooctane amido betaine
PFOAAmS	Perfluorooctaneamido ammonium iodide
PFOS	Perfluorooctane sulfonic acid
PFPeA	Perfluoropentanoic acid
PP	Polypropylene
PRBs	Permeable reactive barriers
RO	Reverse osmosis
SCWO	Supercritical water oxidation
SOM	Soil organic matter
TOC	Total organic carbon
US	United States
6:2 FTS	6:2 fluorotelomer sulfonic acid
8:2 FTS	8:2 fluorotelomer sulfonic acid

Chapter 1
Introduction

1.1 Background

Groundwater is a key component of the water cycle and serves as the main source of drinking water for nearly half of the global population (The Nature Conservancy, 2023). As global surface water reserves become increasingly scarce, groundwater will become an even more crucial drinking water resource. This valuable resource is being threatened by contaminants, which are often released into the environment from leaking chemical storage tanks, improper waste disposal, motor vehicle or railway accidents, and as byproducts from industrial processes (Government of Canada, 2017). In fact, groundwater contamination is an issue that is directly targeted by the United Nations Sustainable Development Goals 6.3 and 6.6, which are to reduce pollution caused by hazardous chemicals and restore water-related ecosystems (United Nations, 2023).

Per- and polyfluoroalkyl substances (PFAS) are synthetic chemicals considered emerging groundwater contaminants (USEPA, 2022). PFAS are thermally and chemically stable, hence are used in everyday products such as waterproof clothing, non-stick cookware and fast-food container linings, and in industrial applications such as lubricants, additives in plastic and rubber manufacturing, and various paints and coatings (Gluge et al., 2020). Most notably, PFAS are an important component of aqueous film-forming foams (AFFF) used in fire-fighting training at airports, military bases, and industrial sites. Unfortunately, the repeated use of AFFF has resulted in the contamination of groundwater resources by PFAS. For example, a recent study estimated that groundwater and soil at 3,493 military sites and 519 airports in the United States (US) are contaminated with PFAS (Salvatore et al., 2022). At one military base, the source zone of a former fire fighting training area (FFTA) had total groundwater PFAS concentrations as high as 51 mg/L (Adamson et al., 2022). McMahon et al. (2022) investigated PFAS concentrations at 254 randomly selected public supply well and domestic well locations across the eastern US. Analytical results from this sampling investigation showed that the concentration of perfluorooctanoic acid (PFOA) and

perfluorooctane sulfonic acid (PFOS) exceeded the recently established maximum contaminant levels (MCLs) of 4 ng/L in 23% and 27% of the collected samples, respectively. Partial dependence plots generated in this study show the probability of PFAS detection increases with closer proximity to an FFTA (McMahon et al., 2022), a trend also observed by Smalling et al. (Smalling et al., 2023). The presence of PFAS in groundwater supplies may contribute to human PFAS exposure, which has been linked to immunological, developmental, endocrine, and cardiovascular disorders, and cancer (ITRC, 2023). To limit human exposure to PFAS-impacted groundwater, there is a need to develop feasible remediation techniques.

The heat-resistant properties which made PFAS the desired group of compounds in AFFF formulations also mean that degradation techniques for the treatment of PFAS-contaminated groundwater are either inefficient or costly. Specifically, the fluorinated tail of PFAS molecules is resistant to degradation by biological processes, and chemical techniques that aim to destroy PFAS incur large lifetime energy costs. The use of activated carbon (AC) as an adsorbent has been a common method to remove PFAS from water. For ex situ applications, granular activated carbon (GAC) (nominal diameter of 0.2 to 5 mm) is widely used as an adsorbent in both drinking water treatment and pump-and-treat groundwater remediation systems (ITRC, 2023; Espana et al., 2015). To avoid the long-term operation and maintenance costs associated with pump-and-treat treatment systems, there has been an interest in immobilizing PFAS in situ to protect downgradient receptors (Fan et al., 2017). In situ immobilization of PFAS could be achieved with permeable reactive barriers (PRBs), which contain adsorbent material that sequester contaminants within the barrier by adsorption (USEPA, 2002). PRBs can be installed by trench excavation where aquifer materials are replaced by an adsorptive media, or by injecting adsorbent slurries into the subsurface (NGWA, 2017). Adsorbent injection is less expensive since it does not involve open trenching and dewatering, and is more feasible for intercepting deeper plumes.

The injection of a slurry of powdered activated carbon (PAC) (15 – 25 μm) or colloidal activated carbon (CAC) (1 – 2 μm) has been suggested as a promising technique for immobilization of PFAS plumes (Fan et al., 2017). An array of strategically located injection

points are normally used to create a barrier perpendicular to a plume of PFAS (Figure 1.1) (McGregor, 2018; Fan et al., 2017; Georgi et al., 2015). While these AC barriers are not able to destroy PFAS, they could mitigate the downgradient transport of these compounds (Fan et al., 2017). For example, McGregor demonstrated in situ immobilization of PFOS and PFOA using injected AC slurry at a former FFTA in central Canada (McGregor, 2018). In this study, concentrations of PFOS and PFOA (3260 and 1450 ng/L respectively) decreased to below the detection limit (< 20 ng/L) 18 months following CAC injection.

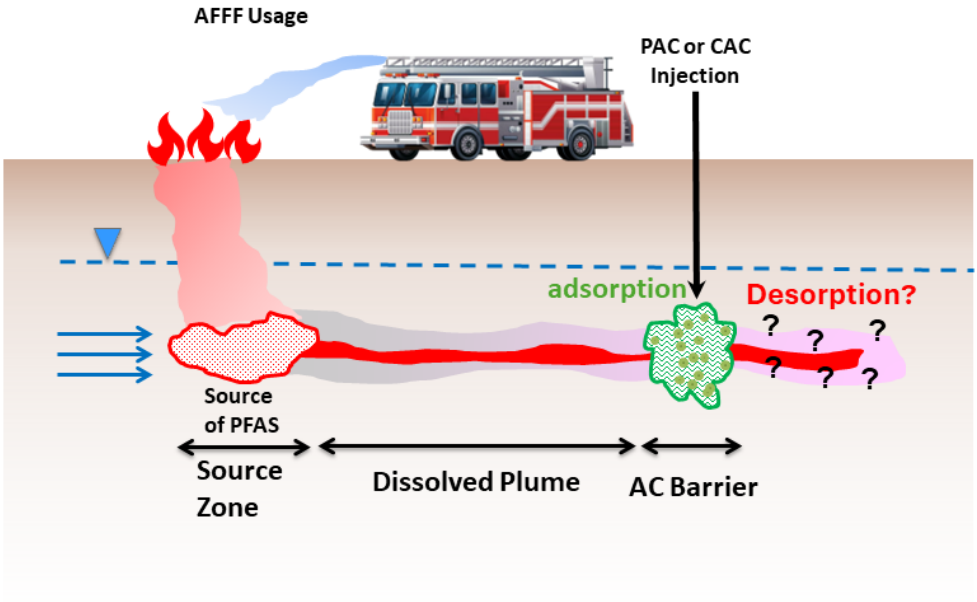


Figure 1.1: Schematic of PFAS immobilization using injectable AC at an AFFF-impacted site.

At a specific location within the barrier following AC injection, the PFAS concentration gradient between the groundwater (C_w, initially high) and the AC (C_s, initially low) drives adsorption. Over time, C_w decreases until it reaches an aqueous phase concentration of C_e that is in equilibrium with the concentration of PFAS on the AC. To predict the affinity of PFAS to these injected AC amendments, *ad*sorption isotherms are often experimentally generated to develop a relationship between C_s and C_e (Cecen and Aktas, 2011). These *ad*sorption isotherms can be used to help estimate the AC dosage required to sequester the mass load of PFAS entering the AC barrier for a given design life. These equilibrium data are

applicable for steady groundwater concentrations; however, these concentrations can fluctuate. If the groundwater PFAS concentration decreases ($C_w < C_e$), the state of equilibrium will be perturbed. This will lead to a reversal of the concentration gradient, resulting in the release of PFAS from the AC back into the groundwater (Figure 1.1). *De*sorption isotherms can be generated experimentally to understand the potential for release of PFAS from the AC when it is subjected to a decrease in aqueous concentration. These adsorption and desorption isotherms can then be compared, where asymmetry between adsorption and desorption data (i.e., $C_{s,\,des} > C_{s,\,ads}$ for a given C_e value) indicates the presence of hysteresis in the system (Xiao et al., 2019). Observed hysteresis may then be classified as reversible sorption (sometimes caused by experimental artifacts) or irreversible sorption (caused by a permanently sorbed mass of PFAS). In the case of reversible sorption, the data may appear hysteretic, but ultimately intersects the origin ($C_e = 0$, $C_s = 0$), suggesting that the adsorbent will eventually release all sorbed PFAS mass over time. If no hysteresis is present (i.e., adsorption and desorption data overlap and pass through the origin), sorption is also considered reversible. Conversely, irreversible sorption occurs when data are hysteretic and desorption data intersects the *y*-axis ($C_e = 0$) at $C_s > 0$. For irreversible sorption, adsorbates may form chemical bonds with functional groups on the surface of adsorbents (Aktas and Cecen, 2006; De Jonge et al., 1996; Petruzelli and Helfferich, 1992) and permanently remove a fraction of PFAS (Yonge et al., 1985). Irreversible sorption could also be caused by structural changes to the adsorbent such as pore deformation, which isolates the adsorbate from the aqueous phase and prevents desorption (Braida et al., 2003; Weber et al., 2002; Kan et al., 1997). Currently, there is a significant knowledge gap surrounding the desorption behavior of PFAS from AC amendments used for in situ applications, including PAC and CAC. A combined understanding of the adsorption and desorption characteristics of PFAS on PAC and CAC will assist with the understanding of the fate and transport of PFAS within and downgradient of an AC barrier.

1.2 Research Scope

The goal of this research is to investigate the desorption behaviour of PFAS from commercially available PAC and CAC products. Desorption data were compared to the 95%

prediction band of the adsorption isotherm to determine if adsorption and desorption behaviours are different. Adsorption and desorption kinetic studies were completed to ensure that the isotherms were generated in a state of equilibrium.

PFAS investigated were limited to PFOS, PFOA and perfluorobutane sulfonic acid (PFBS) since they are commonly found at AFFF sites. Experiments conducted with these different compounds also allowed the investigation of the effect of chain length and functional group type on adsorption and desorption behaviour. Adsorption and desorption experiments were completed using reaction solutions containing a single PFAS and sodium bicarbonate ($NaHCO_3$), which served as a pH buffer. As such, the competitive effects between compounds and the impact of solution chemistry were not considered in this work.

1.3 Thesis Overview

Chapter 2 reviews the existing literature, focusing on PFAS treatment technologies, the use of AC as an adsorbent, adsorption and desorption hysteresis, and existing published data on PFAS desorption. Chapter 3 details the materials and methods used in this research, including the adaptation of existing methods for use with fine-grained adsorbent materials (i.e., CAC). Chapter 4 reports the results of adsorption and desorption kinetic and isotherm experiments and includes a discussion that compares results to existing literature. Chapter 5 summarizes the main findings from this research, highlights limitations in the experimental data and provides recommendations for future work.

Chapter 2
Literature Review

2.1 Per- and polyfluoroalkyl Substances

Per- and polyfluoroalkyl substances (PFAS) are a group of synthetic fluorinated compounds, often referred to as “forever chemicals” for their persistence in the environment (Government of Canada, 2023). According to CompTox, a chemical database by the US EPA, there are nearly 15,000 different PFAS (US EPA, 2024). PFAS consist of a hydrophilic head group and a hydrophobic tail, and are classified based on the length and degree of fluorination of the tail and the type of the head group. Specifically, PFAS are called *per*fluorinated if the tail is fully fluorinated, and *poly*fluorinated if the tail contains hydrogenated carbons alongside fluorinated carbons (ITRC, 2023). Within the perfluorinated group, the compounds with a carboxylate or a sulfonate head group are called perfluoroalkyl carboxylic acids (PFCAs) and perfluoroalkyl sulfonic acids (PFSAs), respectively. PFCAs with carbon chain lengths of C8 and higher, and PFSAs with chain lengths of C6 and higher are considered long chained (OECD, 2024). Conversely, PFCAs and PFSAs are considered short chained if there are less than C8 and C6 in the chain, respectively. PFOS and PFBS are examples of long and short chained PFSAs, while PFOA and perfluorohexanoic acid (PFHxA) are examples of long and short chained PFCAs. The chemical structures of PFOS, PFOA and 6:2 fluorotelomer sulfonic acid (6:2 FTS, which is a polyfluorinated compound), which are PFAS commonly found at AFFF sites, are displayed in Figure 2.1.

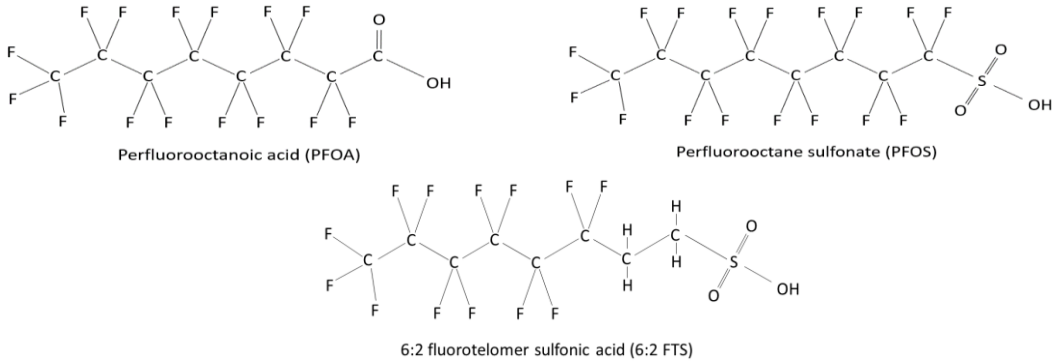


Figure 2.1: Chemical structures of PFOA, PFOS and 6:2 FTS

PFAS are oleophobic (i.e., they repel both oil and water) and are highly resistant to thermal and chemical degradation due to the strong C-F bonds (O'Hagan, 2008; Kissa, 2001; Moody and Field, 2000). Owing to these properties, PFAS have found use in numerous products, including in non-stick cookware, rain-repellent clothing, lubricants, pipe liners, and AFFF (Gluge et al., 2020**)**. The discharge of PFAS-containing wastes and effluents from manufacturing processes, and most notably, from the release of AFFF at FFTAs have resulted in widespread PFAS environmental contamination (Li and Liu, 2022). Carey et al. compiled concentrations from 96 AFFF-impacted sites and reported a median maximum groundwater concentration of 37 µg/L and 7 µg/L for PFOS and PFOA, respectively (Carey et al., 2022). It is important to note that these concentrations varied greatly between sites, and maximum concentrations of 2,500 µg/L and 2,000 µg/L for PFOS and PFOA were noted (Carey et al., 2022).

Since PFAS are resistant to degradation by chemical or biological means, PFAS persist in the environment and can migrate significant distances from the release point. As such, sites where PFAS have been released have the potential to contaminate downgradient drinking water supplies. Consumption from these contaminated drinking water sources is recognized as one of the main routes of PFAS exposure to humans (NGWA, 2017), with lifetime exposures linked to the development of cancer, and are expected to impact the immunological, developmental, endocrine, and cardiovascular systems (ITRC, 2023). To limit these effects, the US EPA established a National Primary Drinking Water Regulation for PFOA, PFOS, perfluorononanoic acid (PFNA), perfluorohexane sulfonic acid (PFHxS), PFBS, and GenX on April 10th, 2024. Under this regulation, maximum contaminant levels (MCLs) for drinking water are set at 4 ng/L for PFOS and PFOA, and 10 ng/L for PFHxS, PFNA, and GenX.

PFAS contamination in drinking water supplies has been commonly found near locations with a known history of PFAS release, such as FFTAs, airports, and waste management areas (Smalling et al., 2023). In a study of 254 public supply and domestic well locations across the Eastern US, McMahon et al. demonstrated that the newly established PFOS and PFOA MCLs were exceeded in 27% and 23% of the collected samples, respectively,

with the probability of detection of PFAS increasing with closer proximity to a FFTA (McMahon et al., 2022). As such, to prevent the spread of PFAS into drinking water supplies, there is a significant need for remedial options to treat PFAS-contaminated waters.

2.2 PFAS Treatment Technologies

2.2.1 Degradation Technologies

The unique physico-chemical properties that make PFAS molecules extremely durable also make PFAS highly resistant to many of the existing degradation technologies. Studies have shown that perfluorinated compounds are resistant to biodegradation (Wackett et al., 2021; Liu and Meija Avendano, 2013; Liou et al., 2010; Key et al., 1998), while polyfluorinated compounds can only be biotransformed into perfluorinated compounds that are resistant to further degradation (ITRC, 2023; Butt et al., 2014). Studies also have shown that advanced oxidation processes (AOPs) such as Fenton's reagent, activated persulfate, and ultraviolet light combined with hydrogen peroxide are generally not effective at destroying PFAS (NGWA, 2017). This is because the hydroxyl radical produced in AOPs, which is one of the most powerful oxidants, is not reactive with perfluorinated compounds (Houtz and Sedlak, 2012; Moriwaki et al., 2005; Schröder and Meesters, 2005). Moreover, hydroxyl radical converts polyfluorinated compounds into perfluorinated compounds, which are resistant to further transformation (Venkatesan et al., 2022; Bruton and Sedlak, 2017).

Unlike conventional AOPs, electrochemical oxidation (EO) has been shown to be capable of degrading not only polyfluorinated compounds but also perfluorinated compounds, including PFOS (Liang et al., 2018; Zhuo et al., 2012; Carter and Ferrell, 2008). In a study using rejectate generated from the treatment of groundwater by reverse osmosis, which contained 4 mg/L PFBS, 10 mg/L PFHxS and 19 mg/L PFOS, EO has been shown to decrease the total PFAS concentrations by 91% when a current density of 2.28 mA/cm^2 was applied for 18 h (Trautmann et al., 2015). During this process, however, concentrations of perfluorobutanoic acid (PFBA), perfluoropentanoic acid (PFPeA), perfluoroheptanoic acid (PFHpA) and PFHxA increased by a factor of 21, 6.7, 2.1 and 4.8 (Trautmann et al., 2015),

demonstrating the generation of shorter-chained PFCAs. It is also important to consider the possible production of toxic byproducts such as bromate and perchlorate in EO (Radjenovic and Sedlak, 2015; Trautmann et al., 2015). Additionally, it has been demonstrated that the rate of PFAS destruction in EO decreased over time due to competition for oxidants and anode surface by organic matter (Zhuo et al., 2012). In waste streams containing low concentrations of PFAS, a scenario that may be encountered in a pump-and-treat system downgradient of a source zone, the inhibitory effect of organic matter on the degradation of PFAS could be expected, which would result in unrealistically long reaction times needed to remove PFAS to below MCLs.

The degradation of PFAS by thermal-based technologies that take advantage of higher temperatures and/or pressures to speed up reaction times has also been explored. One technique for the destruction of PFAS is incineration. It has been demonstrated that incineration of PFAS-contaminated waste resulted in the destruction of PFAS with high efficiencies (Shields et al., 2023; Taylor et al., 2014; Yamada et al., 2005). However, there is a growing concern with products of incomplete combustion, which may form stable fluorinated carboxylic acids when released into the atmosphere (Shields et al., 2023). Currently, there are analytical challenges associated with measuring these fluorinated byproducts, resulting in a lack of a complete understanding of the formation of these byproducts during incineration of PFAS (US EPA, 2020). An alternative to incineration is supercritical water oxidation (SCWO). It has been demonstrated that SCWO was capable of removing PFAS to non-detect levels at temperatures over 600°C and a pressure of 24 MPa, with no decrease in removal efficiency in the presence of VOCs and diesel fuel as co-contaminants (Scheitlin et al., 2023). Field-scale SCWO removal systems, such as Battelle's PFAS Annihilator™, have been validated at the bench scale and are currently being implemented for PFAS removal in field sites (Scheitlin et al., 2023). A study by Krause et al. investigated SCWO systems designed by Batelle (Columbus, USA), Aquarden Technologies (Skaeving, Denmark) and 374Water (Durham, USA), testing each system's ability to destroy PFAS in an AFFF mixture (Krause et al., 2021). While all three systems provided over 99% PFAS removal, effluent PFOS and PFOA concentrations still

exceeded the USEPA MCL of 4 ng/L and, thus, would require further treatment. Another thermal technology, hydrothermal alkaline treatment (HALT), uses high temperatures and pressures with sodium hydroxide to mineralize PFAS under alkaline conditions. Unlike SCWO, HALT operates below the critical point of water. HALT has been demonstrated at the lab scale to destroy PFAS in AFFF formulations (Hao et al., 2021), in addition to destroying PFAS in soil and groundwater (Hao et al., 2023; Hao et al., 2022). However, owing to the large energy cost, HALT is thought to be best suited for treating low-volume, concentrated PFAS waste streams generated in other treatment processes such as foam fractionation (Hao et al., 2023).

All the thermal technologies mentioned above can only be implemented ex situ, requiring the continual pumping of groundwater. Currently, there is no proven in situ destruction technology for PFAS-contaminated groundwater.

2.2.2 Separation Technologies

Since PFAS are highly resistant to degradation and require significant energy input, technologies focusing on the physical removal of PFAS from contaminated water have been the most popular approach. Membrane technologies such as nanofiltration (NF) and reverse osmosis (RO) are ex situ processes that remove PFAS by size selection, or "sieving", holding back PFAS compounds larger than the pores of the membrane (NGWA, 2017). Tang et al. compared the performance of eight thin film composite polyamide RO and NF membranes at a constant PFOS influent concentration of 10 mg/L (Tang et al., 2007). In this study, the RO and NF membranes achieved a > 99% and 90-99% rejection efficiency, respectively. Similarly, Liu et al. compared a RO and NF membrane for a diluted AFFF mixture and reported overall removal efficiencies of > 99% and > 98%, respectively (Liu et al., 2021). While significant PFAS removal is possible with NF and RO, membrane fouling over time means higher pressures must be applied, leading to an energy-intensive operation (US EPA, 2018). In all NF and RO membranes, a secondary aqueous waste stream called retentate is created (Abbasian and Foudazi 2022; US EPA, 2018), meaning further cost is incurred to properly handle the concentrated PFAS stream.

Perhaps more common than membrane filtration is the ex-situ removal of PFAS from groundwater using adsorbents. GAC and ion exchange (IX) resins are commonly used adsorbents in drinking water treatment processes but are also effective for the removal of PFAS from groundwater using ex-situ pump-and-treat systems. Significant removal of PFAS mass has been demonstrated for both GAC and IX resins, making their use promising for treating contaminated groundwater (McCleaf et al., 2017; Woodard et al., 2017; Ochoa-Herrera et al., 2008). Within these studies, GAC and IX demonstrate a higher affinity to the longer chained compounds, such as PFOS and PFOA, compared to shorter chained compounds, such as PFBS (US EPA, 2018; Xiao et al., 2017; Ochoa-Herrera et al., 2008). Within the GAC or IX media exist a limited number of adsorption sites for PFAS removal. Once these adsorption sites are saturated, breakthrough will occur, at which point the adsorbent must be replaced. Due to the lower affinity of short chained compounds to adsorbents, they will break through first. Therefore, depending on the type of PFAS present and their concentration in the influent stream, adsorbent replacement might be more frequent to ensure all PFAS are removed to below regulatory levels (ITRC, 2023).

Passive in situ technologies aim to lower the lifetime costs of ex-situ methods by creating a long-term solution that does not require continuous energy input. Injected activated carbon has been suggested as a promising remedial option since it can achieve the same sequestration and removal of PFAS from the aqueous phase at significantly lower lifetime costs. Advantages of in situ injectable PAC and CAC slurries are that once injected, little to no intervention is required, as they are passive technologies that rely on natural groundwater flow to transfer PFAS-laden groundwater into the adsorptive AC barrier (Fan et al., 2017). Currently, there exist several studies that demonstrate the relatively short-term success of implementing in-situ activated carbon immobilization (McGregor, 2023; Niarchos et al., 2023; McGregor, 2020; McGregor, 2018). Specifically, McGregor demonstrated the in-situ reduction of source zone PFOS and PFOA concentrations (3260 and 1450 ng/L) to below the detection limit (< 20 ng/L) within 18 months after CAC injection (McGregor, 2018).

The dosing of activated carbon amendments in these field studies is based on laboratory experiments that investigate the adsorption characteristics of various PFAS on AC. Specifically, these experiments predict the state of equilibrium that is established between the aqueous phase groundwater (C_e) and solid phase concentration (C_s) within the barrier, where most of the PFAS mass is associated with the solid phase. With AC barriers, the groundwater concentration entering the barrier, C_w, may lower over time ($C_w < C_e$), perturbing the state of equilibrium within the AC barrier. When this occurs, PFAS may desorb from the AC, and re-enter the groundwater downgradient. This complex AC barrier behaviour requires an in-depth understanding of the adsorption and desorption characteristics of PFAS and AC.

2.3 Activated Carbon

The use of charcoal as an adsorbent was first cited in Egyptian papyri from 1550 BC for treating odorous vapours from the intestinal tract and wounds (Cecen and Aktas, 2011). By 450 BC, charcoal filters were used by the Hindus for water treatment (Cecen and Aktas, 2011). Though activated charcoal had been used throughout history, it was not until the 19th century when the production was streamlined through research of source materials, activation methods and particle size. PAC was first used commercially in the early 20th century for food production and solution decolorization, and commercially produced GAC products were first used in gas masks in World War 1 (Cecen and Aktas, 2011).

Commonly used materials for AC production include coconut shells, bituminous coal and lignite (Li et al., 2002). These source materials are pretreated to remove impurities and subsequently activated thermally (using steam) or chemically using potassium hydroxide, phosphoric acid, or zinc chloride (Cecen and Aktas, 2011; Suzuki, 1990). The large surface area generated in this process makes AC a desirable adsorbent material for use in drinking and wastewater treatment. AC products differ greatly by grain size and are commonly classified as either granular, powdered, or colloidal AC, with average grain sizes of 0.2 – 5 mm, 15 – 25 µm, and 1 - 2 µm, respectively (Cecen and Aktas, 2011). The particle size of the AC chosen depends on whether it is being used for in-situ or ex-situ applications. Larger-grained AC such as GAC are widely used in drinking water and wastewater treatment, since they can be held in

place in a flow-through reactor or column. GAC is also used in situ for PRB applications that require trenching and backfilling with an adsorptive media. Finer-grained carbons such as PAC and CAC have become increasingly popular for in situ applications, as they are able to establish a more homogeneous distribution in the subsurface when injected (Fan et al., 2017).

2.3.1 Mechanisms of Adsorption to Activated Carbon

Adsorption is the attachment of an adsorbate (i.e., the molecule being adsorbed) to a surface. For AC, the activation process creates a heterogeneous distribution of micropores (< 2 nm), mesopores (2-50 nm), and macropores (> 50 nm) on the carbon surface (Figure 2.2) that act as the main adsorption sites (Cecen and Aktas, 2011; Gadkaree et al., 1996; Suzuki, 1990).

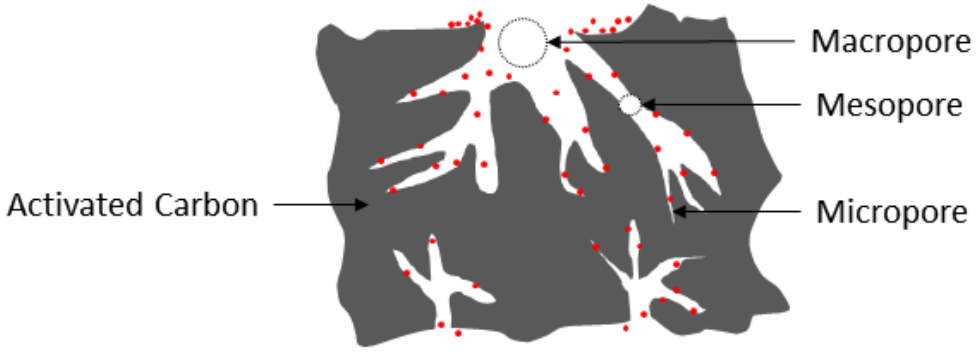


Figure 2.2: Schematic of activated carbon pore structure demonstrating the accumulation of PFAS ● on the surface of the carbon, and the adsorption of PFAS ● within the pore structure

The large pore volume within AC is crucial for the effective removal of contaminants, as they create a high specific surface area on the carbon (Cecen and Aktas, 2011). Of the three mentioned pore sizes, macropores are so large that the adsorptive properties mimic that of a flat carbon surface and are insignificant to the overall adsorption capacity (Cecen and Aktas, 2011). Conversely, mesopores and micropores make up most adsorption sites and are thus crucial for PFAS removal. In general, the strength of adsorption increases with decreasing pore sizes due to the closer proximity of the adsorbate to the pore wall, until the point of size exclusion, where the adsorbate is too large to enter (Li et al., 2002; Newcombe et al., 1996). This means that longer-chained PFOS and PFOA with effective diameters of 0.9 and 0.99 nm,

respectively (Tsai et al., 2010), may be too large to enter some micropores, whereas shorter-chained compounds like PFBS (effective width ~0.79 nm) are more likely to adsorb to micropores (Park et al., 2020). In the selection of an adsorbent for PFAS removal, the pore sizes should be large enough to prevent size exclusion of larger molecular weight compounds but small enough to provide sufficient attachment of PFAS to the pore walls (Krebsbach et al., 2023).

Within the pore structure of AC, sorption may be dominated by physical or chemical mechanisms, depending on the molecular structure of the adsorbent and adsorbate, and environmental conditions. Physical adsorption refers to the attachment of molecules by intermolecular forces (van der Waals forces) whereas chemical adsorption is the attachment by covalent bonds to the adsorbent (Hu and Xu, 2020; Cecen and Aktas, 2011). Physical adsorption has a weaker overall attraction compared to chemical adsorption (Hu and Xu, 2020). In the context of carbon-based adsorbents such as PAC and CAC, sorption is observed to be dominated by physical adsorption, specifically hydrophobic interactions (Hakimabadi et al., 2023; Carter and Farrell, 2010). In the selection of an AC product for the removal of PFAS, preliminary experiments are conducted to determine the extent to which an AC product can sequester an adsorbate from an aqueous phase.

2.3.2 Adsorption Isotherm

The affinity of an adsorbate to an adsorbent is usually reflected in the adsorption isotherm, which describes the relationship between the mass of an adsorbate sorbed to the adsorbent and the mass of the adsorbate remaining in the bulk solution (Cecen and Aktas, 2011). To generate an adsorption isotherm, batch experiments are often conducted using one variation of the bottle-point (BP) method, where all bottles have the same starting concentration of adsorbate, and the adsorbent dose is adjusted so the equilibrium aqueous phase concentrations span a desired range. After adsorption equilibrium is established (meaning that there is no significant change in the mass of sorbed adsorbate with continued reaction time), the adsorbent is separated by settling, filtration, or centrifugation, and an aliquot

of the aqueous phase is analyzed for C_e. The solid phase concentration C_s can then be calculated using mass balance:

$$C_s = \frac{(C_{w,0} - C_e)V_{bottle}}{M_{ads}} \quad (2.1)$$

where $C_{w,0}$ is the initial aqueous concentration of PFAS (mg/L), C_e is the measured, aqueous phase concentration after equilibrium has been reached (mg/L), V_{bottle} is the solution volume (L), and M_{ads} is the mass of adsorbent in the system (g). For the range of adsorbent doses used, a set of points [C_e, C_s] are generated that represent the relationship between C_s and C_e. These data can be fit to isotherm models to generate parameters that indicate adsorption characteristics.

Two commonly used models in activated carbon studies to fit the isotherm data are the Freundlich and Langmuir models. The Freundlich model assumes that the adsorbent surface is heterogeneous, with surface sites having different sorption energies (Cecen and Aktas, 2011). According to the Freundlich model, the relationship between C_s and C_e is as follows:

$$C_s = K_f {C_e}^{n_f} \quad (2.2)$$

where C_s is the concentration of adsorbate on the adsorbent (mg/g), C_e is the concentration of adsorbate in the bulk solution (mg/L), K_f is the Freundlich sorption coefficient $[(\mathrm{mg/g})(\mathrm{mg/L})^{-n_f}]$ that represents adsorption capacity when C_e = 1 mg/L, and n_f is a fitting parameter [-] that represents the non-linearity of the isotherm. According to the Freundlich isotherm theory, n_f represents the heterogeneity of adsorptive sites, with a value of 1 indicating a homogeneous distribution of sorption energies (Newcombe et al., 1996). At high aqueous concentrations, the Freundlich isotherm still exhibits an increase in sorbed concentration and will not asymptotically reach a maximum value.

Contrary to the Freundlich model, the Langmuir model assumes monolayer adsorption, where each adsorption site has the same sorption energy and thus the model will asymptotically reach a maximum value of $C_{s,max}$ at high aqueous concentrations (Cecen and Aktas, 2011). The Langmuir model is represented by:

$$C_s = \frac{C_{s_{max}} K_L C_e}{1 + K_L C_e} \quad (2.3)$$

where $C_{s,max}$ is the maximum adsorption capacity of the adsorbent (mg/g), and K_L is the Langmuir sorption coefficient (L/g). While PFAS and AC adsorption data may fit the Langmuir isotherm model on occasion, it usually does not correspond to an improved fit over the Freundlich isotherm for the concentration ranges studied (Chen et al., 2016). When experimental concentrations are low enough such that the data does not asymptotically reach a maximum, the Freundlich isotherm is preferred and is the most common model used to describe the adsorption of PFAS and carbon-based adsorbents (Chen et al., 2024; Hakimabadi et al., 2023; Zhi & Liu, 2018; Chen et al., 2016). Depending on the adsorbent type, the Freundlich isotherm parameters may vary greatly, but in general, the Freundlich model fits the existing data very well, as indicated by the high r-squared values (Table 2.1).

Table 2.1: Summary of Reported Freundlich Adsorption Parameters for PFOS, PFOA and PFBS on Carbon-Based Adsorbents

PFAS	Reference	Adsorbent Material	K_f $[(mg/g)(mg/L)^{-n_f}]$	n_f [-]	r^2
PFOS	Hakimabadi et al., 2023	Polymer-free CAC	5348	0.92	0.94
	Chen et al., 2024	Activated Hydrochar	83	0.62	0.94
	Liu et al., 2020	DARCO PAC	629	0.3	0.99
	Siriwardena et al., 2019	Coconut-Based GAC	18.9	0.24	0.85
PFOA	Hakimabadi et al., 2023	Polymer-free CAC	79	0.56	0.99
	Qu et al., 2009	PAC (>100 mesh)	24	0.45	0.96
	Liu et al., 2020	DARCO PAC	135	0.54	0.99
	Siriwardena et al., 2019	Coconut-Based GAC	13.7	0.26	0.99
PFBS	Hakimabadi et al., 2023	Polymer-free CAC	12	0.5	0.98
	Chen et al., 2024	Activated Hydrochar	13	0.71	0.91

Prior to conducting experiments to generate an isotherm, kinetic experiments should be performed to determine the contact time required for equilibrium to be reached. Kinetic data are often generated by analyzing the remaining adsorbate concentration in the aqueous phase at designated time intervals. The concentration of PFAS on the adsorbent is then calculated by mass balance (Equation 2.1). These concentration-time profile data are often fit by a pseudo first-order kinetic function for adsorption (Agbovi and Wilson, 2021), as given by:

$$C_s(t) = C_s^{eq}(1 - e^{-k_{ads}t}) \tag{2.4}$$

where C_s^{eq} is the solid phase concentration at equilibrium (mg/g), k_{ads} is the adsorption rate coefficient (/h), and t is time (h). The magnitude of k_{ads} depends on the rate of external diffusion and intraparticle diffusion, either of which may be rate-limiting in the adsorption process (Cecen and Aktas, 2011).

2.4 Desorption and Hysteresis

Desorption is the opposite process of adsorption, where the adsorbate is removed from the adsorbent. For in-situ barrier applications, a state of adsorption equilibrium between C_e and C_s is applicable for constant C_w. However, over time, it is possible that C_w decreases due to either heterogeneities in the groundwater plume or exhaustion of the contaminant source. When the concentration entering the barrier drops (i.e., $C_w < C_e$), the state of equilibrium is perturbed, which leads to the desorption of contaminant mass (e.g., PFAS) from the AC back into the aqueous phase. This desorption potential can be determined by generating desorption isotherms using batch experiments that employ a decant-refill procedure. In this procedure, the adsorbent-free aqueous phase of the adsorption bottle is removed and replaced with an equal volume of adsorbate-free solution to initiate desorption from the solid phase adsorbent (Bowman and Sans, 1985). As in the procedures used to generate adsorption isotherms, desorption bottles must be at equilibrium before sampling, meaning that no further mass of adsorbate will desorb from the adsorbent into the aqueous phase with continued time. To investigate desorption kinetics, experiments can involve sampling desorption bottles at specified time points to measure the concentration of the adsorbate in the aqueous phase. Once

converted to solid phase concentrations using Equation 2.1, the concentration of the adsorbate on the adsorbent over time can be fit with the first-order kinetic function:

$$C_s(t) = C_s^0 e^{-k_{des}t} + C_s^{eq}(1 - e^{-k_{des}t}) \quad (2.5)$$

where C_s^0 is the solid phase concentration at the beginning of the desorption experiment (mg/g), C_s^{eq} is the solid phase concentration at equilibrium (mg/g), k_{des} is the desorption rate coefficient, and t is time (h). If C_s^0 and C_s^{eq} are known based on experimental data, the best fit of Equation 2.5 will generate a value for k_{des}. The plotting of these transient data and fitting of a common kinetic function helps to determine adequate contact time for the desorption equilibrium to be established. This contact time is then adopted for each desorption step. The steps of removing and replacing the aqueous phase to initiate desorption are repeated multiple times, generating a set of desorption data points that relate the concentration of the aqueous phase ($C_{e,des}$) to the solid phase concentration ($C_{s,\,des}$) at equilibrium [$C_{e,des}$, $C_{s,\,des}$]. These desorption data are then compared to the adsorption isotherm data to determine if sorption is hysteretic.

Hysteresis is often indicated by asymmetry between adsorption and desorption data (Xiao et al., 2019), where desorption data lie above adsorption data (i.e., $C_{s,\,des} > C_{s,\,ads}$ for a given C_e value). Further, sorption may either be reversible (i.e., if desorption data passes through the origin) or irreversible (if $C_s > 0$ when $C_e = 0$) (Figure 2.3), causing differences in the desorption path. Thus, when sorption is hysteretic, the desorption characteristics of the adsorbent are dependent on the adsorption-desorption history of the system. Note that reversible sorption is sometimes referred to as artificial hysteresis, as it may be caused by experimental artifacts such as sorption of the adsorbate to container walls, or insufficient contact time between the adsorbent and adsorbate (Sander et al., 2005). If sorption is reversible, continual flushing of the system with adsorbate-free water will eventually displace all the sorbed adsorbate from the adsorbent surface.

In contrast, irreversible sorption is considered true hysteresis (Sander et al., 2005). Irreversible sorption could be the case for systems where adsorbates form strong chemical bonds with functional groups on the surface of adsorbents (Aktas and Cecen, 2006; De Jonge

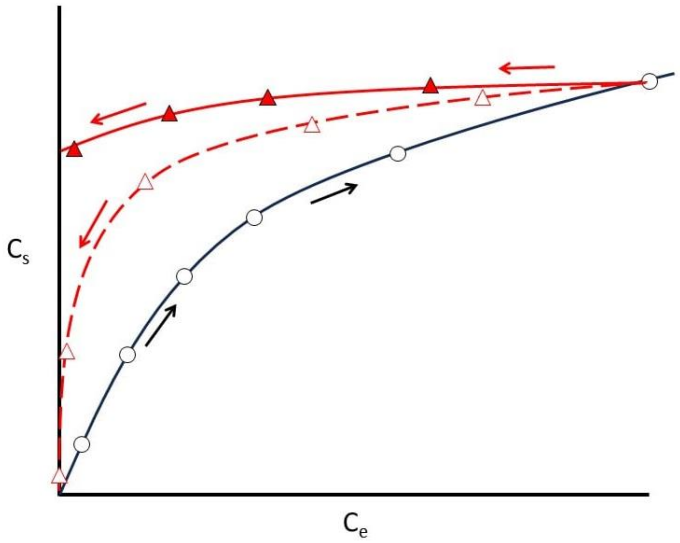


Figure 2.3: Examples of adsorption ─○─, reversible sorption ─Δ─, and irreversible sorption ─▲─ in sequential desorption experimental data

et al., 1996; Petruzzeli and Helfferich, 1992). Irreversible sorption could also be attributable to structural changes of the adsorbent over time, which would mean that the contaminant is desorbing from a material that is different from the original material (Adamson and Gast, 1997). One example of a structural change to the adsorbent is pore deformation, which inhibits desorption by permanently isolating the adsorbed species from the aqueous phase (Braida et al., 2003; Weber et al, 2002; Kan et al., 1997). Pore deformation could be caused by the swelling of adsorbent when exposed to high concentrations of adsorbate (Sander et al., 2005). The high adsorbate concentration in the aqueous phase was also suggested to be the reason for adsorption hysteresis on AC in several studies (Xiao et al., 2019; Aktas and Cecen, 2006; Huang and Weber, 1997). According to Chen et al., high aqueous concentrations at low adsorbent doses could cause saturation of the irreversible adsorptive pores (Chen et al., 2022). However, it was also suggested that the appearance of hysteresis could be due to experimental artifacts (Rao and Davidson, 1980).

One example of experimental artifacts that could result in observed hysteresis is a lack of adsorption and/or desorption equilibrium (Braida et al., 2003; Huang and Weber, 1998; Bowman and Sans, 1985; Rao and Davidson, 1980). In a study using CAC, Hakimabadi et al.

found shorter-chained PFBS and PFBA reached adsorption equilibrium within 24 h, while longer-chained PFOS and PFOA exhibited a slower adsorption phase between 24 and 168 h, with additional mass adsorbed over that time (Hakimabadi et al., 2023). While it was observed that over 99% of the initial PFAS mass was removed within the first 48 h (Hakimabadi et al., 2023), the aqueous phase concentrations measured were still declining, indicating a lack of complete equilibrium under the experimental conditions studied. If the adsorption data are gathered before adsorption equilibrium is reached, the measured aqueous phase concentrations will be higher than the actual equilibrium values, shifting the adsorption curve to the right (i.e., higher C_e). Similarly, if the solution in the desorption experiment is not at equilibrium with the adsorbent when sampled, the reported aqueous phase concentration will be lower than the equilibrium concentration, shifting the desorption curve to the left (i.e., lower C_e). The combined lack of equilibria in the adsorption and desorption experiments can lead to the asymmetry between adsorption and desorption C_e – C_s profiles, which will be perceived incorrectly that hysteresis exists.

Similar to a lack of equilibrium, experimental designs may also lead to the presence or absence of hysteretic behaviour. For desorption experiments with high-capacity adsorbents, the volume of solution that is replaced with adsorbate-free solution must be large enough, such that sufficient sorbed mass is removed to reach lower C_e values and determine whether sorption is reversible or irreversible (Fleer et al., 1993). This can be experimentally challenging since orbital shakers used to mix bottles have weight and size limitations. To avoid this experimental challenge, many researchers employed single-step desorption experiments where the aqueous phase of each adsorption isotherm bottle is decanted and replaced with a clean solution one time, yielding an equal number of "desorption" points. This approach creates a desorption isotherm that covers approximately the same concentration range as adsorption (Figure 2.4). As mentioned earlier, however, desorption processes are dependent on the past adsorption/desorption history of the system. Thus, not only should the desorption points in this method not be fit with an isotherm model, but also they should not be used to determine if sorption is hysteretic (Bowman, 1979; Bowman and Sans, 1977).

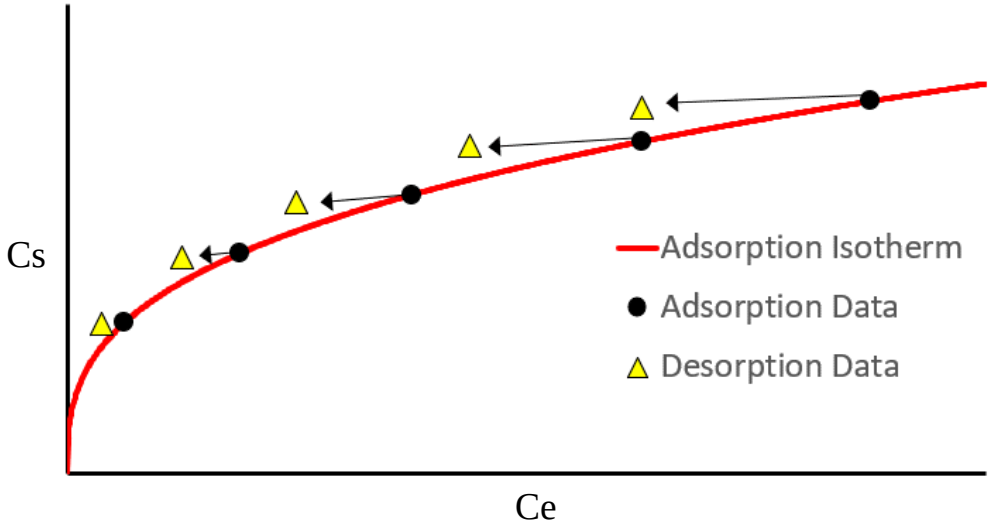


Figure 2.4: Visual demonstration of hysteretic desorption data generated using the single-step desorption approach

An alternative method to studying desorption based on serial dilution was proposed by Swanson and Dutt (Swanson and Dutt, 1973). In this method, the supernatant is decanted and replaced with a clean solution multiple times in successive steps to initiate the desorption from the adsorbent in the same bottle (Figure 2.5). Experiments following this approach are intended

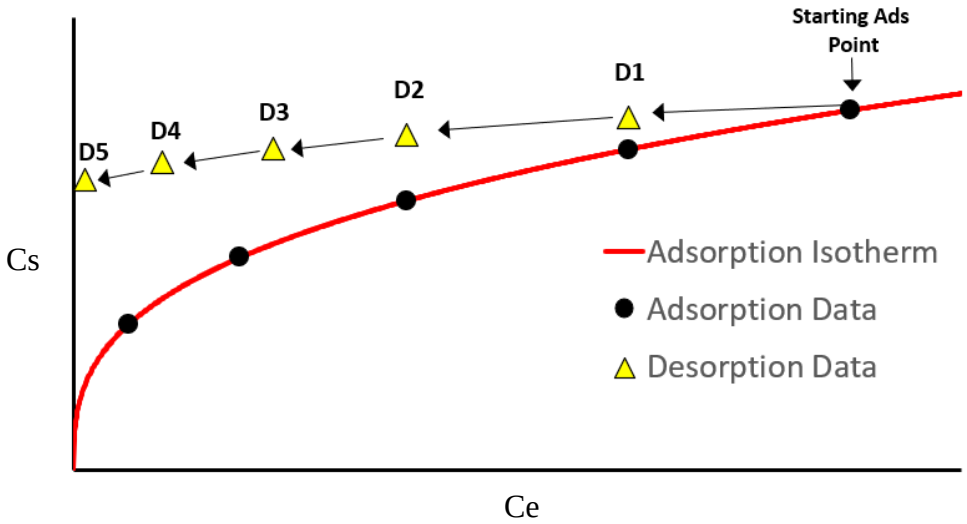


Figure 2.5: Visual demonstration of irreversible desorption data generated using the batch serial dilution approach. D1 to D5 represent the desorption step number, where D5 intersects the y-axis ($C_e = 0$) at $C_s > 0$, indicating irreversible sorption

to demonstrate the desorption characteristics of an adsorbent when it is subjected to aqueous phase flushing over time in the subsurface (Bowman and Sans, 1985; Rao and Davidson, 1980). For compounds having a high affinity to the studied adsorbent, each decant step will remove a very small mass of adsorbate from the system (Bowman and Sans, 1977). As such, without sufficient dilution volumes in desorption experiments to remove the sorbed mass, the batch serial dilution method may prove difficult to generate low C_e values (Fleer et al., 1993).

2.5 Adsorption and Desorption of PFAS on Aquifer Materials

Investigating the retention of PFAS on various aquifer materials is a crucial step in evaluating the fate of PFAS in the subsurface (Li and Liu, 2022). As such, developing an understanding of the desorption potential of PFAS from these materials is a continuing focus of the research community, as described in this section.

Millinovic et al. studied the desorption of PFOS, PFOA, and PFBS in six different aquifer materials using the single-step desorption method (Millinovic et al., 2015). They observed that the sorption of PFOS was highly irreversible, while the sorption of PFOA and PFBS was only slightly irreversible (Millinovic et al., 2015). In this study, the contact time between the adsorbent and the solution was only 24 h in both the adsorption and desorption steps. Because the authors did not provide kinetic data, it is unclear whether adsorption and desorption equilibria had been established after 24 h. Similarly, Xiao et al. investigated the desorption hysteresis of PFOA, perfluorooctaneamido ammonium iodide (PFOAAmS) and perfluorooctane amido betaine (PFOAB) from five soil samples using the single-step desorption method (Xiao et al., 2019). This study showed a weakly hysteretic behaviour for PFOA, fully reversible sorption for PFOAAmS, and significant hysteresis for PFOAB (Xiao et al., 2019). However, as mentioned earlier, there are shortcomings associated with the single-step desorption approach.

Chen et al. investigated the adsorption and desorption of PFAAs to sediment from an urban reservoir using the batch serial dilution method (Chen et al., 2016). Results from this study indicated that for the stronger sorbing PFOS, PFNA, and PFDA, sorption was

significantly irreversible. However, since a desorption kinetic study was not included in this work, it is unclear whether desorption equilibrium was reached. A later study by Chen et al. found that irreversible sorption was the greatest at the highest starting adsorbate concentration (Chen et al., 2022). Based on this observation, they hypothesized this concentration-dependent irreversibility may be caused by the higher potential for saturation of the irreversible pores at higher concentration gradients (Chen et al., 2022). Pan et al. also observed that the sorption of PFOS on sediments from the Miyun reservoir in Beijing, China was hysteretic (Pan et al., 2009). In this study, adsorption equilibrium was established by 24 h, which was then used as the contact time for all adsorption and desorption experiments. Since desorption has been shown to be a slower process in sediments (Xiao et al., 2019; Zhi and Liu, 2018), it is unclear whether desorption equilibrium was truly reached in this study.

Schaefer et al. used the batch serial dilution method to investigate the desorption of PFAS from soils collected from an AFFF source zone (Schaefer et al., 2022). The desorption isotherms generated in this work show the potential for irreversible sorption, as the isotherms appear to intersect the y-axis ($C_e = 0$) at $C_s > 0$. After seven sequential desorption steps, the same reactors containing one of PFOA, PFHPS PFOS, or 8:2 FTS and sediment were allowed to equilibrate for an additional 9 months on an orbital shaker table. In the case of PFOA, PFOS, PFHPS, additional mass was desorbed over these 9 months, resulting in a higher aqueous phase concentration than previously reported. This highlights slow desorption kinetics of PFAS from soil, which could be an experimental artifact when generating a desorption isotherm with aquifer materials. An earlier kinetic study by Schaefer et al. also demonstrated continued release of shorter chained PFAS over 400 h of monitoring (Schaefer et al., 2021). As such, it is suspected that less hydrophobic shorter chained compounds show kinetic controlled desorption in field-aged soils (Schaefer et al., 2021).

2.6 Adsorption and Desorption of PFAS on Engineered Adsorbents

The extensively studied adsorbents for PFAS sequestration vary from GAC (Park et al., 2020; McCleaf et al., 2017; Carter and Farrell, 2010), PAC (Liu et al., 2020; Partlan et al., 2020), CAC (Hakimabadi et al., 2023), biochar (Chen at al., 2024; Zhi and Liu, 2018;

Thompson et al., 2016), IX resins (Mccleaf et al., 2017; Carter and Farrell, 2010) and polymers (Olshansky et al., 2022). While the research on these adsorbents comprises of multiple comparisons of their ability to remove PFAS from the aqueous phase, few studies investigated PFAS desorption.

Zhi and Liu applied the single-step dilution approach to study the adsorption and desorption of PFOS, PFOA, PFOAAmS, PFOAB and 6:2 fluorotelomer betaine (6:2 FTAB) from Pahokee peat soil organic matter (SOM) and pyrogenic carbonaceous materials, including biochar, soot, and oil-free soot (Zhi and Liu, 2018). They reported that the adsorption and desorption isotherm fits were statistically different at the 95% confidence interval, and thus, concluded that the sorption of PFAS on these materials was hysteretic (Zhi and Liu, 2018). Except for 6:2 FTAB and biochar which showed significant hysteresis at every point, the overall desorption data for all PFAS follows adsorption quite well. Though the desorption isotherm "best fit" was located above the adsorption isotherm for some compounds, many desorption points were located either on the adsorption curves, or below them (Zhi & Liu, 2018). Desorption hysteresis has also been observed using activated hydrochar derived from food waste materials in single dilution experiments (Chen et al., 2024). Chen et al. adopted a variation of the BP method where the mass of activated hydrochar was held constant, and PFAS concentrations were varied from 2–3500 µg/L (Chen et al., 2024). Their study found a positive correlation between starting PFAS concentration and degree of hysteresis for PFBA, PFPeA, PFHxA, PFHpA, PFBS, PFHxS, PFOS, GenX and 6:2 FTS. Experimentally, this appears as a desorption curve that is above the adsorption isotherm only at higher concentrations. Similar observations were seen by Chen et al., who hypothesized that this observation was due to saturation of the irreversible pores at the higher starting concentrations (Chen et al., 2022).

Olshansky et al. investigated the adsorption and desorption of PFAS from polyaniline-derived polymers by performed single-step dilution experiments (Olshansky et al., 2022). Desorption of PFOS and PFOA from these polymers was found to exhibit extreme hysteresis at lower equilibrium aqueous phase concentrations (Olshansky et al., 2022). This means that

at lower concentrations, there are desorption-resistant sites that are occupied by PFOS and PFOA first, compared to at higher concentrations where sites of lesser sorption strength may be occupied as well. Similar to other research, however, it is unclear whether this data exhibits true or artificial hysteresis since the single-step dilution method was used, which does not show the desorption trend from the same starting mass of adsorbent.

2.7 Summary

Many published PFAS desorption studies indicate some degree of hysteresis, suggesting that there is a fraction of sorbed PFAS on aquifer materials or engineered adsorbents that are permanently removed from the aqueous phase. However, a common theme among many of these studies is the absence of desorption kinetic data to support contact times adopted in experiments. If reactor bottles are not at equilibrium when sampled, the isotherms generated are not a true representation of the adsorption and desorption characteristics of the system. It is therefore crucial to understand adsorption and desorption kinetic behaviour prior to the evaluation of hysteresis. Based on the available literature, it appears that the sequential dilution methodology has not been adopted to investigate the desorption of PFAS from AC particulate amendments.

Chapter 3
Materials and Methods

In this chapter, the materials and methods used to complete batch adsorption and desorption experiments with PFOS, PFOA and PFBS on commercially available AC particulate amendments are described. PFOS, PFOA, and PFBS were chosen as the representative PFAS in this research, as this selection allows the comparison of short versus long chain PFAS (i.e., PFBS versus PFOS), as well as investigates the impact of carboxylate versus sulfonate functional groups (i.e., PFOS vs PFOA) on the reversibility of sorption. These three compounds are also frequently observed at AFFF sites (Houtz et al., 2013). The adsorption and desorption experiments described are divided into PAC and CAC experiments since different methodologies were required to generate desorption data.

Experiments with PAC were completed to determine the presence or absence of desorption hysteresis by generating adsorption and desorption isotherm data. For adsorption, the bottle-point method was used where the adsorbate concentration was held constant, and the mass of PAC was adjusted to create a set of isotherm points. For desorption experiments, the batch serial dilution method was used to create a series of desorption points starting from the highest adsorption isotherm point. Depending on the PFAS compound used, the volume of supernatant replaced at each dilution step was adjusted so that the desorption points spanned, where possible, the approximate range of the generated adsorption isotherm. At each dilution step, the aqueous phase concentration (C_e) was measured using Liquid Chromatography Tandem Mass Spectrometry (LC-MS/MS), and the associated solid phase concentration (C_s) was estimated using a mass balance approach. Adsorption and desorption kinetic experiments were performed to determine the time to reach equilibrium.

Experiments with CAC were also completed to determine if hysteretic behaviour is exhibited during the desorption of PFAS. Similar to the experiments with PAC, the BP method was adopted for adsorption experiments. Since the grain size of CAC is too small to settle in a reasonable time frame (< 24 h), two desorption methodologies were used. The first method

involved sub-sampling different volumes from the adsorption bottle containing the highest aqueous phase concentration of adsorbate, and diluting them to initiate desorption. Each sub-sample was assumed to have a proportional fraction of the initial CAC mass. The second method involved the creation of additional bottles that replicated the upper adsorption isotherm point. After equilibrium was reached, the contents of the entire bottle were diluted into larger volume bottles to initiate desorption. CAC adsorption and desorption kinetic experiments were also completed to determine the time to reach equilibrium.

3.1 Materials

3.1.1 Adsorbents

For the experiments with PAC, the coconut shell-based PAC product (WPC PAC, Calgon Carbon, Moon Township, Pennsylvania, USA) was used. Grain size analysis of this product was performed by Regenesis (San Clemente, California, USA) using a laser diffraction particle size analyzer (Horiba LA-960). This analysis indicated that WPC PAC has a mean grain size of 13.1 µm, a D90 of 23.7 µm, and a D10 of 4.0 µm.

For the CAC experiments, a polymer-free form of Plumestop™ obtained from Regenesis was used. Grain size analysis, also performed by Regenesis, indicated that Plumestop™ CAC consists of particles with a mean grain size of 1.8 µm, a D90 of 2.8 µm, and a D10 of 0.9 µm. Commercially available Plumestop™ contains polymers as a stabilizing agent that prevent aggregation of the small (1-2 µm) carbon grains, and assist with deposition of CAC onto sediment particles in the subsurface. The presence of these polymers leads to a decreased affinity for PFAS, believed to be caused by competitive sorption of the polymer to the carbon surface (Hakimabadi et al., 2023). Therefore, since this work involved sequential dilution steps to initiate desorption, a polymer-free form of Plumestop™ CAC was used to prevent any influence of the polymer on PFAS adsorption and desorption.

3.1.2 Chemicals

PFOS, PFOA, and PFBS were purchased from Sigma Aldrich (St. Louis, Missouri, USA), while the native and isotopically labelled PFAS standards were purchased from

Wellington Laboratories (Guelph, ON, Canada). Concentrated PFAS stocks were prepared by dissolving each PFAS in LCMS-grade methanol (> 99.9%, obtained from Fisher Scientific, Hampton, New Hampshire, USA) to concentrations of 4500 mg/L, 2500 mg/L and 600 mg/L for PFOS, PFOA and PFBS, respectively.

Sodium bicarbonate ($NaHCO_3$, > 99.7%) was purchased from VWR (Radnor, Pennsylvania, USA) to make a 1 mM buffer solution, which was used as the reaction solution in all experiments.

3.2 Methods

3.2.1 Carbon Processing

WPC PAC was received dry. Thus, specific amounts were weighed on an analytical balance before being added to experimental bottles. As noted above, the as-received WPC PAC contained a wide range of particle sizes, which limited complete settling in a reasonable time frame (< 24 hr). In many desorption experiments, the adsorbent is allowed to settle before the aqueous phase is replaced with an adsorbate-free solution. If the PAC does not settle completely, then a small amount of adsorbent mass might be removed along with the aqueous phase. Additionally, during preliminary experiments, small PAC particles were observed to attach to the side walls of containers, presumably due to static attraction. Therefore, it was decided to remove the smaller particle size of the PAC. To this end, a known mass of PAC was sieved with a 20-micron (US #635) sieve (W.S Tyler™, Laval Labs, Montreal, QC, CAN). Approximately 10% of the initial mass was retained by the sieve, consistent with the D90 of 23.7 µm. Bright-field microscopy (Zeiss 700 confocal microscope) was used to image samples of the as-received and retained WPC PAC (Figure 3.1). While it appears that the original WPC PAC has a greater particle size than the PAC retained on the sieve, this is likely due to imaging

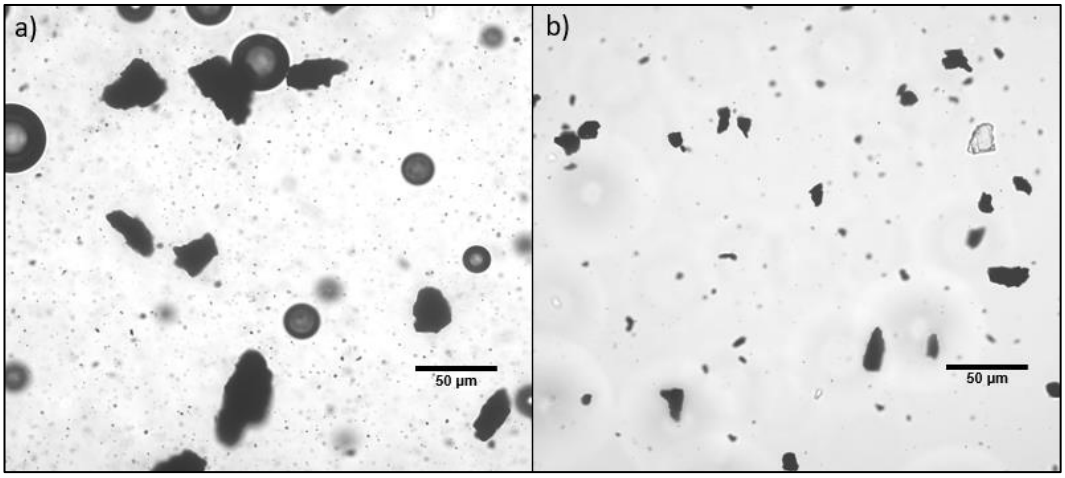


Figure 3.1: Comparison between (a) as-received WPC PAC and (b) retained WPC PAC. Image taken at 40x objective, 1.3 numerical aperture. Circular ordnances within the image are air bubbles trapped under the microscope cover slides.

an area that is not representative. Another possible explanation could be that during the hand-sieving procedure, the large particles may have been ground against the stainless-steel mesh therefore decreasing the particle size. Of importance here is that within panel (b) there is a lack of superfine particles, which are seen in a greater quantity throughout panel (a). This indicated the successful sorting of PAC grains using the sieving procedure.

During this sieving process, the attachment of remnant sub-micron particles to the larger >20 µm particles may be possible, which would lead to the retention of an undesired fine fraction. To investigate the settling behaviour of the PAC retained on the sieve, 100 mg of retained PAC was loaded into a 1000-mL high density polyethylene (HDPE) bottle from VWR, which was then filled with Milli-Q water (Milli-Q IQ 7000 coupled with Q-POD) and placed on an orbital shaker at 125 rpm for 24 h. The bottle contents were then allowed to settle for 24 h. After settling, the large particles had visibly settled to the bottom of the HDPE bottle. The upper 900 mL of the supernatant in the 1000-mL bottle was passed through a vacuum filter (GAST 0523 Vacuum Pump, connected to Kontes Scientific vacuum filter base) with a 0.45-µm cellulose nitrate vacuum filter paper. Approximately 1 mg of the initial 100 mg was retained on the filter, indicating that 1% of the PAC > 0.45 µm did not settle within 24 h, and would be lost in the replacement of supernatant during experimentation. This small percentage

of carbon remaining in the upper 90% of the supernatant was considered adequate to proceed with the use of the retained mass (> 20 µm) for the adsorption and desorption experiments.

Since water is added during the wet-milling process to create polymer-free CAC, the product was received as a stock containing 35% carbon by weight. This 35 wt. % stock of CAC and water was diluted to 20 wt. % of carbon with the addition of ultrapure Milli-Q water in a 250-mL HDPE bottle from VWR. As CAC is a slurry, it could not be weighed on the analytical balance like the dry PAC, and, therefore, it was added to the reaction solution as needed using micropipettes.

3.2.2 Adsorption and Desorption Isotherm Experiments with PAC

Adsorption data were generated using the BP method, where the adsorbent mass was adjusted while keeping the initial adsorbate concentration constant. Six-point isotherms were generated in triplicate for PFOS, PFOA, and PFBS, at starting concentrations of 4500, 2500, and 600 µg/L, respectively. Of the three studied compounds, PFOS is the most hydrophobic and, thus, was expected to have the highest affinity for AC. Therefore, to ensure the range of C_e in all experiments is similar (1–100 µg/L), the concentration of PAC in the PFOS experiment must be the lowest. Preliminary experiments indicated that PAC masses below 5 mg caused an increase in experimental errors, due to inaccuracies when weighing this small mass on the analytical balance used (QUINTIX224-1S, Sartorius, Goettingen, Germany). As such, the low AC concentration in the PFOS experiment could only be achieved by increasing the solution volume. Thus, while 50-mL conical bottom polypropylene (PP) centrifuge tubes from VWR were appropriate for PFOA and PFBS experiments, 125-mL HDPE bottles from VWR were used for PFOS experiments. All bottles were filled with the buffer solution using an electric pipet controller (Fisher Scientific, Waltham, Massachusetts, USA) connected to a 50-mL serological pipette (VWR, Radnor, Pennsylvania, USA). PAC concentrations were adjusted (0.08–1 g/L for PFOS, 0.12–0.6 g/L for PFOA, and 0.12–1.2 g/L for PFBS) for all isotherm points so the equilibrium aqueous concentrations were within the targeted range. Bottles were placed on their sides on an orbital shaker (Solaris, Thermo Scientific, Waltham, Massachusetts, USA) at 125 rpm for 168 h. Subsequently, the bottles were removed, and the

PAC was allowed to settle for 24 h. A 13.2 mL aliquot of supernatant was ultracentrifuged then analyzed to determine C_e.

Desorption data were generated by adapting the sequential dilution method employed by Zhao et al. (Zhao et al., 2002) (Figure 3.2). In each desorption step, 90% of the supernatant in the adsorption bottle was removed with an electronic pipet controller and a 50-mL serological pipet. The supernatant was removed in this manner as opposed to decanting to avoid disturbing the settled PAC. The remaining aqueous phase and the settled PAC were then poured into a larger 500-mL (PFBS) or 1000-mL (PFOA, PFOS) HDPE bottle from VWR, which was then filled with the buffer solution. After 7 days on the orbital shaker, the larger HDPE bottle was placed upright for 24 h to allow the PAC to settle. Again, 13.2 mL of supernatant was ultracentrifuged and then analyzed to determine C_e.

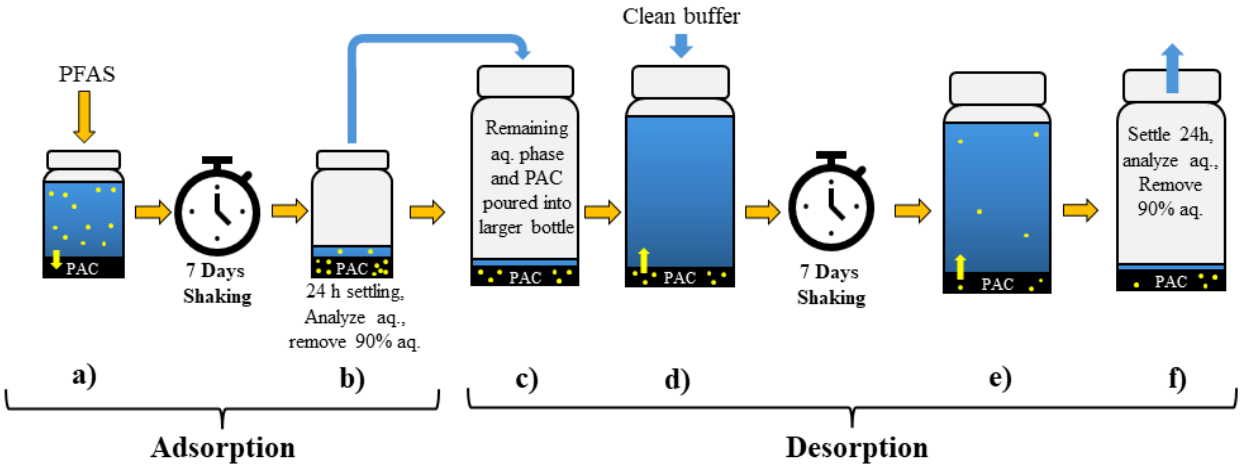


Figure 3.2: Schematic of the experimental approach used to investigate the desorption of PFBS, PFOA, and PFOS from PAC. After the adsorption bottle reached equilibrium (a-b), 10% of the aqueous phase (including all PAC) was transferred to a larger HDPE bottle (c). Multiple desorption steps (d-f) were then repeated where 90% of the supernatant was replaced with buffer solution, shaken for 7 days, then the aqueous concentration was determined.

These desorption steps were completed weekly until the aqueous concentration data covered the same aqueous concentration range as the adsorption data. Based on preliminary calculations, it was expected that this may only be possible for PFBS, since it has a lower affinity for AC, meaning sufficient mass could be removed with each desorption step. For

PFOS and PFOA, since they have a higher affinity for AC, it was recognized that desorption data spanning the same range as adsorption may not be feasible. This is because each successive desorption step incrementally desorbs less mass of PFAS from the PAC, resulting in smaller decreases in the aqueous phase concentration. The inability to reach smaller C_e values when using high-affinity adsorbents highlights the drawback of the batch serial dilution method (Fleer et al., 1993). In this research, PFOS and PFOA having greater affinity to the PAC compared to PFBS means much larger dilutions than 1000 mL would be required to reach lower C_e values. To prevent wear to the orbital shaker with long-term, repeated shaking, a 1000-mL desorption bottle was deemed the largest to be used for the PAC desorption experiments. As such, desorption experiments for PFOS and PFOA were continued until mass removal between successive desorption steps became too small to generate desorption data near MDL (i.e., experiments were stopped when mass desorbed was < 3% of the original sorbed PFAS mass). The pH of the solution in each desorption bottle was measured after each adsorption or desorption step.

As was mentioned in Section 3.2.1, approximately 1% of the PAC representing the unsettled PAC fraction is lost during removal of supernatant for the first desorption step. Since this fraction is also laden with PFAS, the measured C_e in this first desorption step will be lower than expected (i.e., the desorption point is shifted to the left on a C_e vs C_s plot). To adjust for this lost mass, the aqueous concentration of the first desorption point was adjusted, assuming there was 1% more PAC (and thus 1% more mass PFAS sorbed to the PAC) available to contribute to the aqueous concentration.

3.2.3 Adsorption and Desorption Kinetic Experiments with PAC

Kinetic experiments were conducted in triplicate in PP centrifuge tubes, each containing 50 mL of the buffer solution. Retained WPC PAC was added to the buffer solution in each tube prior to the addition of PFAS stock solutions. Initial concentrations were 4500 µg/L, 2500 µg/L and 600 µg/L for PFOS, PFOA, PFBS, respectively, and the PAC mass was adjusted so the targeted equilibrium concentration would be between 20 and 60 µg/L (i.e., the targeted mid-range C_e of the adsorption isotherms). A total of 24 tubes were constructed for

each PFAS. The tubes were placed on the orbital shaker at 125 rpm. At specified times (2, 6, 12, 24, 48, 72, 120 and 168 h), three tubes were removed and centrifuged at 4000xg for 10 min to separate most of the PAC. The supernatant was then subjected to ultracentrifugation and PFAS analysis.

The desorption kinetic tubes were prepared with the same carbon and PFAS dosage as in the adsorption kinetic experiment. After spiking with PFAS and PAC, they were placed on the orbital shaker at 125 rpm for 1 week, before being centrifuged at 4000xg for 10 min to separate the PAC. Like the batch desorption experiments, 90% (or 45 mL) of the aqueous phase from each tube was removed and replaced with a clean buffer solution using a 50-mL serological pipet. At specified times (2, 6, 12, 24, 48, 72, 120, and 168 h), three tubes were removed and again centrifuged at 4000xg for 10 min to separate the PAC. A 13.2 mL aliquot of the supernatant was ultracentrifuged and then analyzed to determine C_w.

3.2.4 Adsorption and Desorption Isotherm Experiments with CAC

Similar to the batch PAC isotherm experiments, the BP method was employed for all CAC adsorption series by adjusting the adsorbent mass and keeping the initial adsorbate concentration constant. Six-point isotherms were generated in triplicate for PFOS, PFOA, and PFBS. Wide-mouth 125-mL HDPE bottles were used for all experiments, utilizing a buffer solution which was added to each bottle using an electronic pipet controller and a 50-mL serological pipet mentioned previously. Initial PFAS concentrations of 4500 µg/L, 2500 µg/L and 500 µg/L for PFOS, PFOA, and PFBS, respectively were replicated from the PAC experiments, except for PFBS, which had a lower starting concentration so that the isotherm data spanned a similar concentration range as the PAC experiments. Dosage of the 20 wt. % polymer-free CAC was varied such that the equilibrium concentrations spanned approximately two orders of magnitude (1 to 100 µg/L). This resulted in CAC concentrations of 0.054 to 0.36 g/L for PFOS, 0.089 to 0.36 g/L for PFOA, and 0.089 to 0.89 g/L for PFBS. The adsorption bottles were allowed to 672 h of contact time to ensure the proceeding desorption experiments were not influenced by a lack of adsorption equilibrium. After 672 h, the bottles were removed from the orbital shaker and a well-mixed 13.2-mL aliquot was subjected to ultracentrifugation

and analysis to determine C_e. The pH of the solution in all adsorption bottles was then measured.

The fine particle size of the CAC used (mean grain size of 1.8 µm) did not allow for separation of the CAC by settling as was completed in the PAC experiments; hence an alternative methodology was developed (Figure 3.3). Assuming that the bottles were well-mixed, the developed method involved taking various aliquots (1, 2, 5, 10, and 25 mL) from an original adsorption bottle and diluting them to a total volume of 125 mL using the same buffer solution. After diluting the aliquots, the desorption bottles are placed on the orbital shaker at 125 rpm for 168 h. After 168 h, a 13.2 mL aliquot was subjected to ultracentrifugation, and handled as outlined in Section 3.2.6. The pH of the solution in all desorption bottles was again measured after 168 h of equilibration.

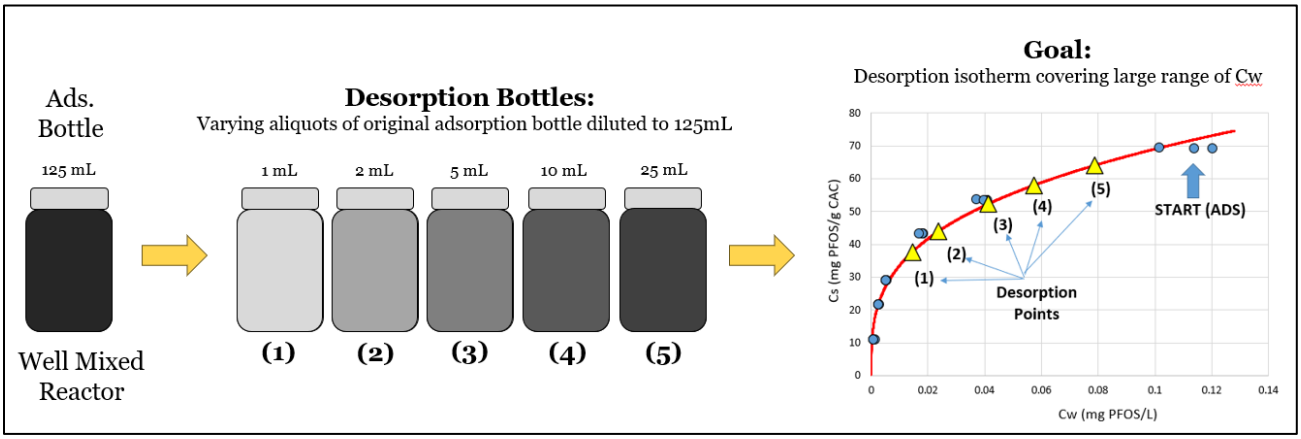


Figure 3.3: Schematic of the experimental approach used to study the desorption of PFOS, PFOA, and PFBS from CAC. After the top adsorption isotherm bottles reached equilibrium (ads bottle), aqueous phase concentrations were measured. Well-mixed aliquots (1, 2, 5, 10, 25 mL) were subsampled from these adsorption bottles and were then diluted to total volumes of 125 mL (bottles 1-5), shaken for 168 h, then the aqueous concentration was determined.

Since there was some uncertainty regarding the well-mixed assumption of CAC within the bottle that the aliquots were collected from, a second alternative method to conduct desorption isotherm experiments was adopted for PFOS only (Figure 3.4). This methodology was adapted from Bowman and Sans, who used a method where additional, replicate

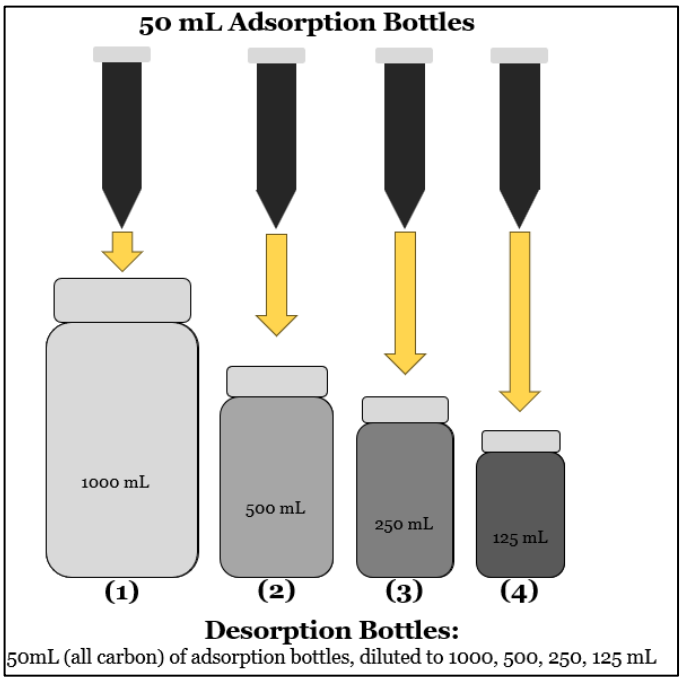


Figure 3.4: Schematic of revised CAC desorption (whole bottle dilution) methodology. After the 50-mL adsorption bottles that replicate the top adsorption isotherm point reached equilibrium, entire bottle contents were poured into larger HDPE bottles (1-4), and filled to total volumes of 125, 250, 500, 1000 mL.

adsorption vials were diluted by the addition of distilled water, rather than diluting a sub-sample from an assumed well-mixed system (Bowman and Sans, 1985). In this method, 50-mL PP centrifuge tubes were filled with the buffer solution with final CAC concentrations ranging from 0.067 g/L to 0.44 g/L, and a target starting concentration of 4500 µg/L of PFOS. Twelve additional 50-mL PP tubes were prepared that replicated the upper adsorption isotherm point (0.067 g/L CAC). All bottles were placed on the orbital shaker at 125 rpm for 168 h, at which point the 18 (6 x 3 replicates) adsorption isotherm tubes were sampled to determine C_e. For desorption, the additional tubes that replicated the upper adsorption point were poured into their respective HDPE bottles, diluted with buffer solution to volumes of 125, 250, 500, or 1000 mL, and placed back on the orbital shaker for 168 h. After shaking, the bottles were sampled to determine C_e.

3.2.5 Adsorption and Desorption Kinetic Experiments with CAC

CAC adsorption kinetic experiments were conducted in triplicate HDPE wide-mouth bottles, each containing 125 mL of buffer solution. Initial PFAS concentrations were 4500 µg/L, 2500 µg/L, and 500 µg/L for PFOS, PFOA, PFBS, respectively, and the volume of 20 wt. % CAC was adjusted so the equilibrium concentrations were in the targeted mid range of the adsorption isotherms. A total of 27 bottles were constructed for each PFAS. The spiked bottles were placed on the orbital shaker at 125 rpm. At selected times (2, 6, 12, 24, 48, 72, 120, 168, and 672 h), three bottles were removed from the orbital shaker, and sampled to determine C_e (Section 3.2.6). The adsorption kinetic experiments were carried out until 672 h (4 weeks) to explore if significant changes in C_e occurred between 1 week (168 h) and 4 weeks.

The desorption kinetic bottles were prepared in the same manner as the sub-sampling desorption isotherm experiments, but the desorption dilution factor was held constant. For all three compounds (PFOS, PFOA, PFBS), 2 mL of well-mixed solution from the highest concentration adsorption isotherm bottle was diluted to 125 mL with the buffer solution. Three bottles were removed from the orbital shaker at each timepoint (2, 6, 12, 24, 48, 72, 120 and 168 h) and sampled to determine C_e.

3.2.6 Sample Preparation and Analysis

To separate adsorbent from aqueous samples prior to LC-MS/MS analysis, adsorption/desorption solutions were ultracentrifuged using an Optima XPN-80 Ultracentrifuge (Beckman Coulter, Brea, California, USA). In all experiments, a 13.2 mL aliquot of the supernatant was transferred to an ultracentrifuge tube (Beckman Coulter Ultra-Clear). To limit sorption to the ultracentrifuge tube walls, the tubes were rinsed with the supernatant for 10 minutes, emptied, and refilled a total of two times. On the third fill, the tubes containing the supernatant were inserted into the centrifuge tube holders. Tubes were then transferred to a swinging bucket centrifuge rotor (Beckman Coulter SW-41 TI), and ultracentrifuged at 230,000xg for 1 h (for PAC-containing samples) and 1.75 h (for CAC-containing samples).

Following ultracentrifugation, PFAS analysis followed the same procedure reported by Hakimabadi et al. (Hakimabadi et al., 2023). Further details on the LC-MS/MS equipment used and operation parameters for analytes are provided in Appendix A (Table A.1).

3.2.7 Data Analysis

Experimental results were plotted using Sigmaplot 10.0 (Systat Software Inc., Chicago, Illinois, USA). Adsorption and desorption data were plotted with error bars representing ± 1 SD from the mean of each triplicate set, for both C_e and C_s. Adsorption isotherms were fit using the Freundlich isotherm model (Equation 2.2), which generated K_f, and n_f values. The adsorption isotherm was plotted along with its 95% prediction band, which represents the expected value of future observations (Kummel et al., 2018; Roth, 2009). Thus, a data point that lies within this prediction band is not statistically different from the entire isotherm population at the 95% level of confidence.

Since the dimensions of K_f are dependent on n_f, it is not defensible to use K_f values as a means to compare different isotherms to evaluate sorption affinity (Higgins and Luthy, 2006). Instead, a K_d (= C_s/C_e) value at a molar concentration of 0.05 µM was used to compare the sorption affinity of PFAS to AC. This molar concentration corresponds to a C_e of 25.0 µg/L, 20.7 µg/L, and 15.0 µg/L for PFOS, PFOA, and PFBS, respectively, which were approximately in the middle of the experimental data range for PAC experiments. For consistency, the K_d of all PFAS were evaluated for CAC at the same concentrations as used for the PAC experiments.

All adsorption kinetic data (C_s vs time (h)) were plotted using Sigmaplot 10.0, and fit to the pseudo first-order kinetic model (Equation 2.4) using nonlinear regression. The solid phase concentration at equilibrium (C_s^{eq}) was set as the average of the 120 h and 168 h timepoints, thus the best-fit result produced rate coefficient (k_{ads}). Based on the solid phase data, the time to reach 98% of equilibrium (t_{98}) was calculated for each adsorption kinetic experiment. The best-fit of the C_s data was used to generate a profile of C_w over time using

$$C_w(t) = C_0 - \frac{m_{AC} C_s^{eq}}{V_w}(1 - e^{-k_{ads}t}) \tag{3.1}$$

where C_0 is the initial aqueous phase concentration (mg/L), m_{AC} is the mass of activated carbon in each bottle (g), and V_W is the total volume of solution in each bottle (L).

In addition to the best-fit rate coefficient (k_{ads}), an initial adsorption rate (R_{ADS}) was estimated using data after the first 6 h of contact, given by:

$$R_{ADS} = \frac{C_s(t = 6\ h) - C_s(t = 0\ h)}{6\ h} \tag{3.2}$$

Similarly, all desorption kinetic data (C_s vs time (h)) was plotted using Sigmaplot 10.0, and fit to the first-order kinetic model (Equation 2.5) using nonlinear regression. The solid phase concentration at equilibrium (C_s^{eq}), was set as the average of the 120 h and 168 h timepoints, therefore the best-fit results produced rate coefficients (k_{des}). Based on the solid phase data, the time to reach 98% of desorption equilibrium (t_{98}) was calculated for each desorption kinetic experiment. The best-fit of the C_s data was used to generate a profile of C_w over time using

$$C_w(t) = \frac{m_{ac}^{des}}{V_w}\left(C_s^0 - C_s^{eq}\right)(1 - e^{-k_{des}t}) + C_w^0 \tag{3.3}$$

where m_{AC}^{des} is the mass of AC in each desorption bottle (g), V_W is the total volume of solution in each bottle (L), Cs^0 is the solid phase concentration at time zero of the desorption experiment (mg/g), Cw^0 is the aqueous phase concentration at the start of the desorption experiment (mg/L). In addition to the best-fit rate coefficient (k_{des}), an initial desorption rate (R_{DES}) was calculated over the first 6 h of contact, given by:

$$R_{DES} = \frac{C_s(t = 0\ h) - C_s(t = 6\ h)}{6\ h} \tag{3.4}$$

Chapter 4
Results and Discussion

4.1 Powdered Activated Carbon Experiments

4.1.1 Adsorption and Desorption Kinetics

During the first 72 h of contact, 99.3%, 98.7%, and 94.4% of the total mass of PFOS, PFOA, and PFBS were removed from the solution, whereas between 72 h and 168 h, an additional 0.005%, 0.14% and 0.69% of the total mass was removed. Since the degree of adsorption observed beyond 72 h was minimal, it was assumed that adsorption of PFOS, PFOA, and PFBS on PAC reached equilibrium by 72 h (Figure 4.1).

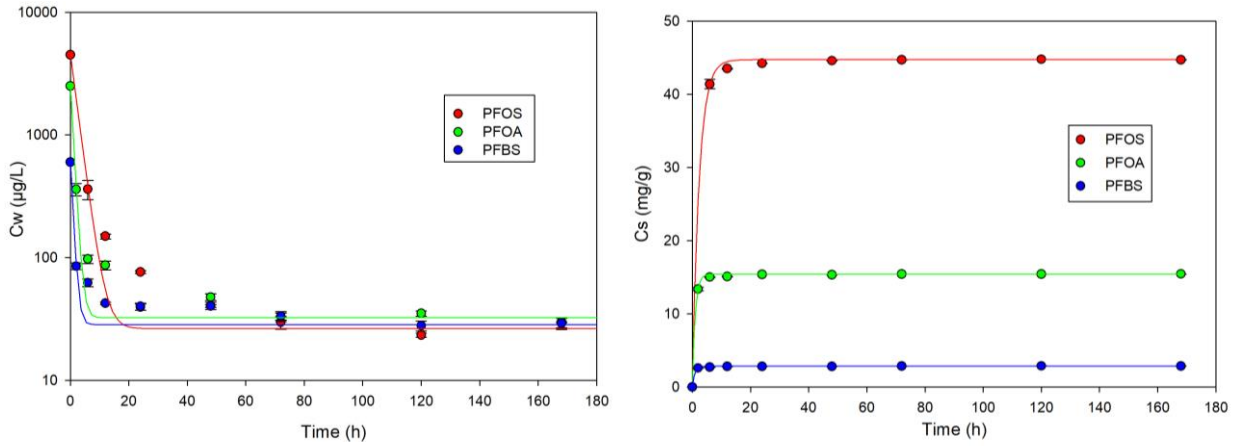


Figure 4.1: The concentration-time profiles for adsorption of PFOS, PFOA, and PFBS in 50-mL reaction solutions containing retained WPC PAC. Reaction solutions contained 0.1 g/L (PFOS), 0.16 g/L (PFOA) or 0.2 g/L (PFBS) of PAC, and either $[PFOS]_0$ = 4500 µg/L , $[PFOA]_0$ = 2500 µg/L, or $[PFBS]_0$ = 600 µg/L. Solid phase concentrations (C_s) were fit to the pseudo first-order kinetic function (the solid lines in the right panel). The model parameters were then used to generate predicted aqueous phase concentrations (solid lines in the left panel). Error bars represent one standard deviation.

Based on the results of the pseudo first-order kinetic model fit to the data (Equation 2.4), *k* values of 0.425 /h (PFOS), 1.01 /h (PFOA), and 1.15 /h (PFBS) were generated when the solid phase concentration at equilibrium ($C_{s,\,eq}$) was set at 44.7 mg/g (PFOS), 15.4 mg/g (PFOA) and 2.86 mg/g (PFBS) (Table 4.1). The solid phase model parameters generated were

used to simulate aqueous phase concentrations using Equation 3.1. The lack of fit between the simulated C_w profile and the observed C_w data at early time is a reflection that most of the PFAS mass is associated with the solid phase and hence a small change in C_s leads to a large change in C_w. As such, a slight lack-of-fit between the early C_s data and the model manifests as a larger variability in the simulated C_w profile relative to the observed C_w data.

The time to reach 98% of equilibrium (t_{98}) was < 10 h for all compounds (Table 4.1). Though a contact time of 72 h was deemed sufficient to reach equilibrium, a contact time of 168 h was used for subsequent adsorption experiments to ensure the manifestation of hysteresis would not be influenced by minor kinetic limitations. The initial adsorption rates based on the mass of PFAS (mg) sorbed per gram of AC over the first 6 h of contact show that PFOS was adsorbed at the fastest rate (6.90 mg/g/h), followed by PFOA (2.50 mg/g/h), then PFBS (0.448 mg/g/h) (Table 4.1). The adsorption of PFOS and PFOA on PAC was observed to consist of two phases: (1) a rapid adsorption rate during the first 6 h, and (2) a slower adsorption rate between 6 h and 72 h. In the second phase, adsorption rates decreased to 0.05, 0.006, and 0.002 mg/g/h for PFOS, PFOA and PFBS, respectively, which represent a 137x, 413x and 203x lower adsorption rate. This suggests that the adsorption process may include a rate-limiting step involving the transport of PFAS to the adsorption sites within the AC pores. One possibility is the presence of an intraparticle diffusion limitation (Cecen and Aktas, 2011), where initially, PFAS rapidly accumulates on the external surface of the PAC particle (during the first 6 h), then slowly diffuses into the deeper pore structure of the PAC.

Table 4.1: Summary of PFAS Adsorption Kinetic Parameters for Retained WPC PAC

Compound	Rate Coefficient, *k* (/h) ± 95% CI	*Cs, eq* (mg/g)	r^2	t_{98} (h)	Initial adsorption rate (6h) (mg sorbed /g AC /h)
PFOS	0.425 ± 0.027	44.7	0.999	9.21	6.90
PFOA	1.01 ± 0.06	15.4	0.999	3.89	2.50
PFBS	1.15 ± 0.15	2.86	0.994	3.41	0.448

Similar to adsorption, the desorption of PFOS, PFOA and PFBS from PAC reached an apparent equilibrium within 72 h (Figure 4.2). The first-order kinetic model (Equation 2.5) fit to the desorption data generated *k* values of 0.239 /h (PFOS), 0.152 /h (PFOA) and 0.341 /h (PFBS) when the solid phase concentration at equilibrium ($C_{s,\,eq}$) was set to 44.6 mg/g (PFOS), 15.3 mg/g (PFOA) and 2.67 mg/g (PFBS) (Table 4.2). Early C_w kinetic data appear to fluctuate, likely due to experimental variability. Similar to the adsorption kinetic data, most of the PFAS mass is associated with the solid phase and a small change in C_s leads to a large change in C_w. As such, a slight lack-of-fit between the early C_s data and the model manifests as a larger variability in the simulated C_w profile relative to the observed C_w data. Between 0 h and 72 h, the maximum difference between the aqueous concentration simulated and the experimental data was 7.1%, 39% and 22% for PFOS, PFOA, and PFBS, respectively. In comparison, between 72 h and 168 h, the maximum difference was 6.6%, 7.6% and 3.3% for PFOS, PFOA and PFBS, respectively, indicating that simulated and observed concentrations converge once near equilibrium conditions are reached.

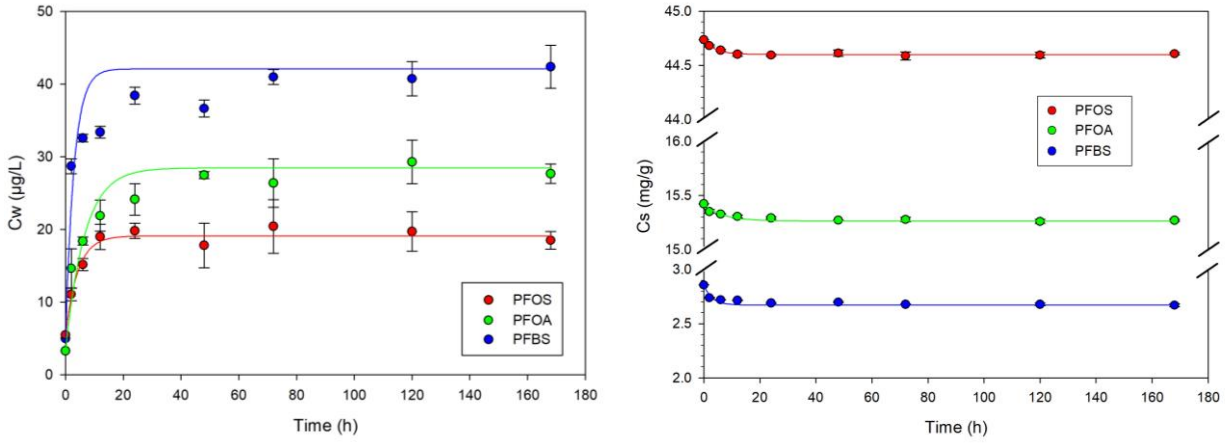


Figure 4.2: The concentration-time profiles for desorption of PFOS, PFOA, and PFBS in 50-mL reaction solutions containing retained WPC PAC. Reaction solutions contained 0.1 g/L (PFOS), 0.16 g/L (PFOA) or 0.2 g/L (PFBS) of PAC, and either $[PFOS]_0$ = 4500 µg/L , $[PFOA]_0$ = 2500 µg/L, or $[PFBS]_0$ = 600 µg/L, and were allowed 168 h to equilibrate. At a time of 0 h, 90% of the PAC-free solution was replaced with adsorbate-free buffer to initiate desorption. Solid phase concentrations (C_s) were fit to the first-order kinetic function (the solid lines in the right panel). The model parameters were then used to generate predicted aqueous phase concentrations (solid lines in the left panel). Error bars represent one standard deviation.

Table 4.2: Summary of PFAS Desorption Kinetic Parameters for Retained WPC PAC

Compound	Rate Coefficient, k (/h) ± 95% CI	$C_{s,\,eq}$ (mg/g)	r^2	t_{98} (h)	Initial desorption rate (6h) (mg desorbed / g AC / h)
PFOS	0.239 ± 0.101	44.6	0.864	16.4	0.0161
PFOA	0.152 ± 0.052	15.3	0.871	25.8	0.0157
PFBS	0.341 ± 0.133	2.67	0.835	11.5	0.0230

t_{98} values for all compounds were < 30 h (Table 4.2), demonstrating near equilibrium was reached by 72 h. However, a contact time of 168 h was used for subsequent desorption experiments to ensure kinetic artifacts were not introduced. Estimated t_{98} values for all compounds were larger for desorption compared to adsorption. The slower rates of desorption compared to adsorption are consistent with the observations made in studies that investigated the adsorption and desorption of PFAS in soil systems (Schaefer et al., 2021; Xiao et al., 2019; Zhi and Liu, 2018; Higgins and Luthy, 2006). The initial desorption rate, calculated as the mass of PFAS (mg) desorbed per gram of AC over the first 6 h of contact, showed that PFBS was desorbed at the fastest rate, followed by PFOS and PFOA, which had very similar desorption rates (Table 4.2). It is hypothesized that the higher PFBS desorption rate is due to its smaller molecular size, which may lead to easier diffusion out of the PAC pore structure.

4.1.2 Adsorption and Desorption Isotherms

All adsorption isotherm experiments with retained PAC had a solution pH between 7.9 and 8.2. Throughout the sequential desorption experiments, the pH change was less than 0.1 pH units. Studies have shown that the affinity of PFAS to surfaces is influenced by the solution pH (Campos-Pereira et al., 2023; Nguyen et al., 2020; Yu et al., 2009; Higgins and Luthy, 2006). In this study, it is deemed that PFAS sorption to PAC was not influenced by the small observed changes in solution pH.

The affinity of the studied PFAS to PAC was in the following order: PFOS > PFOA > PFBS (Figure 4.3). The Freundlich model was fit to the adsorption data using nonlinear

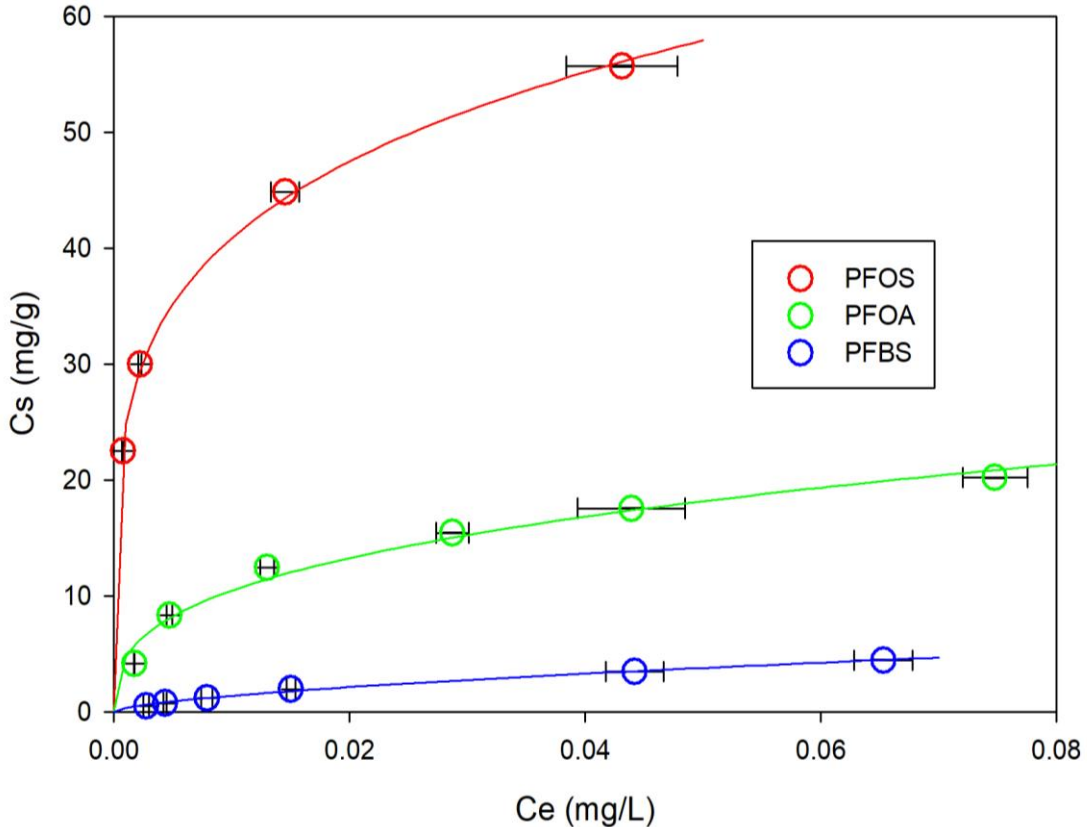


Figure 4.3: Adsorption isotherms for PFOS, PFOA, and PFBS on retained WPC PAC. The experimental data (circles) are fit to the Freundlich Isotherm model (solid lines). Error bars on each point represent one standard deviation from the mean of three replicates.

regression, generating best-fit K_f values of 111 $[(mg/g)(mg/L)^{-n_f}]$ (PFOS), 50.8 $[(mg/g)(mg/L)^{-n_f}]$ (PFOA) and 24.5 $[(mg/g)(mg/L)^{-n_f}]$ (PFBS), and best-fit n_f values of 0.217 (PFOS), 0.343 (PFOA) and 0.625 (PFBS) (Table 4.3). Resulting 0.05 µM K_d values were 1,990 L/g, 648 L/g and 119 L/g for PFOS, PFOA, and PFBS, respectively, indicating that the sorption affinity of PFOS is approximately 3.07x greater than that of PFOA and 16.7x greater than that of PFBS. Considering the best fit isotherm parameters and the resulting 95% confidence intervals, the n_f values are statistically different and follow the trend of PFBS > PFOA > PFOS (Table 4.3). As mentioned in Chapter 2, n_f represents the heterogeneity of adsorptive sites, with a value of unity representing a homogeneous distribution of sorption energies. Since the n_f of PFOS is the smallest of the studied compounds, the sorption energies of the sites that PFOS adsorbs to are thought to be the most heterogeneous. The heterogeneity

of sorption sites is reflected in the highly non-linear shape of the adsorption curve for PFOS (Figure 4.3).

Table 4.3: Summary of Freundlich Adsorption Parameters for Retained WPC PAC

Compound	K_F $(mg/g)(mg/L)^{-n_f}$	n_f	r^2	0.05 µM K_d (L/g)
PFOS	111 ± 5	0.217 ± 0.011	0.995	1.99×10^3
PFOA	50.8 ± 6.0	0.343 ± 0.034	0.974	648
PFBS	24.5 ± 2.5	0.625 ± 0.032	0.994	119

PFOS desorption experiments were concluded after five sequential desorption steps (Figure 4.4), as the mass desorbed at step D5 was only 2.4% of the original sorbed mass at D0, which was below the threshold of 3% (see Section 3.2.2). As the desorption data does not extend completely to a C_e near the MDL, it is uncertain whether the desorption of PFOS is reversible (intersects origin) or irreversible (intersects C_e = MDL at $C_s > 0$). Nevertheless, the desorption data lie within the 95% prediction band (Figure 4.4), indicating that the desorption points were not statistically different from the entire adsorption population at the 95% confidence level. Therefore, it was concluded that the desorption of PFOS from WPC PAC was not hysteretic under the experimental conditions used.

The mass of PFOA desorbed from the PAC during the ninth desorption step was 2.8% of the original sorbed mass, which was below the threshold of 3%, and thus the sequential desorption procedure stopped at step D9 (Figure 4.5). Desorption data D2 to D9 lie within the 95% prediction band, indicating that these desorption data were not statistically different from the adsorption population at the 95% level of confidence, and do not indicate hysteretic behaviour. However, desorption point D1 is located slightly outside of the 95% prediction band (C_s of D1 was 0.53 mg/g above the 95% prediction band), despite being corrected for the assumed 1% PAC lost in the first desorption step. The reason why D1 lies outside of the

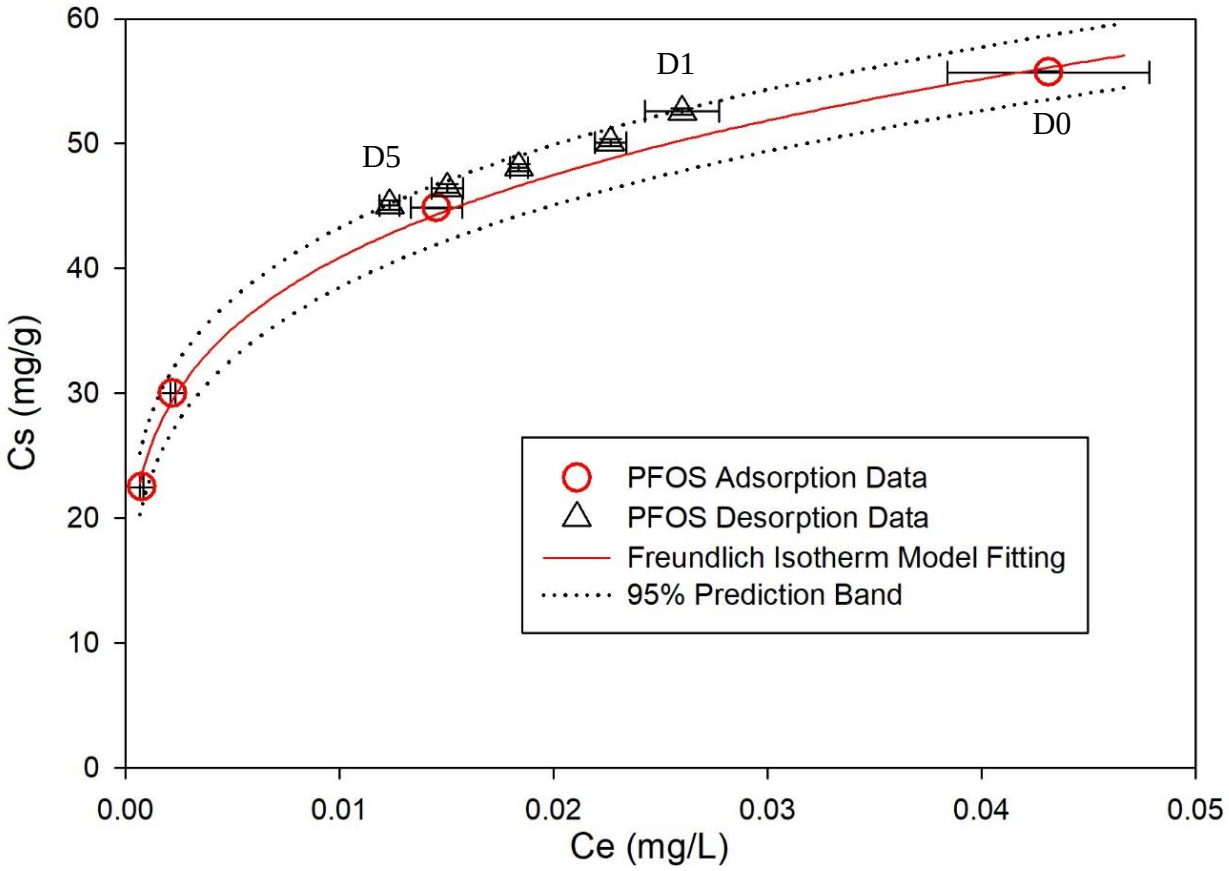


Figure 4.4: Adsorption and desorption of PFOS on retained WPC PAC. The experimental data (circles) are fit to the Freundlich Isotherm model (solid line), with the 95% prediction band of adsorption overlayed (dotted lines). Adsorption reaction solutions contained a range of 0.08–1 g/L of retained WPC PAC, and $[PFOS]_0$ = 4500 µg/L. Following adsorption, 90% of the PAC-free supernatant from D0 was removed, and the remaining solution was diluted with adsorbate-free buffer to 1000 mL. Desorption points D1 through D5 (triangles) represent the sequential desorption steps completed. Error bars on each point represent one standard deviation from the mean of three replicates.

prediction band is unclear. However, since every subsequent desorption point was located within the 95% prediction band, it was concluded there was no hysteretic behaviour for PFOA and PAC under the experimental conditions used.

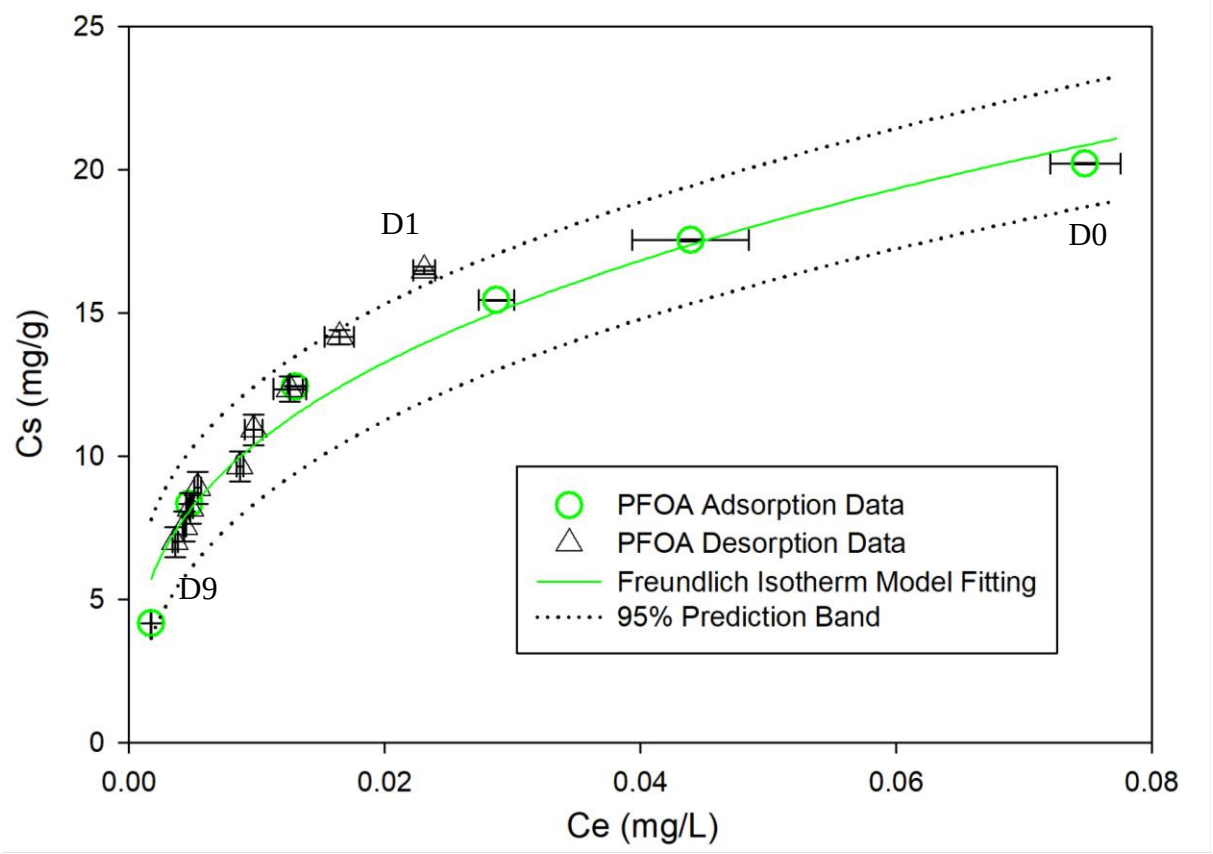


Figure 4.5: Adsorption and desorption of PFOA on retained WPC PAC. The experimental data (circles) are fit to the Freundlich Isotherm model (solid line), with the 95% prediction band of adsorption overlayed (dotted lines). Adsorption reaction solutions contained a range of 0.12–0.6 g/L of retained WPC PAC, and $[PFOA]_0$ = 2500 µg/L. Following adsorption, 90% of the PAC-free supernatant from D0 was removed, and the remaining solution was diluted with adsorbate-free buffer to 1000 mL. Desorption points D1 through D9 (triangles) represent the sequential desorption steps completed. Error bars on each point represent one standard deviation from the mean of three replicates.

In the PFBS desorption experiment, only four desorption steps were required to cover the same range of aqueous phase concentration as the adsorption isotherm, and thus, the experiment was terminated after desorption step 4 (Figure 4.6). Despite desorption data located on either side of the adsorption isotherm, all desorption data are contained within the 95% prediction band, indicating no hysteretic behaviour under the experimental conditions used.

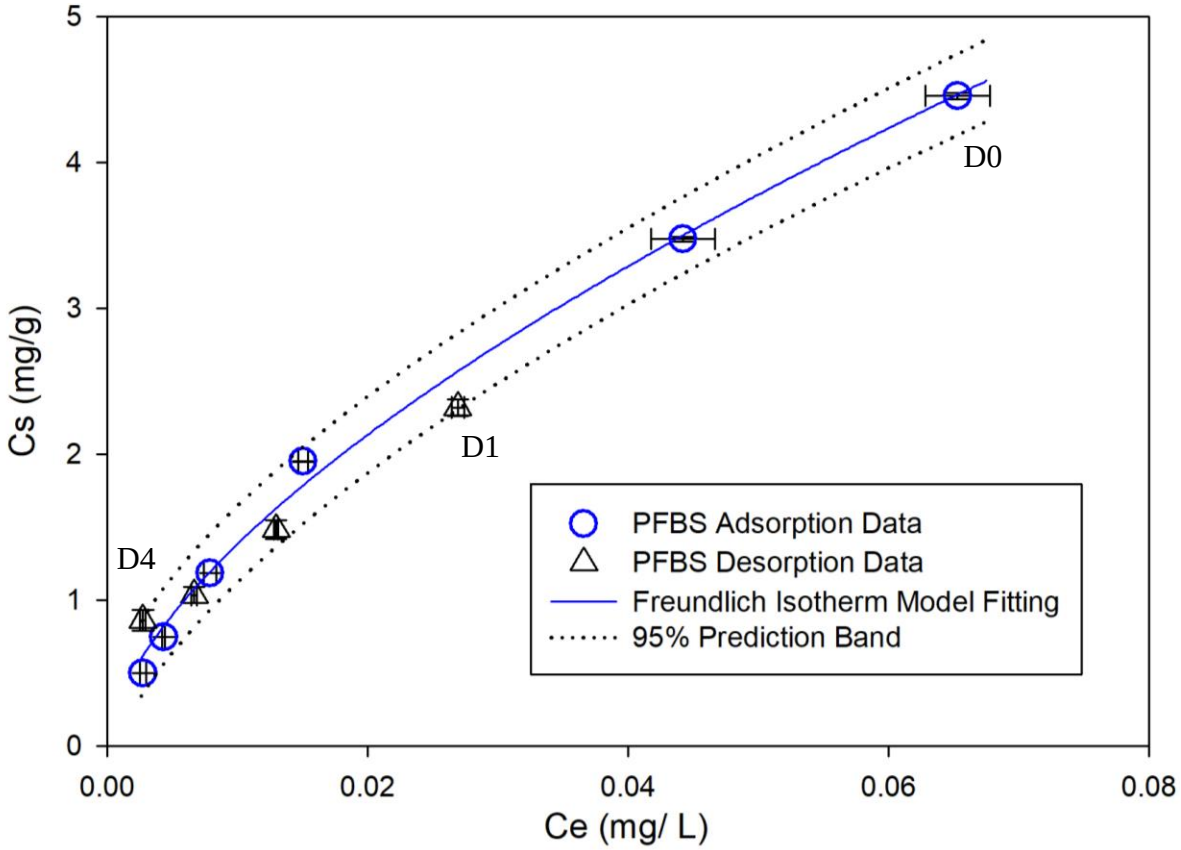


Figure 4.6: Adsorption and desorption of PFBS on retained WPC PAC. The experimental data (circles) are fit to the Freundlich Isotherm model (solid line), with the 95% prediction band of adsorption overlayed (dotted lines). Adsorption reaction solutions contained a range of 0.12–1.2 g/L of retained WPC PAC, and $[PFBS]_0$ = 600 µg/L. Following adsorption, 90% of the PAC-free supernatant from D0 was removed, and the remaining solution was diluted with adsorbate-free buffer to 500 mL. Desorption points D1 through D4 (triangles) represent the sequential desorption steps completed. Error bars on each point represent one standard deviation from the mean of three replicates.

4.2 Colloidal Activated Carbon Experiments

4.2.1 Adsorption and Desorption Kinetics

During the first 120 h of contact, 99.1%, 98.3%, and 94.1% of the total mass of PFOS, PFOA, and PFBS were adsorbed by the CAC. For both PFOS and PFOA, the mass adsorbed at 120 h and 168 h differed by less than 0.1%. Thus, equilibrium was assumed to be established by 120 h for both compounds (Figure 4.7). For PFBS, the adsorption equilibrium appeared to be reached by 72 h since the mass adsorbed at 72 h and 168 h differed by less than 0.1%. The pseudo first-order kinetic model (Equation 2.4) fit to the adsorption data generated k values of 0.706 /h (PFOS), 0.635 /h (PFOA), and 0.294 /h (PFBS) when $C_{s,eq}$ was set at 62.6 mg/g (PFOS), 18.5 mg/g (PFOA), and 2.66 mg/g (PFBS) (Table 4.4). Similar to the PAC results, although the pseudo first-order kinetic model fits the C_s data very well ($r^2 > 0.98$), there is an observed lack of fit between the observed C_w data and the simulated C_w profile at early time (0–48 h). Since most of the PFAS mass is associated with the solid phase, a slight lack of fit between the early C_s data and the model manifests as a larger variability in the simulated C_w

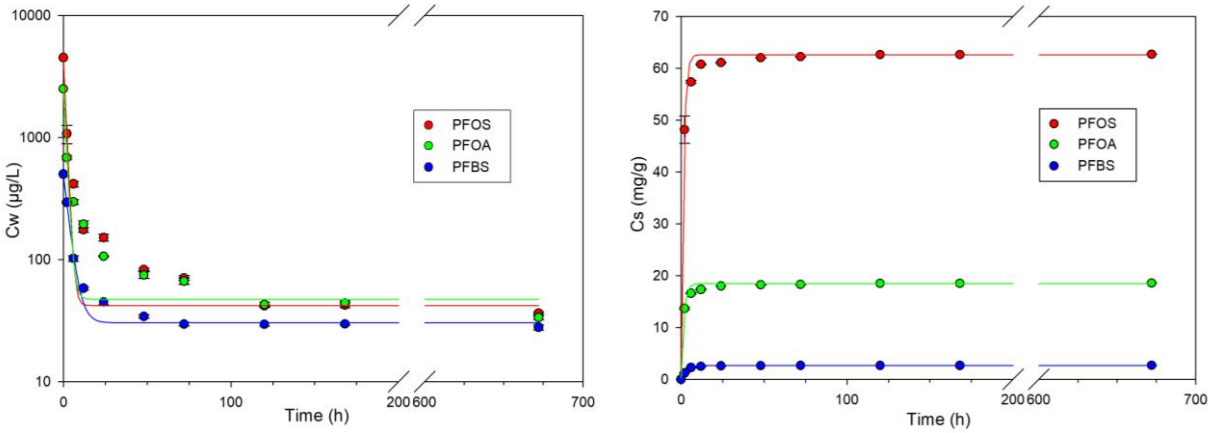


Figure 4.7: The concentration-time profiles for adsorption of PFOS, PFOA, and PFBS in 125-mL reaction solutions containing polymer-free CAC. Reaction solutions contained 0.0712 g/L (PFOS) or 0.133 g/L (PFOA and PFBS) of CAC, and either $[PFOS]_0$ = 4500 µg/L, $[PFOA]_0$ = 2500 µg/L, or $[PFBS]_0$ = 500 µg/L. Solid phase concentrations (C_s) were fit to the pseudo first-order kinetic function (the solid lines in the right panel). The model parameters were then used to generate predicted aqueous phase concentrations (solid lines in the left panel). Error bars represent one standard deviation.

profile relative to the observed C_w data. Despite this lack of fit to the early time data, t_{98} values for all compounds were < 15 h, which supports the assumption that equilibrium was established by 120 h (PFOS, PFOA) and 72 h (PFBS).

The initial adsorption rates, calculated based on the mass of adsorbate removed from the solution after 6 h, indicate that PFOS was adsorbed at the fastest rate (9.56 mg/g/h), followed by PFOA (2.76 mg/g/h), and then PFBS (0.374 mg/g/h) (Table 4.4). This trend is similar to that observed in the experiments with PAC. As in the kinetic experiments with PAC, the adsorption of PFOS and PFOA on CAC was observed to consist of two phases, namely a rapid adsorption phase during the first 6 h and a slower adsorption phase between 6 h and 120 h. In the second phase, adsorption rates decreased to 0.08, 0.03, and 0.006 mg/g/h for PFOS, PFOA, and PFBS, respectively, corresponding to a rate reduction of 120x, 95x and 62x. This two-phase adsorption behavior was also observed by Hakimabadi et al., who employed the same CAC material (Hakimabadi et al., 2023). It is hypothesized that this observation was caused by an intraparticle diffusion limitation where the diffusion of longer-chained PFAS is hindered due to their molecular size. This intraparticle diffusion limitation for larger PFAS might explain why PFBS reached equilibrium faster than PFOS and PFOA. Faster sorption of PFBS was also observed by Chen et al. who studied the adsorption of PFAS on polyacrylonitrile fiber-derived activated carbons (Chen et al., 2017).

Table 4.4: Summary of PFAS Adsorption Kinetic Parameters for Polymer-free CAC

Compound	Rate Coefficient, k (/h) ± 95% CI	Cs, eq (mg/g)	r^2	t_{98} (h)	Initial adsorption rate (6h) (mg sorbed /g AC /h)
PFOS	0.706 ± 0.070	62.6	0.991	5.54	9.56
PFOA	0.635 ± 0.073	18.5	0.987	6.16	2.76
PFBS	0.294 ± 0.013	2.66	0.997	13.3	0.374

Between 168 h and 672 h, C_w decreased from 42 to 36 µg/L for PFOS, 44 to 34 µg/L for PFOA, and 30 to 28 µg/L for PFBS. This change in C_w represents an additional 0.13%,

0.42%, and 0.36% of total mass adsorbed between 168 and 672 h for PFOS, PFOA, and PFBS, respectively, indicating minimal mass removal with extended contact time. To further verify that adsorption equilibrium was reached within 168 h, adsorption isotherms for PFOS, PFOA and PFBS were generated using contact times of 168 h and 672 h (Figure B.1). Since the 95% CI of both isotherms overlap, they were not considered statistically different, confirming that a contact time of 168 h would be sufficient for adsorption experiments. Although 168 h was deemed sufficient to reach equilibrium, the adsorption experiments that had a contact time of 672 h were used for the proceeding sub-sampling desorption experiments to ensure any additional mass removal did not impact desorption results.

In the desorption kinetic experiments, an apparent desorption equilibrium was reached by 120 h for PFOS, and 72 h for PFOA and PFBS (Figure 4.8). The first-order kinetic model (Equation 2.5) fit to the desorption data generated k values of 0.0443 /h (PFOS), 0.100 /h (PFOA), and 0.0989 /h (PFBS) when $C_{s,eq}$ was set to 31.7 mg/g (PFOS), 5.36 mg/g (PFOA) and 0.301 mg/g (PFBS) (Table 4.5). The first-order kinetic model appears to fit the PFOS and

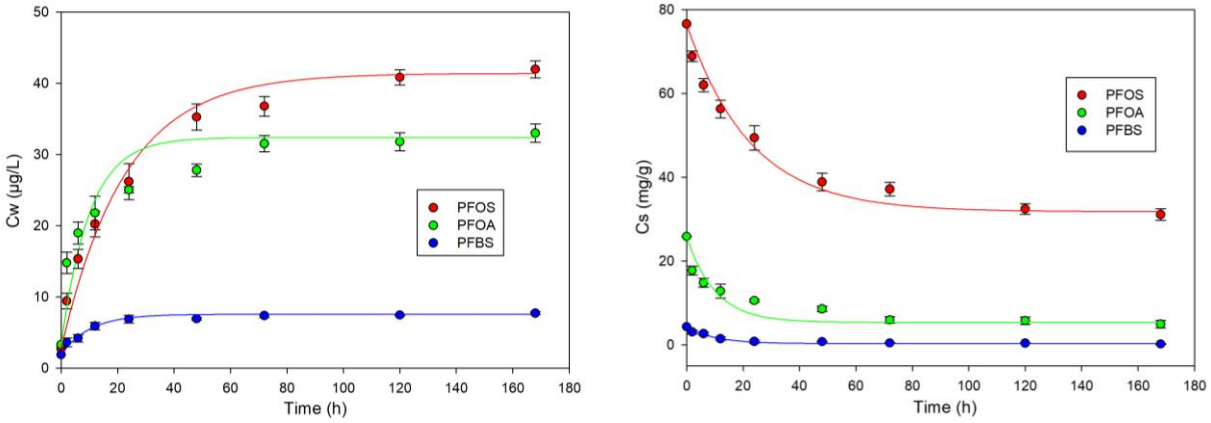


Figure 4.8: The concentration-time profiles for desorption of PFOS, PFOA, and PFBS in 125-mL reaction solutions containing polymer-free CAC. Original reaction solutions contained 0.0539 g/L (PFOS), or 0.0887 g/L (PFOA and PFBS) of CAC, and either $[PFOS]_0$ = 4500 µg/L , $[PFOA]_0$ = 2500 µg/L, or $[PFBS]_0$ = 500 µg/L, and were allowed 168 h to equilibrate. At a time of 0 h, 2 mL aliquots of well-mixed solution were diluted to 125 mL with adsorbate-free buffer to initiate desorption. Solid phase concentrations (C_s) were fit to the first-order kinetic function (the solid lines in the right panel). The model parameters were then used to generate predicted aqueous phase concentrations (solid lines in the left panel). Error bars represent one standard deviation.

PFBS C_s data well ($r^2 > 0.94$). However, for PFOA, the slight lack of fit to the C_s data between 2–48 h resulted in a lower r^2 of 0.87. Again, since most of the PFOA mass is associated with the solid phase, this lack of fit to the C_s data led to a larger variability in the simulated C_w profile compared to the observed C_w data between 2–48 h.

Larger t_{98} values (40–90 h) were observed for the desorption of the studied PFAS from CAC compared to PAC (12–26 h). The initial desorption rate over 6 h was in the following order: PFOS > PFOA > PFBS. Visually, the desorption of all compounds from CAC appears more gradual compared to PAC over 168 h. This may be indicative of deeper pores within the CAC that result in a more tortuous path for the PFAS to desorb from, compared to PAC.

Table 4.5: Summary of PFAS Desorption Kinetic Parameters for polymer-free CAC

Compound	Rate Coefficient, k (/h) ± 95% CI	Cs, eq (mg/g)	r^2	t_{98} (h)	Initial desorption rate (6h) (mg desorbed /g AC /h)
PFOS	0.0443 ± 0.0088	31.7	0.966	88.3	2.43
PFOA	0.100 ± 0.034	5.36	0.866	39.1	1.84
PFBS	0.0989 ± 0.0235	0.301	0.945	39.6	0.271

4.2.2 Adsorption and Desorption Experiments

In the adsorption isotherm experiments, PFOS exhibited the highest adsorption affinity, followed by PFOA, then PFBS (Figure 4.9), with K_d values of 2,130 L/g, 751 L/g, and 121 L/g for PFOS, PFOA, and PFBS, respectively, indicating that the sorption affinity of PFOS is approximately 2.84x greater than PFOA and 17.6x greater than PFBS. The best fit Freundlich model generated K_f values of 124 $[(mg/g)(mg/L)^{-n_f}]$ (PFOS), 38.6 $[(mg/g)(mg/L)^{-n_f}]$ (PFOA) and 11.0 $[(mg/g)(mg/L)^{-n_f}]$ (PFBS) and n_f values of 0.230 (PFOS), 0.234 (PFOA) and 0.430 (PFBS) (Table 4.6). At the 95% confidence, the n_f values of PFOS and PFOA are not statistically different. Small n_f values for PFOS and PFOA compared to PFBS demonstrate that the sorption energies of the sites PFOS and PFOA interact with are very heterogeneous, as demonstrated by the non-linearity of their adsorption curves (Figure 4.9).

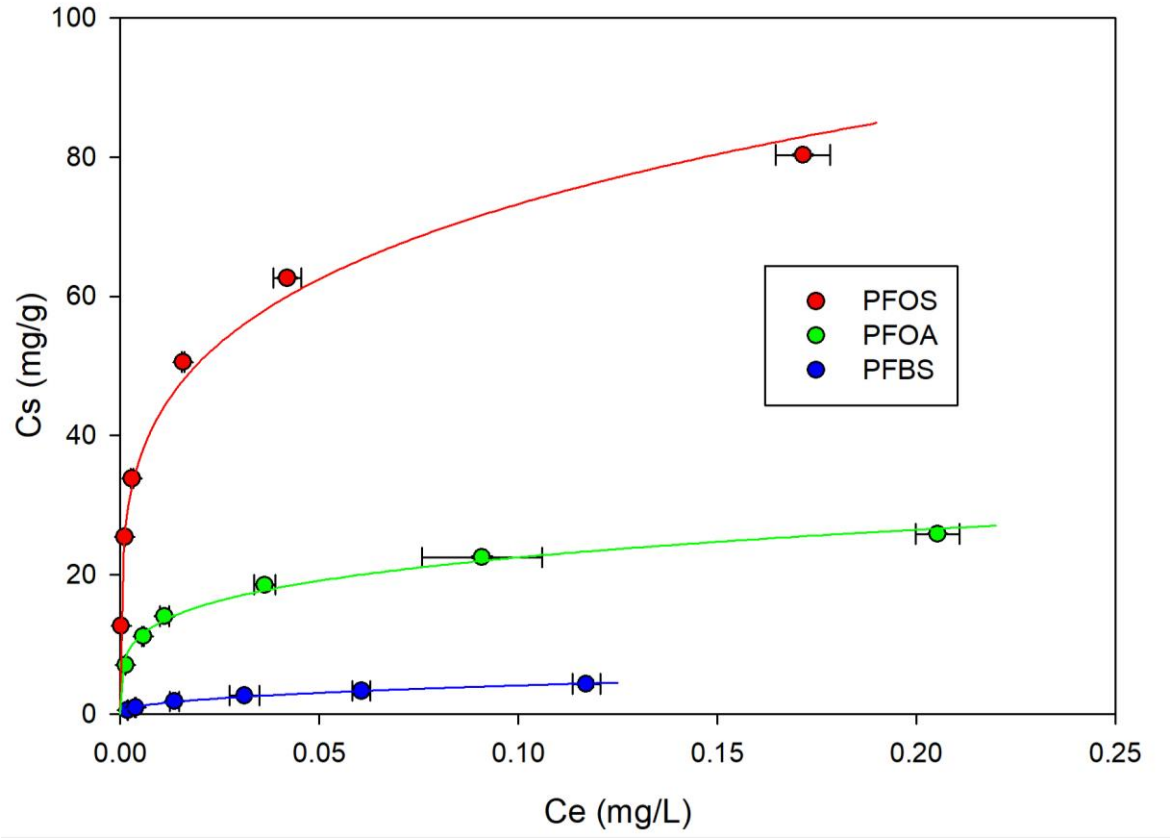


Figure 4.9: Adsorption isotherms for PFOS, PFOA, and PFBS on polymer-free CAC. The experimental data (circles) are fit to the Freundlich Isotherm model (solid lines). Error bars on each point represent one standard deviation from the mean of three replicates.

Table 4.6: Summary of Freundlich Adsorption Parameters for Polymer-Free CAC

Compound	K_F $(mg/g)(mg/L)^{-n_f}$	n_f	r^2	0.05 µM K_d (L/g)
PFOS	124 ± 8	0.230 ± 0.017	0.983	2130
PFOA	38.6 ± 2.0	0.234 ± 0.017	0.984	751
PFBS	11.0 ± 0.9	0.430 ± 0.028	0.990	121

For all three PFAS used, the desorption data are located below the adsorption curve (Figures 4.10 to 4.12). Possible explanations for this observation include:

(1) There were physical/chemical changes to the adsorbent, resulting in a decrease of sorption affinity over time. Physical/chemical changes to AC are often referred to as "carbon aging" (National Academy of Sciences, 1980), and could be caused by oxidation or fouling of the carbon surface (Cookson, 1978). In this research, long-term adsorption kinetics experiments (Figure 4.7) did not demonstrate a rebound of the aqueous phase concentrations between 168 h and 672 h of contact time. Furthermore, adsorption isotherms generated at 168 h and 672 h of contact are comparable (Figure B.1), indicating that physical/chemical changes to the AC did

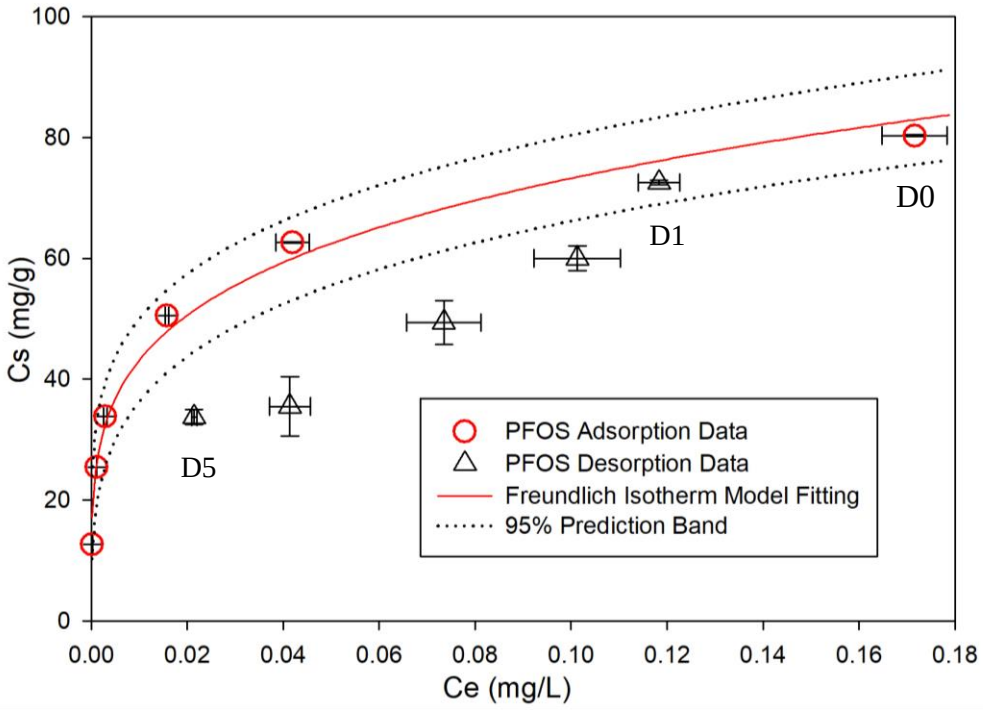


Figure 4.10: Adsorption and desorption of PFOS on polymer-free CAC. The adsorption data (circles) are fit to the Freundlich Isotherm model (solid line), with the 95% prediction band of adsorption overlayed (dotted lines). Adsorption reaction solutions contained a range of 0.054–0.36 g/L of polymer-free CAC, and $[PFOS]_0$ = 4500 µg/L. Following adsorption, varying sub-samples (1, 2, 5, 10, 25 mL) of D0 were diluted with adsorbate-free buffer to 125 mL to initiate desorption, creating desorption points D1 through D5 (triangles). Error bars on each point represent one standard deviation from the mean of three replicates.

not occur over time. As such, AC aging is unlikely the reason for the observed desorption behavior.

(2) The aqueous solution chemistry changed when the aliquot of suspended CAC from the adsorption step was diluted in the desorption experiments. During preliminary experimentation it was found that the polymer-free CAC added was basic, which can lead to a basic adsorption solution pH. As such, when an aliquot of well-mixed adsorption bottle solution is diluted to larger volumes, the pH of the new, desorption bottle solution may be different. Since the adsorption of PFAS has been shown to be dependent on the solution pH (Campos-Pereira et al., 2023; Nguyen et al., 2020; Yu et al., 2009; Higgins and Luthy, 2006), large changes to solution pH in the

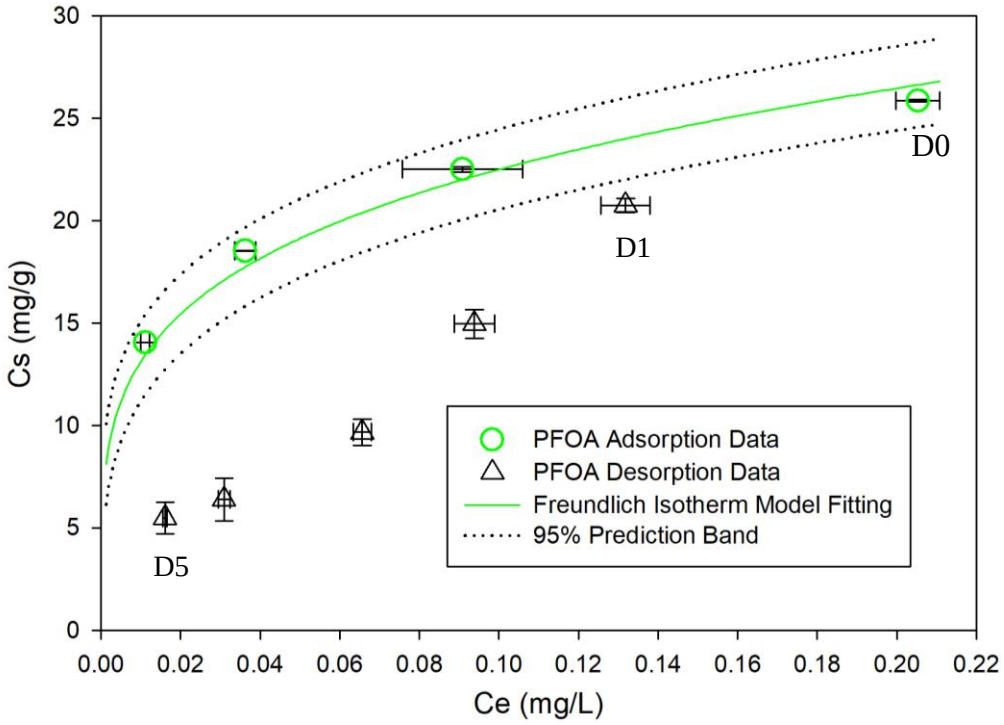


Figure 4.11: Adsorption and desorption of PFOA on polymer-free CAC. The adsorption data (circles) are fit to the Freundlich Isotherm model (solid line), with the 95% prediction band of adsorption overlayed (dotted lines). Adsorption reaction solutions contained a range of 0.089–0.36 g/L of polymer-free CAC, and $[PFOA]_0$ = 2500 µg/L. Following adsorption, varying sub-samples (1, 2, 5, 10, 25 mL) of D0 were diluted with adsorbate-free buffer to 125 mL to initiate desorption, creating desorption points D1 through D5 (triangles). Error bars on each point represent one standard deviation from the mean of three replicates.

desorption steps means the data can not be directly compared to adsorption. During adsorption experiments with polymer-free CAC, the pH ranged from 8.1 to 8.5 due to the different volumes of polymer-free CAC added. Throughout the desorption experiments, the solution pH dropped by less than 0.1 pH units from the desorption starting point, D0, to the final desorption point, D5. This small pH change was unlikely the cause, especially since a decrease in pH is expected to lead to enhanced adsorption, which would have shifted the desorption data to lower C_e values.

(3) The aliquots of well-mixed solution collected from the original adsorption bottles contained more CAC mass than anticipated. If there was more CAC than expected

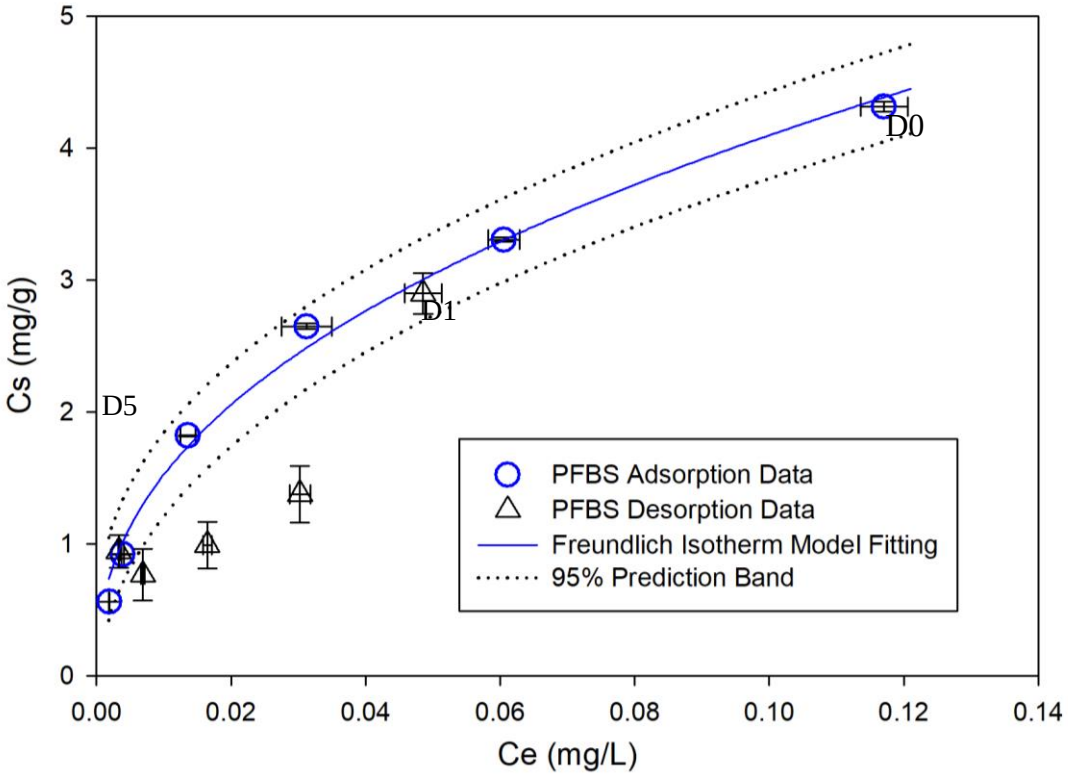


Figure 4.12: Adsorption and desorption of PFBS on polymer-free CAC. The adsorption data (circles) are fit to the Freundlich Isotherm model (solid line), with the 95% prediction band of adsorption overlayed (dotted lines). Adsorption reaction solutions contained a range of 0.089–0.89 g/L of polymer-free CAC, and $[PFBS]_0$ = 500 µg/L. Following adsorption, varying sub-samples (1, 2, 5, 10, 25 mL) of D0 were diluted with adsorbate-free buffer to 125 mL to initiate desorption, creating desorption points D1 through D5 (triangles). Error bars on each point represent one standard deviation from the mean of three replicates.

in these aliquots, there would be more PFAS available to desorb throughout experimentation, which may explain why the desorption data are shifted to a higher C_e.

To test hypothesis (3), an alternative method used by Bowman and Sans (Bowman and Sans, 1985) was adopted. In this method, several bottles replicating D0 are created. To initiate desorption, the entire well-mixed bottle solution is poured into larger bottles and diluted using adsorbate-free solution to varying total volumes. This whole bottle dilution method eliminates potential errors associated with the sub-sampling methodology. This methodology was tested for PFOS and polymer-free CAC and the results are shown in Figure 4.13. The Freundlich

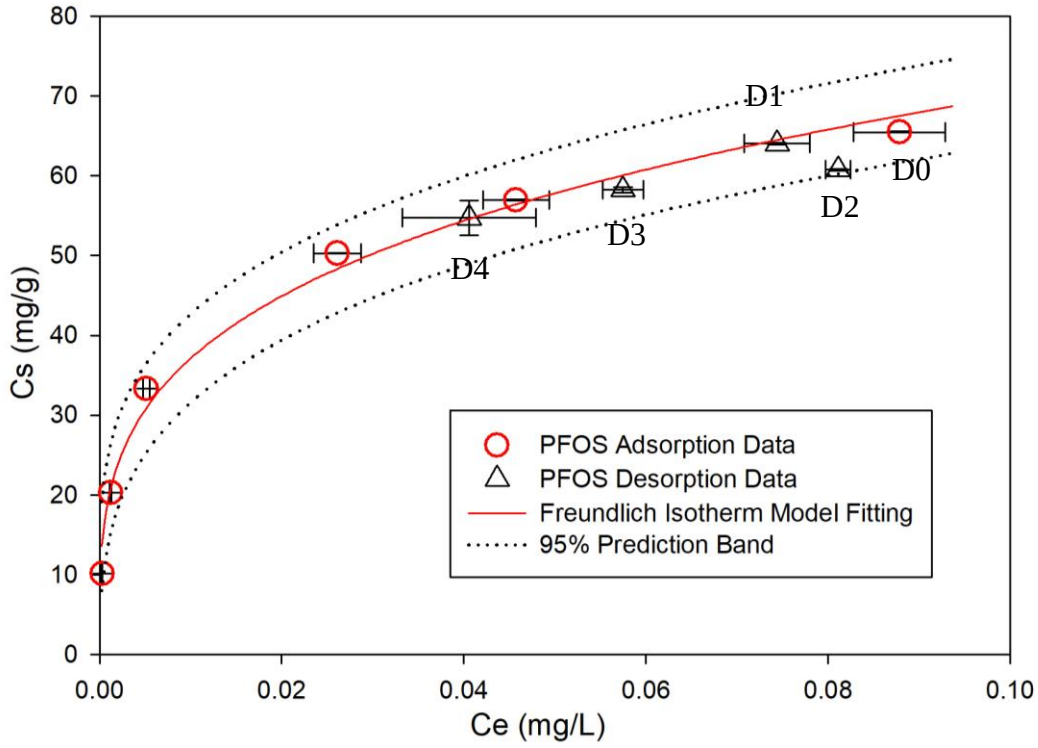


Figure 4.13: Adsorption and desorption of PFOS on polymer-free CAC. The adsorption data (circles) are fit to the Freundlich Isotherm model (solid line), with the 95% prediction band of adsorption overlayed (dotted lines). Adsorption reaction solutions contained a range of 0.067–0.44 g/L of polymer-free CAC, and $[PFOS]_0$ = 4500 µg/L. Following adsorption, whole bottles (50 mL) replicating D0 were diluted with adsorbate-free buffer to 125, 250, 500 and 1000 mL to initiate desorption, and represent desorption points D1 to D4 (triangles), respectively. Error bars on each point represent one standard deviation from the mean of three replicates.

model was fit to the adsorption data and generated a K_f of 132 $[(\mathrm{mg/g})(\mathrm{mg/L})^{-n_f}]$, n_f of 0.275 and r^2 of 0.986. With this method, all desorption data existed within the 95% prediction band of adsorption, indicating that the desorption data are not statistically different from the adsorption population. Therefore, under the experimental conditions used, it was determined that there is no apparent desorption hysteresis for a polymer-free CAC and PFOS system.

4.3 Discussion of Desorption Results Reported in the Literature

Previous studies reported that the sorption of PFAS on aquifer materials (Chen et al., 2022; Xiao et al., 2019; Millinovic et al., 2015; Pan et al., 2009), biochar (Zhi and Liu, 2018) and activated hydrochar (Chen et al., 2024) is hysteretic. Given that hydrophobic contaminants have higher affinity to PAC and CAC, the non-hysteretic behaviors of PFOS, PFOA, and PFBS on WPC PAC, and PFOS on CAC are somewhat surprising. Factors that may have led to these differences are discussed below.

The AC products used in this research adsorb PFAS mainly by hydrophobic interactions (Hakimabadi et al., 2023). Conversely, the adsorption of PFAS to sediments is driven by both hydrophobic and electrostatic effects (Li and Liu, 2022; Zhang et al., 2013; Johnson et al., 2007; Higgins and Luthy, 2006). In particular, in soils with high TOC, the predominant mechanism of PFAS adsorption by sediments is hydrophobic interactions, whereas surface electrostatic interactions are predominant for low TOC sediments (Johnson et al., 2007). The sorption of PFAS to soils may also be influenced by ligand and ion exchange (Barzen-Hanson et al., 2017; Wei et al., 2017; Du et al., 2014), indicating the potential for chemisorption. It is hypothesized that the PFAS sorption hysteresis on aquifer sediments was due to the ligand and ion exchange mechanisms, which result in chemical bonding between the adsorbate and adsorbent. It is also worth noting that the sorption of PFAS to soils is also controlled by salinity and the presence of cations (e.g., Ca^{2+}) (Wang et al., 2022; You et al., 2009; Higgins and Luthy, 2006). Specifically, it has been shown that increasing $CaCl_2$ concentrations in the desorption solutions leads to greater irreversibility of sorption, which was described as an effect of the cation-bridging mechanism (You et al., 2009). Therefore, it is possible that aquifer sediments taken from a site with elevated concentrations of salinity and

cations may demonstrate hysteretic behaviour since these constituents can be bound to the sediment surface.

It is also worth noting that a lack of adsorption and desorption equilibrium is a recognized experimental artifact in isotherm experiments (Huang and Weber, 1998). While desorption hysteresis for PFAS from sediments has been reported in previous studies, a common thread in those studies is the possibility that the reactor bottles used might not be at equilibrium when sampled. For example, in the work reported by Chen et al., significant desorption hysteresis of PFAS from urban water body sediments was observed (Chen et al., 2016). In this study, the contact time for equilibrating the adsorption solution was also adopted for their sequential desorption steps. However, the assumption that desorption kinetics can be approximated by the adsorption kinetic data may not be valid, especially since desorption of PFAS from aquifer sediments is observed to be slower than adsorption (Xiao et al., 2019; Zhi and Liu, 2018; Higgins and Luthy, 2006). It is hypothesized that the slow desorption kinetics of some PFAS from soils, as indicated by Schaefer et al., (Schaefer et al., 2021), may cause the appearance of hysteresis.

Chapter 5
Conclusions, Insights and Recommendations

5.1 Conclusions

To understand the fate and transport of PFAS within in-situ AC barriers, a thorough understanding of both adsorption and desorption processes is required. The generation of adsorption and desorption data [C_e, C_s] allows the comparison of desorption data to the adsorption data. Asymmetry between adsorption and desorption data (i.e., $C_{s,\,des} > C_{s,\,ads}$ for a given C_e value) is a known indication of hysteresis (Xiao et al., 2019). Desorption data can also be classified as reversible (AC will eventually release the sorbed PFAS as the aqueous concentration decreases) or irreversible (a fraction of PFAS is permanently sorbed that will not be released).

The research reported in this thesis is believed to be the first that implemented a batch serial dilution method to investigate the sequential desorption of PFOS, PFOA and PFBS from AC. The research focused specifically on the desorption behavior of these three PFAS on WPC PAC and a polymer-free form of Plumestop™ CAC, which are the adsorbents that are being used for the in-situ immobilization of PFAS. Adsorption and desorption kinetic experiments were completed for both WPC PAC and polymer-free CAC to ensure data represented near equilibrium conditions. The bottle-point method was adopted to generate adsorption isotherm data using a single PFAS, and PAC or CAC. For desorption experiments with PAC, the aqueous phase was replaced with adsorbate-free solution at each desorption step, generating a sequential desorption dataset. For desorption experiments with CAC, two methodologies were adopted. The first was a sub-sampling method, where assumed well-mixed aliquots were diluted with adsorbate-free buffer solution to initiate desorption. The second methodology was a whole-bottle dilution method, where the contents of the entire bottle were diluted to larger volumes to initiate desorption. Desorption was considered not hysteretic if data were located inside of the 95% adsorption prediction band.

The adsorption and desorption of PFOS, PFOA or PFBS on retained (>20 µm) WPC PAC reached equilibrium by 72 h and consisted of a fast adsorption phase within the first 6 h, followed by a slower adsorption phase between 6 h and 72 h. During the sequential desorption experiments with PFOS, PFOA and PFBS, a total of five, nine, and four desorption steps were completed, respectively. These sequential desorption experiments did not show evidence of hysteretic behaviour for PFOS, PFOA, or PFBS, as indicated by the desorption data contained within the 95% prediction band of the adsorption data. Within the concentration ranges explored, sorption of PFOS, PFOA and PFBS to retained WPC PAC appears reversible.

Adsorption of PFOS, PFOA or PFBS on polymer-free CAC reached equilibrium by 120 h, and consisted of a fast adsorption phase within the first 6 h, followed by a slower adsorption phase between 6 h and 120 h. This two-phase adsorption rate was most apparent for the longer-chained PFOS and PFOA. For experiments that adopted the sub-sampling method, the resulting desorption data for PFOS, PFOA and PFBS were located below their respective adsorption isotherms (i.e., $C_{s,\ des} < C_{s,\ ads}$ for a given C_e value). This was attributed to unrepresentative sub-sampling from the initial adsorption bottle, where more CAC than expected was present in each assumed well-mixed aliquot. When the whole-bottle dilution method was adopted with PFOS on polymer-free CAC, the resulting desorption data was located within the 95% prediction band of the adsorption data. This result demonstrated no hysteretic behaviour between polymer-free CAC and PFOS, and sorption appears reversible within the concentration ranges explored.

Although the goal of this research was not to directly compare the performance of AC particulate amendments, the dataset assembled provided the opportunity to contrast some PAC and CAC behaviours. First, the initial adsorption rates to PAC and CAC were similar with PFOS > PFOA > PFBS (9.56 to 0.374 mg/g/h), while the first-order reaction rate coefficients were higher for CAC (PFOS ≈ PFOA > PFBS; k ranged from 0.706 to 0.294 /h) than for PAC (PFBS ≈ PFOA > PFOS; k ranged from 1.15 to 0.425 /h). Second, the initial desorption rates were greater from CAC (PFOS > PFOA > PFBS; 2.43 to 0.271 mg/g/h) compared to PAC (PFBS > PFOS > PFOA; 0.0230 to 0.0157 mg/g/h) while the pseudo first-order reaction rate

coefficients for desorption from PAC (PFBS > PFOS ≈ PFOA; *k* ranged from 0.341 to 0.152 /h) where higher than from CAC (PFOA ≈ PFBS > PFOS; *k* ranged from 0.100 to 0.0443 /h). Third, the K_d values at an aqueous concentration of 0.05 µM follow PFOS > PFOA > PFBS and were higher for CAC (2130 to 121 L/g) than for PAC (1990 to 119 L/g). Adsorption isotherms for PAC and CAC show that for PFOS, CAC exhibits a higher sorbed phase concentration over the entire range of aqueous concentrations explored. For PFOA and PFBS, the isotherms generated for PAC and CAC cross, and at concentrations > 0.1 mg/L for PFOA and > 0.01 mg/L for PFBS, PAC exhibited a higher sorbed phase concentrations than CAC. Lastly, there was no evidence of desorption hysteresis for PAC (PFOS, PFOA, PFBS) and CAC (PFOS) under the experimental conditions used.

5.2 Limitations and Recommendations

Since this is the first known study that investigated desorption of PFAS from AC particulate amendments using a sequential desorption methodology, the experimental design was simplified to limit the factors that may influence hysteretic behaviour. As a result, the following limitations of this research have been identified and recommendations are suggested for future work:

a) The whole-bottle dilution method using polymer-free CAC was only adopted for a single PFAS (PFOS). It is possible that not all PFAS will exhibit reversible sorption, as was observed for PFOS. Hence the desorption data for polymer-free CAC are limited and may not be sufficient to understand the fate and transport of other PFAS within an AC barrier.

   To address the lack of studied compounds the whole-bottle dilution method should be implemented to investigate the desorption of other PFAS from polymer-free CAC. Doing so will establish a greater understanding PFAS desorption behaviour from polymer-free CAC.

b) Since the mass removal at each desorption step was extremely small compared to the sorbed fraction, the collected desorption data did not span the entire concentration range and reach aqueous equilibrium concentrations near MDL. Therefore, it is unclear whether

sorption of PFAS to these AC amendments is reversible or irreversible. When using high-affinity adsorbents, the batch serial dilution method (PAC) and the whole bottle dilution method (CAC) used would require much larger dilution volumes than employed in this research to assess reversibility.

To overcome these dilution limitations adsorption-desorption column studies should be considered to determine the potential irreversibly of PFAS on AC.

c) The experiments used an idealized 1 mM sodium bicarbonate buffer solution for all adsorption and desorption experiments. In actual groundwater systems near AFFF sites, there is expected to be a complex mixture of PFAS combined with other co-contaminants that may compete for sorption sites (Fan et al., 2017; Moody and Field, 2000). The competition between co-contaminants and PFAS for sorption sites on AC may lead to the desorption of weaker-sorbing PFAS. This effect of co-contaminants on PFAS adsorption and desorption was not investigated in this research. Similarly, the effect of groundwater chemistry on adsorption and desorption of PFAS was not evaluated in this research. As such, the results obtained may not be fully representative of the in-situ desorption behaviour of PFAS from AC.

   To address the simplified solution chemistry used, future desorption experiments should incorporate an aqueous solution that is representative of typical groundwater at AFFF sites. This will allow the investigation of whether groundwater chemistry affects hysteretic behaviour.

d) This research did not investigate the impact of biofilm growth on AC following the adsorption of PFAS. If groundwater conditions are amenable to microbial growth (i.e., a biodegradable substrate is present), this process has the potential to trap sorbed PFAS within the AC pore structure, which may lead to irreversible sorption.

   To address the lack of understanding of biofilm growth on AC desorption research should incorporate the growth of biofilm on AC following adsorption of PFAS, to see if biofilm-coated AC will impact desorption processes.

References

Abbasian Chaleshtari, Z., and Foudazi, R. (2022). A Review on Per- and Polyfluoroalkyl Substances (PFAS) Remediation: Separation Mechanisms and Molecular Interactions. In *ACS ES and T Water* (Vol. 2, Issue 12, pp. 2258–2272). American Chemical Society. https://doi.org/10.1021/acsestwater.2c00271

Adamson, D. T., Kulkarni, P. R., Nickerson, A., Higgins, C. P., Field, J., Schwichtenberg, T., Newell, C., and Kornuc, J. J. (2022). Characterization of relevant site-specific PFAS fate and transport processes at multiple AFFF sites. *Environmental Advances, 7*. https://doi.org/10.1016/j.envadv.2022.100167

Adamson, A.W., Gast, A.P. (1997). Physical Chemistry of Surfaces, 6th ed. John Wiley and Sons, Inc. New York.

Agbovi, H. K., & Wilson, L. D. (2021). Adsorption processes in biopolymer systems: fundamentals to practical applications. In Natural Polymers-Based Green Adsorbents for Water Treatment (pp. 1–51). Elsevier. https://doi.org/10.1016/B978-0-12-820541-9.00011-9.

Aktaş, Ö., & Çeçen, F. (2006). Effect of type of carbon activation on adsorption and its reversibility. *Journal of Chemical Technology and Biotechnology*, *81*(1), 94–101. https://doi.org/10.1002/jctb.1363

Barzen-Hanson, K. A., Davis, S. E., Kleber, M., & Field, J. A. (2017). Sorption of Fluorotelomer Sulfonates, Fluorotelomer Sulfonamido Betaines, and a Fluorotelomer Sulfonamido Amine in National Foam Aqueous Film-Forming Foam to Soil. Environmental Science and Technology, 51(21), 12394–12404. https://doi.org/10.1021/acs.est.7b03452

Bowman, B. T. (1979). Method of repeated additions for generating pesticide adsorption-desorption isotherm data. *Can. J. Soil Sci. 59*, 435-437. https://doi.org/10.4141/cjss79-050

Bowman, B. T., & Sans, W. W. (1985). Partitioning Behavior of Insecticides in Soil-Water Systems: II. Desorption Hysteresis Effects. *Journal of Environmental Quality*, *14*(2), 270–273. https://doi.org/10.2134/jeq1985.00472425001400020023x

Bowman, B. T., & Sans, W. W. (1977). Adsorption of Parathion, Fenitrothion, Methyl Parathion, Aminoparathion and Paraoxon by Na+, Ca2+, and Fe3+ Montmorillonite Suspensions. *Soil Science Society of America Journal*, *41*(3), 514–519. https://doi.org/10.2136/sssaj1977.03615995004100030016x

Braida, W. J., Pignatello, J. J., Lu, Y., Ravikovitch, P. I., Neimark, A. v., & Xing, B. (2003). Sorption hysteresis of benzene in charcoal particles. *Environmental Science and Technology*, *37*(2), 409–417. https://doi.org/10.1021/es020660z

Bruton, T. A., & Sedlak, D. L. (2017). Treatment of Aqueous Film-Forming Foam by Heat Activated Persulfate under Conditions Representative of in Situ Chemical Oxidation. *Environmental Science and Technology*, *51*(23), 13878–13885. https://doi.org/10.1021/acs.est.7b03969

Butt, C. M., Muir, D. C. G., & Mabury, S. A. (2014). Biotransformation pathways of fluorotelomer-based polyfluoroalkyl substances: A review. *Environmental Toxicology and Chemistry*, *33*(2), 243–267. https://doi.org/10.1002/etc.2407

Campos-Pereira, H., Kleja, D. B., Ahrens, L., Enell, A., Kikuchi, J., Pettersson, M., & Gustafsson, J. P. (2023). Effect of pH, surface charge and soil properties on the solid–solution partitioning of perfluoroalkyl substances (PFASs) in a wide range of temperate soils. *Chemosphere*, *321*. https://doi.org/10.1016/j.chemosphere.2023.138133

Carey, G. R., Hakimabadi, S. G., Singh, M., McGregor, R., Woodfield, C., van Geel, P. J., & Pham, A. L. T. (2022). Longevity of colloidal activated carbon for in situ PFAS remediation at AFFF-contaminated airport sites. *Remediation*, *33*(1), 3–23. https://doi.org/10.1002/rem.21741

Carter, K. E., & Farrell, J. (2008). Oxidative destruction of perfluorooctane sulfonate using boron-doped diamond film electrodes. *Environmental Science and Technology*, *42*(16), 6111–6115. https://doi.org/10.1021/es703273s

Carter, K. E., & Farrell, J. (2010). Removal of perfluorooctane and perfluorobutane sulfonate from water via carbon adsorption and ion exchange. *Separation Science and Technology*, *45*(6), 762–767. https://doi.org/10.1080/01496391003608421

Çeçen, F., Aktaş, Ö. (2011). *Activated carbon for water and wastewater treatment: integration of adsorption and biological treatment.* Wiley-VCH.

Chen, F., Chen, J., Liu, X., Zhi, Y., Qian, S., Li, W., & Wang, X. (2024). Removal of per- and polyfluoroalkyl substances by activated hydrochar derived from food waste: Sorption performance and desorption hysteresis. *Environmental Pollution*, *340*, 122820. https://doi.org/10.1016/j.envpol.2023.122820

Chen H., Reinhard M., You L., Gin, K. (2022). Effect of repeated sorption-desorption on

irreversible and reversible adsorption of hydrophobic perfluoroalkyl acids to freshwater sediment. Environ. Sci. Innov. 28. 102673. https://doi.org/10.1016/j.eti.2022.102673.

Chen, H., Reinhard, M., Nguyen, V. T., & Gin, K. Y. H. (2016). Reversible and irreversible sorption of perfluorinated compounds (PFCs) by sediments of an urban reservoir. *Chemosphere*, *144*, 1747–1753. https://doi.org/10.1016/j.chemosphere.2015.10.055

Chen, W., Zhang, X., Mamadiev, M., & Wang, Z. (2017). Sorption of perfluorooctane sulfonate and perfluorooctanoate on polyacrylonitrile fiber-derived activated carbon fibers: In comparison with activated carbon. *RSC Advances*, *7*(2), 927–938. https://doi.org/10.1039/c6ra25230c

Cookson, J.T. (1978). *Adsorption mechanisms: the chemistry of organic adsorption on activated carbon*. Carbon Adsorption Handbook (Pp. 241–279). Ann Arbor Science Publishers, Inc., Ann Arbor, Mich.

de Jonge, R. J., Breure, A. M., & van Andel, J. G. (1996). Reversibility of Adsorption of Aromatic Compounds onto Powdered Activated Carbon (PAC). In *Wat. Res 30*(4). https://doi.org/10.1016/0043-1354(95)00248-0.

Du, Z., Deng, S., Bei, Y., Huang, Q., Wang, B., Huang, J., & Yu, G. (2014). Adsorption behavior and mechanism of perfluorinated compounds on various adsorbents-A review. In Journal of Hazardous Materials (Vol. 274, pp. 443–454). Elsevier. https://doi.org/10.1016/j.jhazmat.2014.04.038

Espana, V. A., Mallavarapu, M., & Naidu, R. (2015). Treatment technologies for aqueous perfluorooctanesulfonate (PFOS) and perfluorooctanoate (PFOA): A critical review with an emphasis on field testing. In *Environmental Technology and Innovation* (Vol. 4, pp. 168–181). Elsevier. https://doi.org/10.1016/j.eti.2015.06.001

Fan, D., Gilbert, E. J., & Fox, T. (2017). Current state of in situ subsurface remediation by activated carbon-based amendments. In *Journal of Environmental Management* (Vol. 204, pp. 793–803). Academic Press. https://doi.org/10.1016/j.jenvman.2017.02.014

Fleer, G.J., Scheutjens, J.M.H.M., Cohen Stuart, M.A., Cosgrove, T., Vincent, B. (1993). Polymers at Interfaces. https://doi.org/10.1007/978-94-011-2130-9

Gadkaree, K.P., Heuchel, M., Jaroniec, M. (1996). Studies of Active Carbons of Controlled Structural Properties. Proceedings of the Fifth International Conference on Fundamentals of Adsorption (pp. 301–308). Kluwer Academic Publishers, Boston, Massachusetts.

Georgi, A., Schierz, A., Mackenzie, K., & Kopinke, F. D. (2015). Colloidal activated carbon for in-situ groundwater remediation - Transport characteristics and adsorption of organic compounds in water-saturated sediment columns. *Journal of Contaminant Hydrology*, *179*, 76–88. https://doi.org/10.1016/j.jconhyd.2015.05.002

Glüge, J., Scheringer, M., Cousins, I. T., Dewitt, J. C., Goldenman, G., Herzke, D., Lohmann, R., Ng, C. A., Trier, X., & Wang, Z. (2020). An overview of the uses of per- And polyfluoroalkyl substances (PFAS). *Environmental Science: Processes and Impacts*, *22*(12), 2345–2373. https://doi.org/10.1039/d0em00291g

Government of Canada (2017, June 9). Groundwater Contamination. https://www.canada.ca/en/environment-climate-change/services/water-overview/pollution-causes-effects/groundwater-contamination.html

Government of Canada (2023). Draft State of Per- and Polyfluoroalkyl Substances (PFAS) Report. https://www.canada.ca/en/environment-climate-change/services/evaluating-existing-substances/draft-state-per-polyfluoroalkyl-substances-report.html

Hakimabadi, S. G., Taylor, A., & Pham, A. L. T. (2023). Factors Affecting the Adsorption of Per- and Polyfluoroalkyl Substances (PFAS) by Colloidal Activated Carbon. *Water Research*, *242*. https://doi.org/10.1016/j.watres.2023.120212

Hao, S., Choi, Y. J., Wu, B., Higgins, C. P., Deeb, R., & Strathmann, T. J. (2021). Hydrothermal alkaline treatment for destruction of per-and polyfluoroalkyl substances in aqueous film-forming foam. *Environmental Science and Technology*, *55*(5), 3283–3295. https://doi.org/10.1021/acs.est.0c06906

Hao, S., Choi, Y. J., Deeb, R. A., Strathmann, T. J., & Higgins, C. P. (2022). Application of Hydrothermal Alkaline Treatment for Destruction of Per- and Polyfluoroalkyl Substances in Contaminated Groundwater and Soil. *Environmental Science and Technology*, *56*(10), 6647–6657. https://doi.org/10.1021/acs.est.2c00654

Hao, S., Reardon, P. N., Choi, Y. J., Zhang, C., Sanchez, J. M., Higgins, C. P., & Strathmann, T. J. (2023). Hydrothermal Alkaline Treatment (HALT) of Foam Fractionation Concentrate Derived from PFAS-Contaminated Groundwater. *Environmental Science and Technology*, *57*(44), 17154–17165. https://doi.org/10.1021/acs.est.3c05140

Houtz, E. F., & Sedlak, D. L. (2012). Oxidative conversion as a means of detecting precursors to perfluoroalkyl acids in urban runoff. *Environmental Science and Technology*, *46*(17), 9342–9349. https://doi.org/10.1021/es302274g

Houtz, E. F., Higgins, C. P., Field, J. A., & Sedlak, D. L. (2013). Persistence of

perfluoroalkyl acid precursors in AFFF-impacted groundwater and soil. *Environmental Science and Technology*, *47*(15), 8187–8195. https://doi.org/10.1021/es4018877

Hu, H., & Xu, K. (2020). Chapter 8 - Physicochemical technologies for HRPs and risk control. *High-Risk Pollutants in Wastewater*, 169–207. https://doi.org/10.1016/B978-0-12-816448-8.00008-3

Huang, W., Weber, W. (1997). A Distributed Reactivity Model for Sorption by Soils and Sediments. 10. Relationships between Desorption, Hysteresis, and the Chemical Characteristics of Organic Domains. *Environ. Sci. Technol. 31*, 2562-2569. https://doi.org/10.1021/es960995e

Huang, W., Yu, H., & Weber, W. J. (1998). Hysteresis in the sorption and desorption of hydrophobic organic contaminants by soils and sediments 1. A comparative analysis of experimental protocols. In *Journal of Contaminant Hydrology* (Vol. 31). https://doi.org/10.1016/S0169-7722(97)00056-9

Higgins, C. P., & Luthy, R. G. (2006). Sorption of perfluorinated surfactants on sediments. *Environmental Science and Technology*, *40*(23), 7251–7256. https://doi.org/10.1021/es061000n

Interstate Technology & Regulatory Council (ITRC) (2023). Per- and Polyfluoroalkyl Substances (PFAS). https://pfas-1.itrcweb.org/#1_7

Johnson, R. L., Anschutz, A. J., Smolen, J. M., Simcik, M. F., & Lee Penn, R. (2007). The adsorption of perfluorooctane sulfonate onto sand, clay, and iron oxide surfaces. *Journal of Chemical and Engineering Data*, *52*(4), 1165–1170. https://doi.org/10.1021/je060285g

Kan, A. T., Fu, G., Hunter, M.A., & Tomson, M.B. (1997). Irreversible Adsorption of Naphthalene and Tetrachlorobiphenyl to Lula and Surrogate Sediments. *Environmental Science and Technology, 31(8),* 2176–2185. https://doi.org/10.1021/es9601954

Key, B. D., Howell, R. D., & Criddle, C. S. (1998). Defluorination of Organofluorine Sulfur Compounds by Pseudomonas Sp. Strain D2. *Environmental Science and Technology, 32(15),* 2283–2287. https://doi.org/10.1021/es9800129

Kissa E. (2001). Fluorinated Surfactants and Repellents, Second Edition. Surfactant science series 97. New York (NY): Marcel Dekker. 640 p. ISBN: 9780824704728.

Krause, M. J., Thoma, E., Endalkachew, S., Crone, B., Whitehill, A., Shields, E., & Gullett,

B. (2021). Supercritical Water Oxidation as an Innovative Technology for PFAS Destruction. *Journal of Environmental Engineering, 148*(2). https://doi.org/10.1061/(ASCE)EE.1943

Kümmel, A., Bonate, P. L., Dingemanse, J., & Krause, A. (2018). Confidence and Prediction Intervals for Pharmacometric Models. *CPT: Pharmacometrics and Systems Pharmacology, 7*(6), 360–373. https://doi.org/10.1002/psp4.12286

Li, L., Quinlivan, P. A., & Knappe, D. R. U. (2002). Effects of activated carbon surface chemistry and pore structure on the adsorption of organic contaminants from aqueous solution. *Carbon, 40*(12), 2085–2100. https://doi.org/10.1016/S0008-6223(02)00069-6

Liang, S., Pierce, R. "David," Lin, H., Chiang, S. Y. D., & Huang, Q. "Jack." (2018). Electrochemical oxidation of PFOA and PFOS in concentrated waste streams. *Remediation, 28*(2), 127–134. https://doi.org/10.1002/rem.21554

Liou, J. S. C., Szostek, B., DeRito, C. M., & Madsen, E. L. (2010). Investigating the biodegradability of perfluorooctanoic acid. *Chemosphere, 80*(2), 176–183. https://doi.org/10.1016/j.chemosphere.2010.03.009

Li, C., & Liu, L. (2022). Fate and transport of perfluorinated compounds in soils and groundwater. In *Emerging Contaminants in Soil and Groundwater Systems: Occurrence, Impact, Fate and Transport* (pp. 119–163). Elsevier. https://doi.org/10.1016/B978-0-12-824088-5.00008-2

Liu, J., & Mejia Avendaño, S. (2013). Microbial degradation of polyfluoroalkyl chemicals in the environment: A review. In *Environment International* 61, (pp. 98–114). Elsevier. https://doi.org/10.1016/j.envint.2013.08.022

Liu, C. J., Strathmann, T. J., & Bellona, C. (2021). Rejection of per- and polyfluoroalkyl substances (PFASs) in aqueous film-forming foam by high-pressure membranes. *Water Research, 188*. https://doi.org/10.1016/j.watres.2020.116546

Liu, C., Hatton, J., Arnold, W. A., Simcik, M. F., & Pennell, K. D. (2020). In Situ Sequestration of Perfluoroalkyl Substances Using Polymer-Stabilized Powdered Activated Carbon. *Environmental Science and Technology, 54*(11), 6929–6936. https://doi.org/10.1021/acs.est.0c00155

McGregor, R. (2018). In Situ treatment of PFAS-impacted groundwater using colloidal activated Carbon. *Remediation, 28*(3), 33–41. https://doi.org/10.1002/rem.21558

McGregor, R. (2020). Six pilot-scale studies evaluating the in situ treatment of PFAS in

groundwater. *Remediation*, *30*(3), 39–50. https://doi.org/10.1002/rem.21653

McGregor, R. (2023). The in situ treatment of PFAS within porewater at the air–water interface of a PFAS source zone. *Remediation*, *33*(4), 265–278. https://doi.org/10.1002/rem.21759

Moody, C. A., & Field, J. A. (2000). Perfluorinated surfactants and the environmental implications of their use in fire-fighting foams. In *Environmental Science and Technology 34*(18), 3864–3870. https://doi.org/10.1021/es991359u

Moriwaki, H., Takagi, Y., Tanaka, M., Tsuruho, K., Okitsu, K., & Maeda, Y. (2005). Sonochemical decomposition of perfluorooctane sulfonate and perfluorooctanoic acid. *Environmental Science and Technology*, *39*(9), 3388–3392. https://doi.org/10.1021/es040342v

McMahon, P. B., Tokranov, A. K., Bexfield, L. M., Lindsey, B. D., Johnson, T. D., Lombard, M. A., & Watson, E. (2022). Perfluoroalkyl and Polyfluoroalkyl Substances in Groundwater Used as a Source of Drinking Water in the Eastern United States. *Environmental Science and Technology*, *56*(4), 2279–2288. https://doi.org/10.1021/acs.est.1c04795

National Academy of Sciences (1980). *Drinking water and Health: Volume 2*. Safe Drinking Water Committee, National Research Council. National Academy Press, Washington, D.C. https://doi.org/10.17226/1904

Newcombe, G., Drikas, M., Hayes, R. (1997). Influence of characterized natural organic matter on activated carbon adsorption: II. Effect on pore volume distribution and adsorption of 2-methylisoborneol. *Water Res 31*(5), 1065–1073. https://doi.org/10.1016/S0043-1354(96)00325-9

Nguyen, T. M. H., Bräunig, J., Thompson, K., Thompson, J., Kabiri, S., Navarro, D. A., Kookana, R. S., Grimison, C., Barnes, C. M., Higgins, C. P., Mclaughlin, M. J., & Mueller, J. F. (2020). Influences of Chemical Properties, Soil Properties, and Solution pH on Soil-Water Partitioning Coefficients of Per- And Polyfluoroalkyl Substances (PFASs). *Environmental Science and Technology*, *54*(24), 15883–15892. https://doi.org/10.1021/acs.est.0c05705

NGWA (2017). Groundwater and PFAS: State of Knowledge and Practice. https://www.ngwa.org/docs/default-source/default-document-library/publications/pfas-doc-section1-overview.pdf?sfvrsn=f4ae9fe6_2

Niarchos, G., Ahrens, L., Kleja, D. B., Leonard, G., Forde, J., Bergman, J., Ribeli, E., Schütz,

M., & Fagerlund, F. (2023). In-situ application of colloidal activated carbon for PFAS-contaminated soil and groundwater: A Swedish case study. *Remediation*, *33*(2), 101–110. https://doi.org/10.1002/rem.21746

Ochoa-Herrera, V., & Sierra-Alvarez, R. (2008). Removal of perfluorinated surfactants by sorption onto granular activated carbon, zeolite and sludge. *Chemosphere*, *72*(10), 1588–1593. https://doi.org/10.1016/j.chemosphere.2008.04.029

Organization for Economic Cooperation and Development (OECD) (2024). Portal on Per and Poly Fluorinated Chemicals. https://www.oecd.org/chemicalsafety/portal-perfluorinated-chemicals/aboutpfass/

O'Hagan D. (2008). Understanding organofluorine chemistry. An introduction to the C-F bond. *Chemical Society reviews*, *37*(2), 308–319. https://doi.org/10.1039/b711844a

Olshansky, Y., Gomeniuc, A., Chorover, J., Abrell, L., Field, J. A., Hatton, J., He, J., & Sierra-Alvarez, R. (2022). Tailored Polyanilines Are High-Affinity Adsorbents for Per- and Polyfluoroalkyl Substances. *ACS ES and T Water*, *2*(8), 1402–1410. https://doi.org/10.1021/acsestwater.2c00166

Petruzelli, D., Helfferich, F.G. (1992). Migration and Fate of Pollutants in Soils and Subsoils. *NATO ASI Series. Series G: Ecological Sciences*, *32*. https://doi.org/10.1007/978-3-642-77862-9

Qu, Y., Zhang, C., Li, F., Bo, X., Liu, G., & Zhou, Q. (2009). Equilibrium and kinetics study on the adsorption of perfluorooctanoic acid from aqueous solution onto powdered activated carbon. *Journal of Hazardous Materials*, *169*(1–3), 146–152. https://doi.org/10.1016/j.jhazmat.2009.03.063

Radjenovic, J., & Sedlak, D. L. (2015). Challenges and Opportunities for Electrochemical Processes as Next-Generation Technologies for the Treatment of Contaminated Water. *Environmental Science and Technology 49*(19), 11292–11302. https://doi.org/10.1021/acs.est.5b02414

Rao, P.S., & Davidson, J.M. (1980). Estimation of pesticide retention and transformation parameters required in nonpoint source pollution models. In M.R Overcash and J.M Davidson (ed.). Environmental impact of nonpoint source pollution. Ann Arbor Science Publishers, Ann Arbor, MI. https://api.semanticscholar.org/CorpusID:133733971

Roth, J. v. (2009). Prediction interval analysis is underutilized and can be more helpful than just confidence interval analysis. *Journal of Clinical Monitoring and Computing*, *23*(3), 181–183. https://doi.org/10.1007/s10877-009-9165-0

Salvatore, D., Mok, K., Garrett, K. K., Poudrier, G., Brown, P., Birnbaum, L. S., Goldenman, G., Miller, M. F., Patton, S., Poehlein, M., Varshavsky, J., & Cordner, A. (2022). Presumptive Contamination: A New Approach to PFAS Contamination Based on Likely Sources. *Environmental Science and Technology Letters*, *9*(11), 983–990. https://doi.org/10.1021/acs.estlett.2c00502

Schröder, H. F., & Meesters, R. J. W. (2005). Stability of fluorinated surfactants in advanced oxidation processes - A follow up of degradation products using flow injection-mass spectrometry, liquid chromatography-mass spectrometry and liquid chromatography-multiple stage mass spectrometry. *Journal of Chromatography A*, *1082*, 110–119. https://doi.org/10.1016/j.chroma.2005.02.070

Schaefer, C. E., Nguyen, D., Christie, E., Shea, S., Higgins, C. P., & Field, J. (2022). Desorption Isotherms for Poly- and Perfluoroalkyl Substances in Soil Collected from an Aqueous Film-Forming Foam Source Area. *Journal of Environmental Engineering*, *148*(1). https://doi.org/10.1061/(asce)ee.1943-7870.0001952

Schaefer, C. E., Nguyen, D., Christie, E., Shea, S., Higgins, C. P., & Field, J. A. (2021). Desorption of Poly- and Perfluoroalkyl Substances from Soil Historically Impacted with Aqueous Film-Forming Foam. *Journal of Environmental Engineering*, *147*(2). https://doi.org/10.1061/(asce)ee.1943-7870.0001846

Scheitlin, C. G., Dasu, K., Rosansky, S., Dejarme, L. E., Siriwardena, D., Thorn, J., Mullins, L., Haggerty, I., Shqau, K., & Stowe, J. (2023). Application of Supercritical Water Oxidation to Effectively Destroy Per- and Polyfluoroalkyl Substances in Aqueous Matrices. *ACS ES and T Water*, *3*(8), 2053–2062. https://doi.org/10.1021/acsestwater.2c00548

Smalling, K. L., Romanok, K. M., Bradley, P. M., Morriss, M. C., Gray, J. L., Kanagy, L. K., Gordon, S. E., Williams, B. M., Breitmeyer, S. E., Jones, D. K., DeCicco, L. A., Eagles-Smith, C. A., & Wagner, T. (2023). Per- and polyfluoroalkyl substances (PFAS) in United States tapwater: Comparison of underserved private-well and public-supply exposures and associated health implications. *Environment International*, *178*. https://doi.org/10.1016/j.envint.2023.108033

Swanson, R.A., Dutt, G.R. (1973).Chemical and physical processes that affect atrazine and distribution in soil systems. *Soil Sci. Soc. Am. J.*, *37*(6) 872–876. https://doi.org/10.2136/sssaj1973.03615995003700060024x

Suzuki, M. (1990). Adsorption Engineering. *Chemical engineering monographs* (Vol. 25). Kodansha Ltd, Tokyo, Japan. ISBN 0-444-41-295-6

Tsai, Y. T., Yu-Chen Lin, A., Weng, Y. H., & Li, K. C. (2010). Treatment of perfluorinated chemicals by electro-microfiltration. *Environmental Science and Technology*, *44*(20), 7914–7920. https://doi.org/10.1021/es101964y

Tang, C. Y., Fu, Q. S., Criddle, C. S., & Leckie, J. O. (2007). Effect of flux (transmembrane pressure) and membrane properties on fouling and rejection of reverse osmosis and nanofiltration membranes treating perfluorooctane sulfonate containing wastewater. *Environmental Science and Technology*, *41*(6), 2008–2014. https://doi.org/10.1021/es062052f

Taylor, P. H., Yamada, T., Striebich, R. C., Graham, J. L., & Giraud, R. J. (2014). Investigation of waste incineration of fluorotelomer-based polymers as a potential source of PFOA in the environment. *Chemosphere*, *110*, 17–22. https://doi.org/10.1016/j.chemosphere.2014.02.037

The Nature Conservancy. (2022). Groundwater: Our Most Valuable Hidden Resource. https://www.nature.org/en-us/what-we-do/our-insights/perspectives/groundwater-most-valuable-resource/

United Nations. (2023). Ensure availability and sustainable management of water and sanitation for all. https://sdgs.un.org/goals/goal6#targets_and_indicators

US EPA (2024). CompTox Chemicals Dashboard v2.4.1. https://comptox.epa.gov/dashboard/

US EPA (2022). Memorandum: Implementation of the Clean Water and Drinking Water State Revolving Fund Provisions of the Bipartisan Infrastructure Law. https://www.epa.gov/system/files/documents/2022-03/combined_srf-implementation-memo_final_03.2022.pdf

US EPA (2020). Per- and Polyfluoroalkyl Substances (PFAS): Incineration to Manage PFAS Waste Streams. https://www.epa.gov/sites/default/files/2019-09/documents/technical_brief_pfas_incineration_ioaa_approved_final_july_2019.pdf

US EPA (2018). Reducing PFAS in Drinking Water with Treatment Technologies. https://www.epa.gov/sciencematters/reducing-pfas-drinking-water-treatment-technologies

USEPA (2002). Field Applications of In Situ Remediation Technologies: Permeable Reactive Barriers. https://clu-in.org/download/rtdf/fieldapp_prb.pdf

Venkatesan, A. K., Lee, C. S., & Gobler, C. J. (2022). Hydroxyl-radical based advanced oxidation processes can increase perfluoroalkyl substances beyond drinking water standards: Results from a pilot study. *Science of the Total Environment, 847*. https://doi.org/10.1016/j.scitotenv.2022.157577

Wackett, L. P. (2021). Why Is the Biodegradation of Polyfluorinated Compounds So Rare? *MSphere*, *6*(5). https://doi.org/10.1128/msphere.00721-21

Wang, W., Rhodes, G., Zhang, W., Yu, X., Teppen, B. J., & Li, H. (2022). Implication of cation-bridging interaction contribution to sorption of perfluoroalkyl carboxylic acids by soils. *Chemosphere*, *290*. https://doi.org/10.1016/j.chemosphere.2021.133224

Weber, W.J., Kim, S.H., & Johnson, M.D. (2002). Distributed Reactivity Model for Sorption by Soils and Sediments. 15. High-Concentration Co-Contaminant Effects on Phenanthrene Sorption and Desorption. *Environ. Sci. Technol*. *36*(16), 3625–3634. https://doi.org/10.1021/es020557

Wei, C., Song, X., Wang, Q., & Hu, Z. (2017). Sorption kinetics, isotherms and mechanisms of PFOS on soils with different physicochemical properties. Ecotoxicology and Environmental Safety, 142, 40–50. https://doi.org/10.1016/j.ecoenv.2017.03.040

Woodard, S., Berry, J., & Newman, B. (2017). Ion exchange resin for PFAS removal and pilot test comparison to GAC. *Remediation*, *27*(3), 19–27. https://doi.org/10.1002/rem.21515

Xiao, X., Ulrich, B. A., Chen, B., & Higgins, C. P. (2017). Sorption of Poly- and Perfluoroalkyl Substances (PFASs) Relevant to Aqueous Film-Forming Foam (AFFF)-Impacted Groundwater by Biochars and Activated Carbon. *Environmental Science and Technology*, *51*(11), 6342–6351. https://doi.org/10.1021/acs.est.7b00970

Xiao, F., Jin, B., Golovko, S. A., Golovko, M. Y., & Xing, B. (2019). Sorption and Desorption Mechanisms of Cationic and Zwitterionic Per- And Polyfluoroalkyl Substances in Natural Soils: Thermodynamics and Hysteresis. *Environmental Science and Technology*, *53*(20), 11818–11827. https://doi.org/10.1021/acs.est.9b05379

Yamada, T., Taylor, P. H., Buck, R. C., Kaiser, M. A., & Giraud, R. J. (2005). Thermal degradation of fluorotelomer treated articles and related materials. *Chemosphere*, *61*(7), 974–984. https://doi.org/10.1016/j.chemosphere.2005.03.025

Yonge, D. R., Keinath, T. M., Poznanska, K., & Jiang, Z. P. (1985). Single-solute irreversible adsorption on granular activated carbon. *Environmental Science and Technology*, *19*(8), 690–694. https://doi.org/10.1021/es00138a006

Yu, Q., Zhang, R., Deng, S., Huang, J., & Yu, G. (2009). Sorption of perfluorooctane sulfonate and perfluorooctanoate on activated carbons and resin: Kinetic and isotherm study. *Water Research*, *43*(4), 1150–1158. https://doi.org/10.1016/j.watres.2008.12.001

Zhang, C., Yan, H., Li, F., Hu, X., & Zhou, Q. (2013). Sorption of short- and long-chain perfluoroalkyl surfactants on sewage sludges. *Journal of Hazardous Materials*, *260*, 689–699. https://doi.org/10.1016/j.jhazmat.2013.06.022

Zhi, Y., & Liu, J. (2018). Sorption and desorption of anionic, cationic and zwitterionic polyfluoroalkyl substances by soil organic matter and pyrogenic carbonaceous materials. *Chemical Engineering Journal*, *346*, 682–691. https://doi.org/10.1016/j.cej.2018.04.042

Zhuo, Q., Deng, S., Yang, B., Huang, J., Wang, B., Zhang, T., & Yu, G. (2012). Degradation of perfluorinated compounds on a boron-doped diamond electrode. *Electrochimica Acta*, *77*(30), 17–22. https://doi.org/10.1016/j.electacta.2012.04.145

Appendix A

Equipment Details

Table A.1: LC-MS/MS Setup

Instrument	Shimadzu LCMS-8030 Triple Quadrupole Mass Spectrometer
Column	Agilent Infinity Lab Poroshell 120 Å EC-C18, 3.0 x 50 mm, 2.7 µm
Precolumn	Agilent ZORBAX Eclipse Plus C18, 95Å, 4.6 x 30 mm, 3.5 µm
Oven Temperature	30 ˚C
Injection Volume	30 µL
Eluent	A: 5mM ammonium acetate in LCMS grade water B: LCMS grade methanol
Flow Rate	0.5 mL/min

Flow Gradient Profile:

Time (min)	Eluent A Conc. (%)	Eluent B Conc. (%)
0	60	40
0.5	60	40
4.5	20	80
10	20	80
10.5	60	40
13.5	Stop	Stop

MS/MS Electrospray Ionization Source Parameters:

Nebulizing Gas Flow (L/min)	Drying Gas Flow (L/min)	Heat Block Temperature (˚C)	Desolvation Line (DL) Temperature (˚C)	Collision-Induced dissociation (CID) gas flow (kpa)	Interface Voltage (V)
3	15	400	250	230	-4500

Monitored Ion Transitions

Analytes	Ion Transitions	Internal Standards	Ion Transitions	Calibration Range (µg/L)
PFOS	499 > 80	[$^{13}C_8$] MPFOS	507 > 99	0.05 - 20
PFOA	413 > 369	[$^{13}C_8$] MPFOA	421 > 376	0.05 - 20
PFBS	299 > 80	[$^{13}C_3$] MPFBS	302 > 99	0.05 - 20

Appendix B
Additional Figures

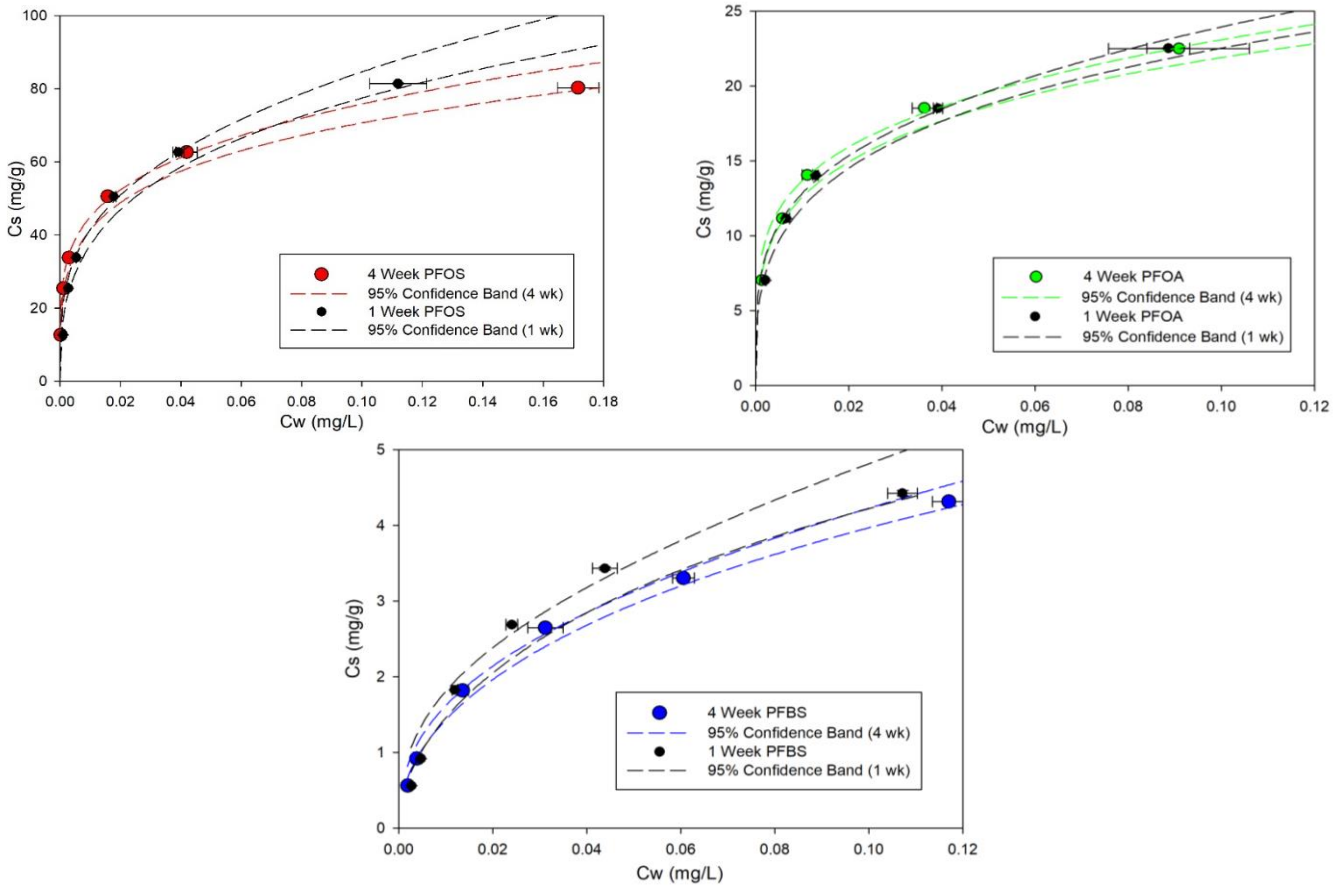


Figure B.1: Comparisons of the adsorption data for PFOS, PFOA or PFBS on polymer-free CAC with contact times of 168 h (black circles) and 672 h (coloured circles). After the data was fit to the Freundlich isotherm model (not shown), the 95% confidence band of adsorption was overlayed (dashed lines). Error bars on each point represent one standard deviation from the mean of three replicates. Overlap of the 95% confidence bands indicates that the isotherms are not statistically different, at the 95% level of confidence.

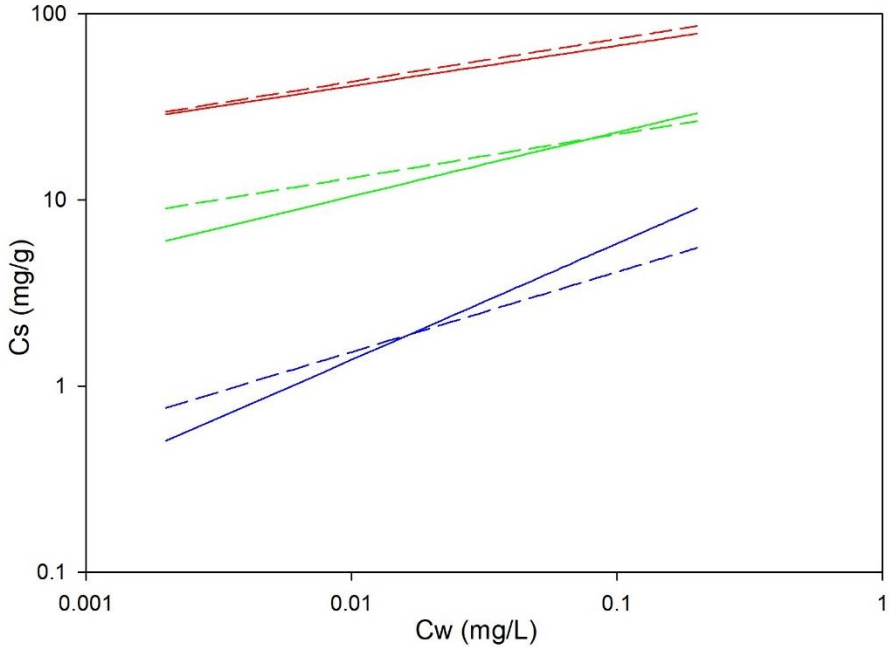


Figure B.2: Comparison of PAC (solid lines) to CAC (dashed lines) adsorption isotherms for PFOS —, PFOA —, PFBS —.